Archives of Civil and Mechanical Engineering (2024) 24:184
https://doi.org/10.1007/s43452-024-00988-5

REVIEW ARTICLE

Latest advances in extrusion processes of light metals

Dariusz Leśniak[1] · Józef Zasadziński[1] · Wojciech Libura[1] · Zbigniew Gronostajski[2] · Romana Śliwa[3] · Beata Leszczyńska-Madej[1] · Marcin Kaszuba[2] · Antoni Woźnicki[4] · Bartłomiej Płonka[5] · Paweł Widomski[2] · Jacek Madura[1]

Received: 18 March 2024 / Revised: 20 May 2024 / Accepted: 1 June 2024 / Published online: 20 June 2024

Abstract

The paper presents a review of the literature and authors' research on the current achievements in the field of extrusion of aluminium alloys, magnesium alloys, powders and aluminium-based composites in particular. The microstructure transformations taking place during homogenisation of billets from the medium- and high-strength heat-treatable aluminium alloys are still an object of interest of researchers. The recently published papers are related to dissolution of soluble phases formed during solidification and elimination of microsegregation, precipitation of the dispersoids, insoluble phases' transformation as well as particles re-precipitation during cooling. The novelties in the extrusion of magnesium alloys and aluminium-based composites are shortly reported. Specifics of the extrusion dies design and their working conditions, which limit the products quality and working life of the tools, are extensively reported. The computer-aided designing (CAD) and finite-element method (FEM) and 3D optical scanning were used in analysis aimed at dimensional deviations of the dies and the extruded products. The surface engineering techniques such as welding techniques, diffusion layers and protective coatings such as produced by physical vapour deposition (PVD), plasma-enhanced physical vapour deposition (PAPVD), chemical vapour deposition (CVD) and plasma-enhanced chemical vapour deposition (PECVD) are described. Various original methods of extrusion including the severe plastic deformation processes (SPD), such as cyclic extrusion compression (CEC), equal-channel angular pressing (ECAP) and hydrostatic extrusion (HE) are discussed. The above techniques as well as the new KOBO extrusion process with oscillating die movement generate significant refining of the microstructure of metals and alloys and enable consolidation of the powdered materials. The application of the rapid solidification process connected with the hot extrusion permits production of beneficial microstructure and above-standard mechanical properties of the extruded products. Finally, the opportunities and directions of development of the extrusion process of metals and alloys are indicated.

1 Introduction

The extrusion is a widespread process for production of various long profiles from metals and alloys. It is particularly valuable to produce extrudates of complex cross-section, even from the materials of poor deformability. The extruded products are characterised by relatively high mechanical properties and the advantageous microstructure. In the paper, the novelties in the traditional extrusion process are described, enabling production of profiles of the unique characteristics which are unattainable in the classic process. The investigations are focussed on the light metals and alloys only, since extrusion of copper and other heavy alloys is based mainly on the traditional and well-known technologies.

The homogenisation of billets is an essential stage within the scope of technological cycle of aluminium alloys

✉ Dariusz Leśniak
dlesniak@agh.edu.pl

[1] AGH University of Kraków, al. Mickiewicza 30, 30-059 Kraków, Poland

[2] Wrocław University of Science and Technology, ul. Wybrzeże Stanisława Wyspiańskiego 27, 50-370 Wrocław, Poland

[3] Rzeszów University of Technology, al. Powstańców Warszawy 12, 35-959 Rzeszow, Poland

[4] Aptiv Services Poland S.A., ul. Podgórki Tynieckie 2, 30-399 Kraków, Poland

[5] Łukasiewicz Research Network – Institute of Non-Ferrous Metals, ul. Józefa Sowińskiego 5, 44-121 Gliwice, Poland

extrusion. It significantly influences billets extrudability, permissible extrusion parameters as well as properties of obtained profiles. The homogenisation is still an object of interest of the researchers, and it is driven by growing demand for extruded products and their properties. The recently published papers are related to all main microstructure transformations taking place during billets homogenisation, i.e. dissolution of soluble phases of particles formed during solidification and elimination of micro segregation, and precipitation of the dispersoids in alloys containing transition elements. This work presents a brief overview of the selected research which describes homogenisation of precipitation hardened aluminium alloys. In particular, these data can be applicable to extrusion billets.

The magnesium alloys are traditionally used as-cast alloys, but plastic deformation of many alloys is also performed successfully, especially in the last 2 decades. Wrought magnesium alloys contain aluminium, zinc, manganese and copper. These additions improve strength properties of these alloys. Recently, rare-earth elements, such as La, Y, Nd, Ce, Dy as well as zirconium are added to magnesium alloys which are subject to plastic deformation. Magnesium and its alloys offer a remarkable potential in the transport industries since their low density makes its alloys the lightest available constructional metals. Magnesium wrought alloy yield stress is between 160 and 240 MPa, whereas tensile strength is of 180–440 MPa and elongation of 7–40%. It is worth noting that the commercial Mg extrusion alloys have a significant tension–compression yield asymmetry. The yield stress in compression is about 0.4–0.8 of that in tension, which is not observed for Al extrusion alloys. The most common wrought magnesium alloys, and the innovations in their extrusion are shortly described below.

Among engineering materials, composites play an important role and increasingly many key products are manufactured from these materials. Due to specifics of their microstructure and resulting unique properties, they can show properties unattainable for metallic materials, ceramics or plastics. Out of different composites, aluminium-based composites obtain wide application, mainly in the automotive and aerospace industry, power engineering and construction. In the work, a classification of the aluminium-based composites is presented and an attempt of their welding extrusion for production of the hollow profiles is undertaken. Then, experiments were performed on the aluminium-based composites containing hard particles of silicon carbide SiC and Al_2O_3. The base materials were aluminium and the 6061 aluminium alloy.

Modern applications of extruded profiles from the aluminium alloys, such as construction industry, automotive including enclosures of the electric vehicles, transport of vans and trucks or aerospace industry, force more and more complex shapes of the hollow profiles, lightness (thin walls), better strength properties, narrow dimensional tolerances and low roughness. The advanced and economically acceptable process parameters are also strongly sought. All the above-mentioned aspects except the strength of the product depend on the die design. The design of the extrusion die affects process parameters, such as extrusion force, maximum permissible exit speed from the die opening, as well as the die life, material yield, scrap and product quality. In particular, designing of the porthole dies for extrusion of the hollow profiles is important. In this work, the procedures were subsequently of designing of the porthole dies for extrusion of the complex hollow profiles from the 6005A and hard 7021 aluminium alloys are presented. Those procedures were subsequently successfully validated in the industrial conditions.

The excessive tool wear in the hot extrusion processes is observed, resulting in early recall of tools from the exploitation. The reason for the observed variety of wear is damage mechanisms present in the extrusion processes. One of these mechanisms specified is the adhesive and abrasive wear, which results in damage of the die bearing length. Besides, the tempering of die elements occurs as a result of high temperature which leads to material cracking under pressure of the extruded material. The other damages result mainly from the overloading of the extrusion dies, as a result of constructional and technological mistakes. The methods of the tool life improvement include both conventional and modern technologies. In the description, the authors are including methods currently investigated and not widely validated in practices but indicate high potential for exploitation.

The SPD processes, frequently extrusion based, include many methods which can be used for the refining grains to nano- or submicron dimensions by causing high plastic strains. They require special devices to be used, allowing for producing very high deformation and preserving cohesion of the deformed material as well its dimensions. It is ideal to apply a hydrostatic compression which prevents cracking of the material. In some SPD methods, the extrusion is the base process, e.g. cyclic extrusion compression (CEC), or equal-channel angular pressing (ECAP). Well known are also the methods of utilising high plastic strains, such as hydrostatic extrusion (HE), or KOBO process. The deformation in these processes leads to significant refining of the microstructure of metals and alloys and enables consolidation of the powdered materials. In the work, the most important SPD methods are described and available mechanical and structural characteristics of the investigated materials are compared.

The KOBO extrusion process is an innovative and attractive method among the SPD processes permitting to produce different products under very positive deformation conditions in terms of product properties and manufacturing costs. In this method, proposed and patented by Korbel and Bochniak, the metal adjacent to the die in the cutting

zone is submitted to reversible torsion by oscillating rotary motion of the die around its axis. The method allows for the decreasing extrusion force without heating of the billet, the increasing of deformation ratio and acceleration of the process. The speed of the process, temperature, deformation ratio and, most importantly, an angle oscillation frequency of the die influence also the mechanical properties of the products. The reason of a typical behaviour of the deformed materials is a localised plastic flow which results from the generating of the vacancies in the amount of even ten orders of magnitude higher in comparison to its steady-state concentration. A dramatic decrease in material viscosity explains the enhanced plasticity, whereas the hardening of the products results from the immediate forming of the clusters of vacancies. The work provides examples of KOBO process including mechanical and structural behaviour of the investigated materials.

The development of modern engineering materials gives an opportunity to produce new variants of materials characterised by new and modified performance properties due to application of special production techniques. This is a technology of plastic consolidation of loose materials (powders, flakes, and chips), classified as powder metallurgy (PM) process. The traditional PM methods ensure production of new materials, from the deformable feedstocks of specified properties using compaction and sintering procedures. In the work, the traditional PM techniques are described based on classic and modified aluminium alloys. Particularly, an emphasis is put on the alloys obtained by the rapid solidification methods, consolidated subsequently by the hot extrusion process. The obtained microstructure and properties of the products are superior to the materials produced by traditional technologies.

2 Extrusion billets

2.1 Medium- and high-strength aluminium alloys

The billets homogenisation is an essential stage of the manufacturing cycle of aluminium alloys extruded products. It significantly influences billets extrudability, permissible extrusion parameters as well as properties of obtained profiles. This process step has quite long history, for Al–Mg–Si alloys, it was introduced in the industry around 1960s. Despite this, homogenisation is still an object of interest of the researchers, which is driven by growing demand for extruded products and requirements regarding their properties. Among the recently published papers, one may find works related to all main microstructure transformations taking place during aluminium alloys billets homogenisation, i.e. dissolution of soluble phases particles formed during solidification and elimination of microsegregation, precipitation of the dispersoids in alloys containing transition elements, transformation and spheroidisation of insoluble particles and finally precipitation during cooling of phases showing limited solubility in aluminium matrix. Below is presented a brief overview of the selected works describing homogenisation of precipitation hardenable aluminium alloys, results of which refer to or are applicable to extrusion billets.

2.1.1 Soluble phases dissolution

The dissolution of soluble phases particles and elimination of microsegregation observed in the direct-chill as-cast billets are considered as the primary microstructural processes occurring during homogenisation heating and soaking. At the end of soaking, a maximum possible enrichment of (Al) solid solution in elements taking part in subsequent precipitation hardening shall be obtained. The full utilisation of alloying additions is a basic condition for achieving the often expected, high-strength properties of the extruded products. Moreover, the undissolved particles generally have negative effects on fatigue resistance and fracture toughness of high-strength alloy products. It is well known that the microstructure of high-strength alloys as-cast billets is often characterised by the presence of several soluble phases. For example, in the case of Al–Zn–Mg–Cu alloys, one may show microstructures containing M-$(Cu, Zn, Al)_2$ Mg, T-$(Cu, Zn, Al)_{49}Mg_{32}$, S-Al_2CuMg, β-Mg_2Si and Al_3Mg_2 or M-$(Cu, Zn, Al)_2$ Mg, θ-Al_2Cu and the metastable, Cu-enriched phase [AlCuMgZn]. For Al–Mg–Si–Cu alloys, phases β-Mg_2Si, Q-$Al_5Cu_2Mg_8Si_6$, θ-Al_2Cu and (Si) may be present. Such complex microstructures result in low unequilibrium solidus temperature, e.g. ~ 460 °C for Al–Zn–Mg–Cu and ~ 485 °C for Al–Mg–Si–Cu alloys. Thus, in order to avoid incipient melting and ensure the expected phases dissolution, a tailored, multi-step homogenisation schedules need to be often designed. Different approaches to this task are described in recent literature: experimental work, thermodynamic calculations or numerical modelling.

In the paper [1], homogenisation of 7 alloys, with Zn content from 6.40 to 7.20%, Mg from 2.11 to 2.37% and Cu from 1.79 to 2.89%, was investigated. On the basis of thermodynamic calculations, modelling of the homogenisation process and experimental work, it was found that the examined alloys can be divided into 3 groups:

- with low Cu + Mg content (4.04–4.16 wt%), for which soluble phases (i.e. M phase, Cu-enriched [AlCuMgZn] phase, when present, and the S phase forming already during annealing) can be fully eliminated after 475 °C/24 h homogenisation;

- with medium Cu + Mg content (4.24 wt%), where the S phase can be eliminated after the homogenisation 475 °C/24 h + 485 °C/24 h;
- with high Cu + Mg content (4.69–5.04 wt%), in which the S phase cannot be completely eliminated even after the two-step homogenisation as mentioned above.

Based on the obtained results and analysis of literature data, the guidelines for designing or optimising of the composition and homogenisation process for Al–Zn–Mg–Cu alloys were presented. The alloys with higher Zn content, about 8.5%, Mg from 1.5 to 2.5% and Cu from 1.5 and 2.9% were analysed in the paper [2] in the view of thermodynamic calculations and experiments. The one-step 460 °C/24 h as well as two-step 460 °C/24 h + 475 °C/24 h homogenisation schedules were applied. For alloys with relatively low Mg or low Mg + Cu concentration, the single-step homogenisation was found to be sufficient for complete dissolution of soluble phases. Alloys richer in the mentioned additions need to be homogenised with two-step schedule and for the alloys with Mg + Cu ≥ 4.35%, the complete dissolution of phases cannot be obtained in the examined conditions.

A different approach to homogenisation design was presented in the work [3], where process parameters for 7050 grade alloy Al–6.2% Zn–2.35% Mg–2.3% Cu–0.13% Zr were proposed on the basis of a numerical study. The model, coupling the microscale model of soluble phases evolution with nanoscale model of Al_3Zr dispersoids precipitation, was developed and verified by experiments. A three-step homogenisation was suggested: 420 °C/10 h + 470 °C/4 h + 480 °C/15 h. The first step was aimed at dispersoids precipitation, second at the η-$MgZn_2$ phase dissolution/transformation to S phase and third at minimising the S-phase fraction in the microstructure. The authors state that the developed model can be a tool for designing homogenisation schedules for other 7xxx alloys.

The homogenisation conditions for Al–Zn–Mg–Cu alloys billets intended for extrusion welding were analysed in the paper [4]. The particular attention was paid on maximisation of the solidus temperature after homogenisation. A high solidus temperature extends the permissible temperature range for the extrusion process, and the material temperature in the welding chamber is one of crucial parameters determining a quality of longitudinal welds. The homogenisation was studied experimentally and the analysis was primarily based on the DSC tests results, showing evolution of solidus temperature and incipient melting heat, supported by SEM/EDS microstructure examination. One- or two-step homogenisation schemes were suggested, they are presented in Table 1, together with conditions mentioned in other papers. In all examined alloys, at the end of the soaking, the significant increase of solidus temperature was achieved, when compared to as-cast state (Fig. 1).

Table 1 Reported homogenisation soaking conditions for selected Al–Zn–Mg–Cu alloys

No.	Alloy	Homogenisation soaking conditions	Remarks	Source
1	Al–5.14% Zn–2.08% Mg–1.22% Cu (7075 Grade-No. 1)	465 °C/4 h		[4]
2	Al–5.94% Zn–2.50% Mg–2.02% Cu (7075 Grade-No. 2)	465 °C/2 h + 475 °C/8 h		[4]
3	Al–5.89% Zn–2.39% Mg–1.54% Cu (7075 Grade-No. 3)	465 °C/12 h or 465 °C/2 h + 475 °C/4 h		[4]
4	Al–8.02% Zn–2.36% Mg–1.57% Cu (7049 Grade-No. 4)	465 °C/12 h		[4]
5	Al–7.20% Zn–2.21% Mg–1.83% Cu	475 °C/24 h		[1]
6	Al–6.86% Zn–2.17% Mg–2.07% Cu	475 °C/24 h + 485 °C/24 h		[1]
7	Al–7.20% Zn–2.11% Mg–2.58% Cu	475 °C/24 h + 485 °C/24 h	S-phase not dissolved completely	[1]
8	Al–6.50% Zn–2.15% Mg–2.89% Cu	475 °C/24 h + 485 °C/24 h	S-phase not dissolved completely	[1]
9	Al–8.74% Zn–1.50% Mg–2.45% Cu	460 °C/24 h		[2]
10	Al–8.76% Zn–2.06% Mg–1.51% Cu	460 °C/24 h		[2]
11	Al–8.73% Zn–1.41% Mg–2.90% Cu	460 °C/24 h + 475 °C/24 h		[2]
12	Al–8.57% Zn–2.52% Mg–1.42% Cu	460 °C/24 h + 475 °C/24 h		[2]
13	Al–8.61% Zn–2.47% Mg–1.90% Cu		M-phase (denoted as σ in the paper) not dissolved completely	[2]
14	Al–8.67% Zn–2.50% Mg–2.50% Cu		M-phase and S-phase not dissolved completely	[2]
15	Al–6.2% Zn–2.35% Mg–2.3% Cu (7050 grade)	420 °C/10 h + 470 °C/4 h + 480 °C/15 h	S-phase not dissolved completely	[3]

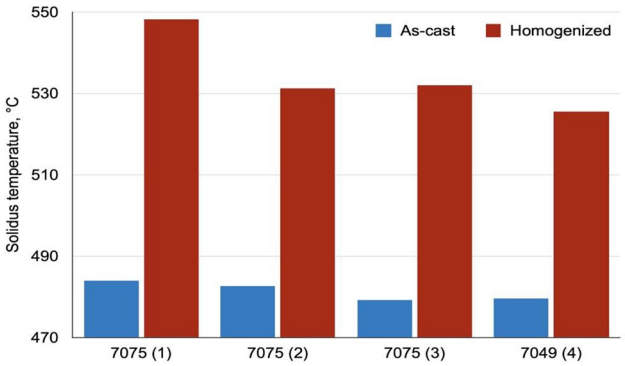

Fig. 1 Solidus temperature of 7xxx alloys from [4-open access]. Number in brackets refers to alloys numbering in Table 1. For alloy 7075 (3), solidus temperature after double-stage homogenisation is presented

In the work [5], the homogenisation conditions for extrusion billet of the alloy Al–0.80% Mg–1.22% Si–1.41% Cu were investigated. The alloy was characterised by higher Cu content than currently applied in the 6xxx series. The experimental method, similarly as in paper [4], was based on the DSC and SEM/EDS techniques.

The homogenisation scheme with three soaking stages: 475 °C/2 h + 530 °C/2 h + 545 °C/8 h was proposed. During the first stage at 475 °C, the θ-Al_2Cu phase and probably (Si) were dissolved, causing solidus increment, which enabled rising the soaking temperature. During the second stage, the dissolution of the Q-$Al_5Cu_2Mg_8Si_6$ phase took place. Despite the further temperature rising, the β-Mg_2Si phase was not fully dissolved during soaking, but its amount was significantly reduced. After completed soaking and water quenching, the solidus temperature of 573.4 °C was noted.

The homogenisation of Al–5.2% Cu–0.9% Mg–0.6% Ag alloy industrial billet of diameter of 252 mm was analysed in the paper [6] on the basis of OM, SEM and DSC examination results. Four three-stage homogenisation, soaking schemes were investigated. The first and second stages were constant and the conditions of the third stage were changed. The scheme 420 °C/5 h + 480 °C/8 h + 515 °C/24 h was proposed for the alloy. Two of soluble phases present in the as-cast state, i.e. the S-Al_2CuMg and the AlCuMgAg quaternary phase, were dissolved. Third one, the θ-Al_2Cu phase was not dissolved completely, but thanks to third-stage conditions selection, reduction of its fraction in the microstructure took place (Table 1).

2.1.2 Dispersoids precipitation

The dispersoids, which precipitate from solid solution during homogenisation, significantly influence the microstructure and properties of high-strength aluminium alloys after further processing stages. They enable the grain size control and increase the fracture toughness. However, to achieve expected results, the dispersoids need to be fine and their distribution is to be dense and uniform. The alloying additions microsegregation within dendrites in the as-cast state and low diffusivity of dispersoids-forming elements hinder obtaining the mentioned effects after standard homogenisation, and considerable research effort is paid on designing of the heat treatment cycles minimising the negative effect of the microsegregation.

The paper [7] presents investigation on three-stage homogenisation schedules of 7085 alloy: 450 °C/12 h + 350 or 250 °C/8 h + 480 °C/12 h, in comparison with two-stage cycle 450 °C/20 h + 480 °C/12 h. During the soaking at 450 °C, the dominant part of soluble phases (eutectics) dissolved in the matrix. In the second stage, accomplished at 350 or 250 °C, precipitation of the η-$MgZn_2$ phase took place, which served as nucleation sites for Al_3Zr dispersoids. The second-stage temperature of 350 °C brought noticeable improvement of the Al_3Zr dispersoids precipitation homogeneity, whereas at 250 °C, inhomogeneous dispersoids precipitation was observed. In the final stage at 480 °C, the soluble phases (η-$MgZn_2$ and S phase, which left after the first stage) dissolved. In conclusion, the three-stage homogenisation process 450 °C/12 h + 350 °C/24 h + 480 °C/12 h (i.e. with extended second-stage duration) was suggested. Although the obtained effects are interesting, one should notice that application of such homogenisation scheme in industrial practice is difficult.

The different implementation of the same idea—making use of the η phase pre-precipitation for improving dispersoids uniformity—was presented in the work [8]. One-, two- and three-stage homogenisation cycles of 7020 alloy billets were compared. For three-stage schedule: 350 °C/8 h + 420 °C/4 h + 470 °C/16 h, the significant increase in dispersoids number density and in the ratio of volume fraction to radius was noted (when compared with one stage homogenisation). Large amount of fine Al_3Zr dispersoids formed near grain boundaries was observed. It is worth noticing that after the first stage, the η-phase precipitates distribution inside the grains was uneven (due to microsegregation). However, this phase tends to segregate in areas near grain boundaries, depleted in Zr, also in areas where it is most needed for Al_3Zr nucleation.

In the work [9], the homogenisation of 2196 alloy Al–2.80% Cu–1.67% Li–0.39% Mg–0.38% Ag was analysed. Two-step schedules were investigated, with varying temperature: 350, 375, 400 and 425 °C and constant time of 10 h for the first step. The second step was constant, 520 °C/24 h. Among the investigated variants, the best results were noted for the first step at 400 °C, for which in grains centres the average particle size was the lowest, whereas the number density and the volume fraction were the highest. Unfortunately, in all cases, in areas close to grain boundaries, a few

Al_3Zr dispersoids were observed, at some distance towards grains centres, low density of dispersoids with relatively large size was noted, and in the grains centres, dense dispersoids were present. In addition, the dispersoids precipitation was found to be non-uniform. One should note that after the first step, the precipitation of the θ′-phase was observed, with precipitate-free zone in grains centres. However, neither the effect of the first stage temperature on this phase precipitation nor its relationship with the dispersoids formation was discussed.

The effect of different two-step homogenisation conditions on the distribution of the α-Al(Mn, Cr)Si dispersoids was shown in the work [10]. Within the first step, the alloy Al–1.03% Mg–0.98% Si–0.44% Cu–0.47% Mn–0.28% Cr was heated at 300 °C/h from ambient temperature to 175, 250 and 300 °C and held for 4, 8, 12, and 24 h (including heating time). After completed first soaking, it was water quenched. Subsequently, the samples were put directly into a furnace at 550 °C, soaked for 10 h and finally water quenched. The results were compared with obtained after one-step homogenisation 550 °C/2–10 h (with the same heating rate). After one-step homogenisation, in areas of grain boundaries and in interdendritic regions, dispersoids-free zones were observed. At the centres of dendritic arms, some larger, sparsely distributed dispersoids were present, and these areas were named CDZ (coarse dispersoid zone). After each two-step homogenisation variant, the fraction area of the CDZ decreased significantly. With the first soaking temperature increases, the CDZ decrease was greater. The effect of soaking time was weaker. The best results were obtained for the first step conditions 300 °C/8 h. The significant improvement in the distribution of α-Al(Mn, Cr)Si dispersoids after two-step homogenisation was attributed to the diffusion of Si and Mg towards depleted areas and, more importantly, to the precipitation of metastable Mg_2Si and Q phases in first step. At higher temperature, during the dissolution of precipitated Mg_2Si or Q-phases, Si atom clusters were released. The α-Al(Mn, Cr)Si dispersoids started to nucleate at the original locations of the dissolved Mg_2Si or Q-phases and took advantage of the Si atom clusters.

2.1.3 Insoluble particles transformation

It is commonly known that the high transformation ratio of the Fe-containing primary particles, from the β-AlFeSi to the α-AlFeSi type, and spheroidisation of the AlFeSi particles are beneficial to the extrudability and surface quality of the extruded products. It is also known that the mentioned transformation is enhanced by the increase of homogenisation soaking temperature and by addition of a small amount of Mn, typically less than 0.03 wt%, to lean Al–Mg–Si alloys. In the 6xxx alloys with low additions content, where dispersoids formation is not an object of interest, the incipient melting is the factor limiting the homogenisation temperature, and the lowered solidus within the inverse segregation zone (ISZ) needs to be taken into consideration. A very interesting research result and practical solution regarding Fe-bearing phases transformation in 6xxx alloys are presented in the work [11]. Thanks to application of the new billet casting technology termed low-pressure casting (LPC), the reduction of ISZ width and decrease of elements concentration within this zone were achieved. This resulted in the significant increase of the solidus temperature of material within mentioned zone, by over 30 °C for 6060 alloy, which in turn enabled application of homogenisation temperature even as high as 600 °C. During soaking at such a high temperature, the high degree of the β-AlFeSi to the α-AlFeSi transformation was obtained for Mn-free alloy. The extrusion trials showed that the lack of Mn in alloy composition and application of the new cooling manner (described in the next section) lead to decrease of extrusion pressure.

Among recent literature data on the considered topic, one may find publications [12, 13], which are not focussed on the selection of homogenisation parameters, but contribute to understanding of the microstructural processes. In the work [12], the β-AlFeSi to the α-Al(FeMn)Si transformation was studied in-situ by TEM for 6005 and 6082 alloys. It was observed that the Mg_2Si particles precipitate in the Al matrix at about 250 °C. This precipitation occurred also at the edges and faces of the β-AlFeSi particles, and the Mg_2Si particles were preferred sites for the α-Al(FeMn)Si phase nucleation. After nucleation, the α-Al(FeMn)Si particles grew and coarsened via two different modes on the expense of the β-AlFeSi.

In the paper [13], the evolution of Fe-bearing particles during direct-chill casting and homogenisation of 6063 alloy industrial billet was investigated. The as-cast microstructure as well as the microstructure after homogenisation 580 °C/5 h were described in details. For example, the different types of the Fe-rich particles and Mg_2Si particles were characterised. In general, the results showed that the initial as-cast microstructure, which is influenced by the solidification conditions, had a strong effect on the final homogenised microstructure, affecting the size, morphology, type, β- to α-phase transformation rate and inter-connectivity of the various phases.

2.1.4 Particles precipitation during cooling

The works of Oddvin Reiso and co-authors, published over 30 years ago, clearly showed that cooling from homogenisation temperature greatly affects the billets extrudability and properties of obtained profiles, solution heat treated on the press. This process stage is still of interest to researchers. In particular, the authors mentioned above published their new results [11]. They found that besides the attention paid on

precipitation of the β-Mg_2Si phase in the form of particles capable for rapid dissolution during subsequent processing, the effect of Mn and Fe in solid solution needs to be considered. These elements also exhibit limited solubility in (Al), decreasing with the temperature lowering. Thus, it may be expected that a slow cooling in the high-temperature regime may allow for some Mn and Fe to go from solid solution to the pre-existing AlFeSi particles. The phase diagrams show that for concentrations present in the 6xxx alloys, the solvi temperatures of Fe and Mn are higher than solvus of the β-Mg_2Si phase, and it is schematically presented in the Fig. 2.

On the basis of this consideration, the new cooling regime from homogenisation temperature, called dual-rate cooling (DRC), was designed. It consists of the slow cooling between the soaking temperature (T1 in the Fig. 2) and the β-Mg_2Si phase solvus temperature (T2), followed by the fast cooling below the latter to avoid formation of coarse β-Mg_2Si particles. The extrusion trials shown that dual-rate cooling cycle has beneficial effect on the extrusion pressure, which can be lowered usually by 2–3%. The decrease may be considered as low, but it is worth to note that in the pursuit of best extrudability, one should take advantage of every opportunity.

As an example of recent works regarding precipitation of β-Mg_2Si particles during billets cooling from homogenisation temperature, one may show paper [14]. The specimens from industrial billet of 6082 alloy were homogenised with soaking at 560 °C for 8 h, followed by cooling at rates over a wide range of 32–120,000 °C/h. The homogenised specimens were examined using multiple techniques. They were also subjected to hot compression test at 500 °C, with water quenching and subsequent artificial ageing (to the T5 temper). On the basis of hardness measurements results of aged material, the cooling rate of 760 °C/h was suggested as suitable for this alloy. Within the work, a new thermodynamic particle-coarsening model was also presented. It may be used for prediction of the evolution of particle size during the cooling process. It presented appropriate agreement with the experimental data, in particular for lower cooling rates.

The process of cooling billets of Al–Mg–Si alloys is often described in the literature, but there is a need for performing similar research on 6xxx alloys containing Cu. In the work [5], a cooling from homogenisation temperature of the Al–0.80% Mg–1.22% Si–1.41% Cu alloy was analysed. Three cooling rates of 50, 300 and 500 °C/h (estimated in the range 545–200 °C) were applied. The ability of precipitated particles to dissolution during rapid heating was evaluated using DSC test: the samples were inserted into the cell with the temperature of 390 °C and heated at 20 °C/min to the temperature of 700 °C in Ar atmosphere (the time of heating to the temperature of 540 °C was about 450 s). As expected, the rising cooling rate contributed to refinement of β-Mg_2Si particles. After cooling from homogenisation at 500 °C/h, the precipitated particles dissolved nearly completely within short time during the DSC test and the fraction of remaining particles was very low, probably negligible in industrial practice. The particles of θ-Al_2Cu phase precipitated during this cooling were also small and capable for fast dissolution. Unexpectedly, even after the fastest examined cooling, in the alloy, microstructure coarse particles of the Q-$Al_5Cu_2Mg_8Si_6$ phase were observed besides fine ones. The presence of coarse particles lowered the solidus temperature, from 573.4 °C noted after water quenching to about 545 °C. The

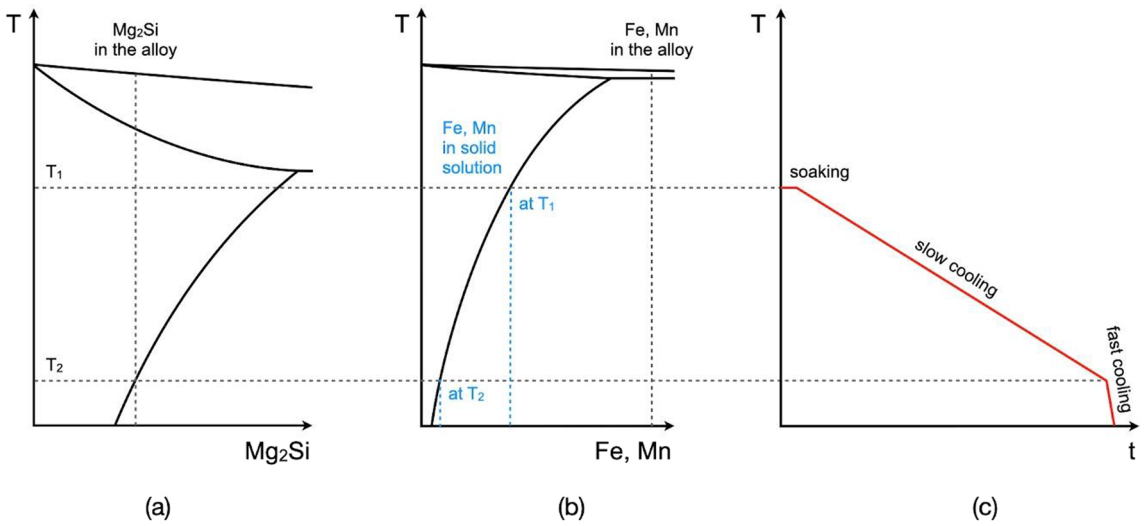

Fig. 2 Schemes of binary diagrams Al–Mg_2Si (**a**) and Al–Fe or Mn (**b**), as well as scheme of cooling cycle for an arbitrary Al–Mg–Si alloy (**c**). The temperature T1 illustrates homogenisation soaking temperature of the alloy, whereas the temperature T2 illustrates a temperature for the onset of fast cooling within the DRC cycle [own source]

very small incipient melting heat indicated that the amount of undissolved Q-$Al_5Cu_2Mg_8Si_6$ particles at the temperature of about 545 °C was very small. It was suggested that in industrial process, where billets heating rate will probably be lower and the plastic deformation during extrusion will facilitate diffusion, these particles will be fully dissolved. Nevertheless, this supposition needs to be verified during extrusion trials and the obtained results show that conditions of billets preheating and extrusion for the examined alloy need to be selected carefully.

The cooling rate after homogenisation soaking needs to be controlled not only in the case of alloys solution heat treated on the press. As it was shown above, among properties influenced by this homogenisation stage is the solidus temperature of the material. In the mentioned earlier work [4], describing homogenisation of 7xxx alloys billets intended for extrusion welding, the effect of cooling from homogenisation temperature was also investigated. It was found that the recommended cooling manner is strongly dependent on the alloy composition. In particular, the lean 7075 alloy (No. 1 in Table 1) can be cooled very slowly, at 60 °C/h, without influencing the solidus temperature. For 7049 alloy (No. 4 in Table 1), the application of a moderate cooling rate from homogenisation temperature, about 120 °C/h, is sufficient. In the case of high-Cu 7075 alloy (No. 2 in Table 1), despite the fast cooling at 500 °C/h, the decrease of solidus temperature was observed (in comparison with water quenching). In order to restore the high solidus temperature noted at the end of soaking stage, the dissolution of the S phase causing this effect must be ensured during careful billets preheating prior to extrusion.

2.2 Magnesium alloys

More than 10,000 papers have been published in the last decade on the topic of Mg extrusion alloys, with the number of papers in 2016 being twice as many as that in 2007 [15]. Therefore, it is difficult to describe exactly recent progress in the magnesium alloys extrusion. Magnesium alloys have a hexagonal lattice structure, which affects fundamental properties of these alloys. Plastic deformation of hexagonal lattice is more complicated than that of cubic-latticed metals. Therefore, magnesium alloys was traditionally used as-cast alloys, but plastic deformation of many alloys is also realised with success especially in the last 2 decades. Wrought magnesium alloys contain aluminium, zinc, manganese and copper. These additions improve strength properties of magnesium alloys. Recently, rare-earth elements, such as La, Y, Nd, Ce, Dy as well as zirconium are added to magnesium alloys which are submitted to plastic deformation to form precipitates that lead to improvements in mechanical properties and creep resistance. Magnesium and its alloys offer a remarkable potential in the transport industries since the low density of magnesium 1.74 g/cm^3 makes its alloys the lightest available constructional metals. Magnesium wrought alloy yield stress is between 160 and 240 MPa, whereas tensile strength is of 180–440 MPa and elongation of 7–40%. It is worth noting that the commercial Mg extrusion alloys have a significant tension–compression yield asymmetry. The yield stress in compression is about 0.4–0.8 of that in tension, which is not observed for Al extrusion alloys. Most common wrought alloys contain mostly Al and Zn.

2.2.1 Mg–Al alloys

Mg–Al alloys are the most widely used alloys of moderate strengths, a relatively high plasticity and a reasonably good corrosion resistance from the all Mg alloys. Among them, AZ, AM, and AE alloys are of high plasticity. For example, AZ31 and AZ61 alloys have elongations higher than 15%. The content of the Al element is less than 10 wt%. The as-cast magnesium alloy consists of $\alpha(Mg) + \beta(Mg_{17}Al_{12})$ phases. The amount of them increases with increasing the content of Al. Microalloying elements, such as Ca, Ti, Bi, Sb, Sn, Sr and rare-earth (RE) elements can change the morphology of β-$Mg_{17}Al_{12}$ phase. Microalloying also leads to the refinement of α-Mg grains and results in the improvement of mechanical properties [16]. In magnesium alloys that contain more than two alloying elements, very stable intermetallic phases are formed that cannot be influenced by additional heat treatment. The toughness and ductility of the AZ series is moderate. For this reason, magnesium alloys with reduced aluminium content were developed, namely AM60 and AM50, and they display improved toughness and ductility due to a reduction of $Mg_{17}Al_{12}$ intermetallic particles.

Mg–Al–Mn (AM) alloys such as AM20, AM5, and AM60 have elongations of 20%, 15%, and 14%, respectively. The brittle β-Mn phase appears as the Mn content is enhanced to more than 1 wt% [16]. The Mg–Al alloys can contain rare-earth elements leading to Al–RE binary phases, such as $Al_{11}RE_3$, with high melting points, resulting in decreased $Mg_{17}Al_{12}$ phase.

Extrusion of tubes from the AZ31 magnesium alloys was performed using porthole die [17]. Extrusion speed had a negative influence on the seam weld quality. The optimum extrusion speed was about 0.5 mm/s for the extrusion of AZ31 magnesium alloy tube at the billet temperature of 400 °C on the 800 T extrusion press.

In the study [18], the extrusion of hollow profiles from AZ31 alloy was investigated and the extrusion trials were conducted in order to show the feasibility of producing magnesium hollow profiles with axially variable wall thickness.

2.2.2 Mg–Zn alloys

Mg–Zn alloys are the most typical Mg alloys subjected to precipitation hardening [19]. When Zn content is low, the alloys exhibit very good extrudability. At the content of about 6 wt% of Zn, the alloys exhibit ageing strengthening effect. After ageing and following extrusion of the MgSnZnMn alloy at 300 °C, the yield stress was of 256.5 MPa, and UTS was of 324.5 MPa [20]. In addition, an alloy with lower Zn content demonstrates better corrosion resistance than an alloy with higher Zn content. When the Zn content exceeds the solid solubility limit, the corrosion performance is greatly reduced. These alloys typically consist of a α-Mg matrix and intermetallic β-$Mg_{17}Al_{12}$ phase, distributed along the α grain boundaries. This phase increases the corrosion resistance of the magnesium alloy [20]. The Mg–Zn alloys are rarely used due to the wide crystallisation temperature range, easy to produce micropores, susceptibility to hot tearing. Therefore, the alloying elements, such as Zr, Mn, Cu and REE, are added to the Mg–Zn binary alloys to improve their structure and properties. The addition of Zr and Mn affects positively an alloy microstructure. Manganese is used also to improve formability.

2.2.3 Mg alloys + REE (WE series)

The addition of rare-earth elements improves magnesium alloy properties. For example, cerium enhances deformability at room temperature, the addition of neodymium decreases the corrosion rate, and yttrium improves the ultimate tensile strength and elongation of magnesium alloys. The REE in Mg–Al–RE alloys involves strengthening effect originating from Al and RE elements' reaction of low melting point and the rearrangement of the second phases [21, 22]. WE series alloys possess excellent mechanical properties at room temperature when compared to other magnesium alloys, and they retain their properties at high temperatures. The dissolving of RE atoms in the Mg matrix, which hinders the dislocation motions and the diffusion of atoms, leads to the pinning of grain boundaries and dislocations, and results in the enhancement of strength. The neodymium, yttrium, cerium, improve the corrosion behaviour of magnesium alloys. WE series alloys are more creep resistant than other magnesium alloys, and display superior ductility, strength, and corrosion resistance [23].

The study conducted on the as-cast Mg–2Y–1Zn–0.6Zr alloy showed that the tensile strength, yield strength and elongation of the as-cast alloy [24] were 245 MPa, 135 MPa and 14.4%, respectively. After hot extrusion, the tensile strength, yield strength and elongation reached 327 MPa, 322 MPa and 24.9%, respectively, but they were slightly different at different extrusion temperatures. The reason for the significant improvement of material properties is mainly due to the dynamic recrystallisation during thermal processing, which produces fine grains of as-cast alloy. Moreover, the second phase broken during the extrusion process hinders grain boundary migration and refines grains. The extruded $MgZn_{14}Y_3$ alloy reviled the UTS of about 420 MPa [15].

2.2.4 Mg–Li alloys

The new Mg–Li alloys demonstrate very attractive properties which enable producing different components for automotive, aerospace and other industries. The advantage of Mg–Li-based alloys is their ultralight weight, and their density is of about 1.4 g/cm^3. Lithium is the lightest metal, whose density is only 0.533 g/cm^3. In addition, Li has significant solubility in Mg. The maximum solubility of Li in Mg is 5.5 wt% at the eutectic temperature of 588 °C, and it almost does not decrease with the decrease in temperature. With the concentration of Li between 5.5 and 11 wt%, the alloy is composed of an α-Mg (hcp) phase and a β-Li phase (bcc). When the concentration of Li is more than ~ 11 wt%, the alloy is composed of single β-Li phase. The high concentration of Li leads to a decrease in alloy density to 1.4–1.5 g/cm^3. The interesting features of these alloys are as follows: good casting properties, good weldability and machinability. The addition of lithium increases corrosion resistance of magnesium alloys, particularly above 12 wt% contents of Li [25].

In order to enhance the strength of Mg–Li extrusion alloys, Zn and Al are commonly added to Mg–Li alloys. The main intermetallic compounds in these alloys are $MgLi_2Al$, $MgLi_2Zn$, AlLi and MgLiZn. To further enhance the strength of these alloys, REE elements are also often added to form some second-phase particles during casting and strengthening precipitates in hot extrusion. The extrusion of the profiles involves billet homogenisation, hot extrusion, solution and quenching treatments, artificial ageing, and others. The article [26] summarises the main applications and key mechanical properties of Al–Li alloy extrusion profiles. The studies related to evolutions of the microstructure and mechanical properties during homogenisation and extrusion processes are also reviewed.

In the work [27], the finite-element simulation model of porthole die extrusion of LZ91 Mg–Li alloy was established. The effects of extrusion ratio on strain, temperature and flow velocity were studied, and the welding quality was quantitatively evaluated. With the increase of extrusion ratio, the welding quality was improved.

Magnesium alloys can be effectively submitted to plastic deformation including hydrostatic extrusion and hot extrusion to produce complex profiles [28]. Typical extrusion parameters and properties for magnesium alloys are presented in Table 2 [15].

Table 2 Extrusion parameters and strength properties of some magnesium alloys

Alloy	Temperature, °C	Exit speed, m/min	Complicated hollow profiles	UTS, MPa
Mg	320–380	15–25	Yes	185
MgMn2	320–380	15–25	Yes	255
MgAl3Zn	320–380	8–15	Yes	260
MgAl6Zn	320–380	2–4	Yes	310
MgAl8Zn	320–380	1–2	No	380
MgZn3 Zr	320–380	3–5	Yes	260

For the difficult-to-extrude Mg alloys, such as Mg6Al1Zn0.3Mn (AZ61) and Mg6ZnZr (ZK60), or for the complicated profiles, the extrusion speed decreases by a factor of 10 or more. Therefore, the realisation of Mg alloy extrusions to-date has been accompanied by significantly lower production rates and lower cost-effectiveness of extruded products compared to Al-alloy extrusions.

2.3 Aluminium-based composites

Composites are a significant group among engineering materials and many reliable products are increasingly manufactured from them. Due to the specificity of their unique structure, which results in unique properties, they exhibit a number of features unattainable by metallic materials, ceramics or plastics [29]. Among various composites based on metals, plastics or ceramics, aluminium-based composites are gaining more and more applications due to their advantages, mainly in the automotive, aviation and space industries, power engineering and construction.

Aluminium-based composites can be divided into the following groups:

- Al composites with reinforcing particles
- Al alloy composites with reinforcing particles
- Al composites or Al alloy with nanoscale reinforcement

The group of Al composites with reinforcing particles distinguishes composites consisting of an aluminium matrix and a reinforcing additive, i.e. hard particles, which most often include ceramics. Such composites may contain one type or several types of reinforcing particles necessary to achieve specific properties of the composite. Among the known reinforcing particles used in this type of composites, the most common are oxides, carbides and nitrides, such as Al_2O_3, ZrO_2, SiC, TiC, AlN, and Si_3N_4.

The second group are composites consisting of Al alloy with particles reinforcing the matrix, which is mainly made of alloys that are susceptible to heat treatment, e.g. the 2xxx, 6xxx or 7xxx series. Similar to the previous group, the reinforcing particles used are most often oxides, carbides and nitrides.

In the last group of composites, which is Al or Al alloy with nanoscale reinforcement, the composite matrix is aluminium or an aluminium alloy, and the reinforcement is obtained by the addition of various nano-particles (0D), nano-fibres (1D) or nano-sheets (2D). Most often, these are nano-particles of various elements, nano-fibres such as SiC or graphene nano-sheets.

The manufacturing process of aluminium-based composites can be carried out using various technologies; however, in practice, casting processes are the most common. The obtained aluminium-based composites must be further processed in order to obtain specific products (elements of machine and equipment parts) that meet specific requirements [30, 31].

Among techniques of composites manufacturing, the following can be distinguished: casting, powder metallurgy, pressing, forging, extrusion, machine cutting and quite recently additive techniques such as 3D printing [32].

In the presented review works on aluminium-based composites [30–32], in addition to their manufacturing techniques, the importance of micro- and nano-particles in achieving the specified properties of the composites is shown. In recent years, we have observed numerous works on aluminium-based composites with increasingly different reinforcing particles, obtained using the hot extrusion technique. Among these works, noteworthy are the studies of composites based on the 6005A alloy with the addition of TiC [33], composites reinforced with glass fibre [34] and composites reinforced with mechanically ground Mg_2Si particles [35]. Interesting results were presented in work [36], which analysed the microstructure and mechanical properties of composites based on 6061 aluminium alloy reinforced with multi-walled carbon nanotubes. Also using alloy 6061 as the matrix of the composite, the authors of work [37] examined the influence of Si_3N_4 on the microstructure, mechanical properties and anisotropy of the composite, finding that the addition of Si_3N_4 contributes significantly to reducing the anisotropy of the material. Another interesting work that investigated the influence of TiB_2 particles and the local shape ratio on the microstructure and mechanical properties of a hot-extruded composite based on the 6061 alloy is the study [38]. The authors of this study found that

the central part of the extruded profile contains more TiB_2 particles than the peripheral parts, which is probably related to the variations in flow of the extruded composite. Among the recently published works, noteworthy are work [39] in which the authors analyse the possibility of using reduced graphene oxide to produce ultra-conductive aluminium composites, and work [40] devoted to the possibility of strengthening aluminium with nanodiamond particles.

Taking into account the limitations associated with the manufacturing processes of aluminium-based composite products within the known production and processing techniques, it is justified to use extrusion technology in the production of aluminium-based composite products.

The input in aluminium-based composite extrusion technologies may include:

- ingots cast from aluminium-based composites
- powder mixtures of aluminium-based composites
- compressed powder mixtures made of aluminium-based composites

Cast ingots from aluminium-based composites and compressed powder mixtures made of aluminium-based composites can be directly extruded both cold and hot into profiles with specific cross-sections. Regarding powder mixtures of aluminium-based composites, extrusion of profiles can be carried out using cartridges filled with the composite powder mixture, or by filling the container directly with the composite powder mixture.

General technological schemes that can be used in practice for the production of composite products, including the extrusion of aluminium-based composites, are presented in work [41].

Analysing literature reports [42], it can be concluded that aluminium-based composites are most often extruded into open shapes of various cross-sections, usually circular cross-sections in the form of rods. There are known cases of extrusion of closed shapes (e.g. tubes) made of aluminium-based composites, however, it involves technology based on extruding ingots with a hole, or extruding ingots with their preliminary piercing, using double-acting presses.

The commonly used technology of extruding closed profiles from aluminium alloys through porthole extrusion dies has not yet been used in the production of closed profiles made of aluminium-based composites due to the difficulties in welding streams of composite material during welding extrusion, as well as the relatively high unit pressures needed to carry out the extrusion process.

Considering the advantages of welding extrusion of closed profiles from aluminium alloys, an attempt was made to adapt this extrusion technique to the production of closed profiles from aluminium-based composites. The test materials were aluminium-based composites containing hard reinforcing particles in the form of SiC and Al_2O_3. The composite matrix was aluminium or 6061 aluminium alloy. The input for the welding extrusion process using porthole extrusion dies were powder mixtures of AlSiC, $AlAl_2O_3$, 6061SiC, and $6061Al_2O_3$.

The selection of the structure of porthole extrusion dies for the production of profiles in the form of pipes from the tested aluminium-based composites was preceded by FEM analysis. As part of the FEM analysis, the compaction of the composite mixture in the container was monitored for three porthole extrusion dies designs—die No. 1 (V1): 2 seam welds are a single-back design with a wedge-shaped back; die No. 2 (V2): 4 seam welds is a four-spine construction in the form of a cone; die No. 3 (V3): 4 seam welds is a four-spine structure in the form of a truncated cone. Figure 3 shows exemplary phases of compaction of the mixture in the container for the optimised matrix

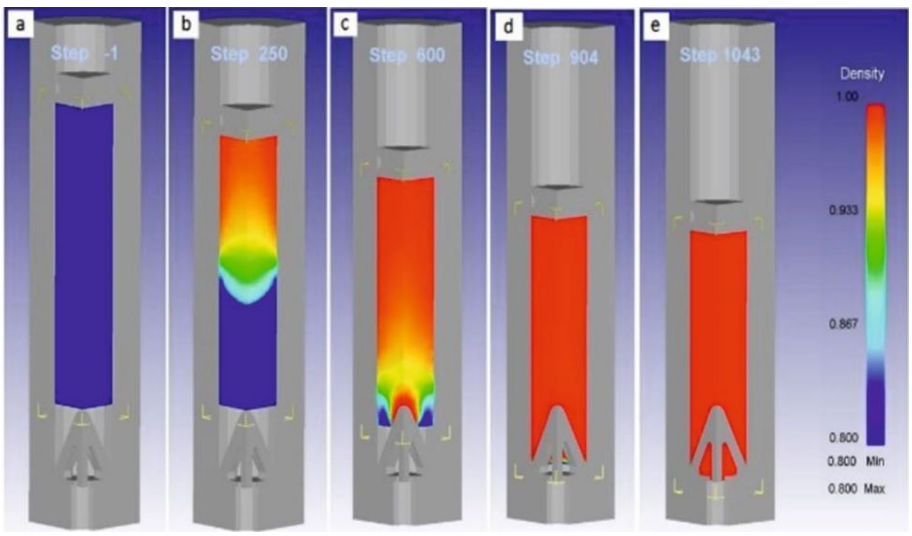

Fig. 3 Phases of compaction of the composite mixture in the container. **a** 0% change in height of the batch (initial state), **b** 7.5% change height of the batch, **c** 15% change height of the batch, **d** 22.5% change height of the batch, **e** 30% change height of the batch [own source]

design (V2). Analysing the individual compaction phases a–e (Fig. 3), it can be concluded that in order to achieve full thickening of the mixture, it is necessary to reduce approximately 1/3 of the height of the batch. The distribution of effective strain during extrusion process of the composite mixture through various dies is shown in Fig. 4. In semi-industrial tests, composite mixtures were hot extruded through a four-ridge porthole extrusion die (V2) to obtain tubes with dimensions of 25 × 2 mm. Figure 5 shows the relation between the tensile strength of welds for the tested aluminium-based composites and their location at the cross-section of the extruded tube. The tensile strength of the welds was determined on ring samples cut from composite pipes after extrusion process.

Based on semi-industrial tests, a basic technological scheme was designed for obtaining profiles from aluminium-based composites extruded using porthole extrusion dies. In order to exploit the maximum potential of the mechanical properties of the tested aluminium-based composites, the hot-extruded composites were further subjected to strain hardening by cold upsetting with deformation of up to 80%. Figure 6 shows how the hardness of the strain-hardened aluminium-based composites tested changes depending on the applied strain. It is worth emphasising that even 80% of cold deformation applied to the tested composites did not lead to cracking, which proves their very high susceptibility to plastic deformation. Based on these studies, a technology for the production of thin-walled drawn composite pipes based on aluminium with high mechanical properties was developed. The verified use of porthole extrusion dies in the technology of extruding aluminium-based composites creates new possibilities for manufacturing products with various shapes and properties.

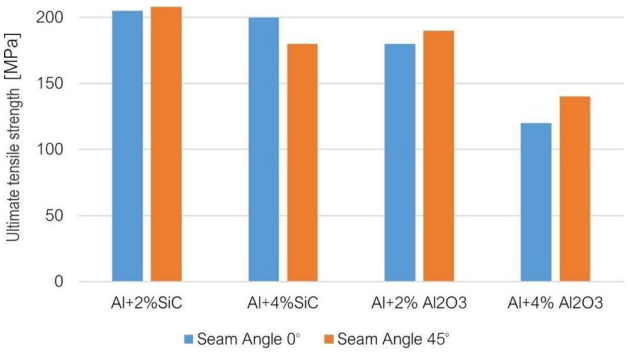

Fig. 5 Ultimate tensile strength of welds depending on their location [own source]

3 Extrusion tools

3.1 Innovative design solutions of extrusion dies for aluminium alloys

Contemporary applications for extruded aluminium alloy profiles, such as modern construction, the automotive industry, including battery housings for electric cars and the transport of vans and trucks, or aeronautics, require the hot-extruded product to have an increasingly complex cross-sectional shape (hollow sections with complex shapes), to be increasingly lighter (thin-walled), to have higher quality characteristics (high tensile strength, close dimensional tolerances, low roughness and high surface class) and to be manufactured with more and more advanced and economically acceptable process parameters.

In addition to maximising the strength properties of the product, which is the domain of material/alloy type, all the above aspects depend on the design of the die. The design of the die for the extrusion of metals and alloys affects the process parameters such as: extrusion force and the maximum

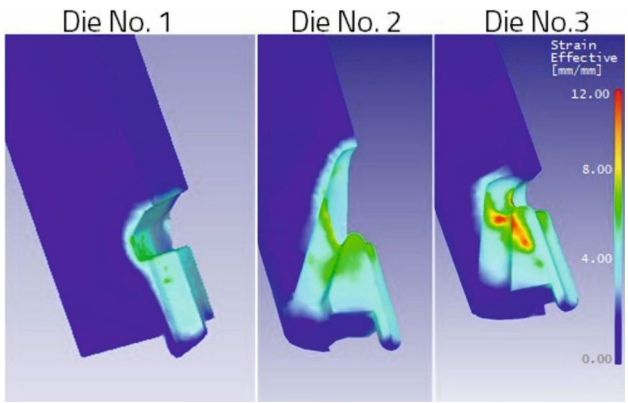

Fig. 4 Distribution of effective strain during extrusion of the composite mixture through various dies [own source]

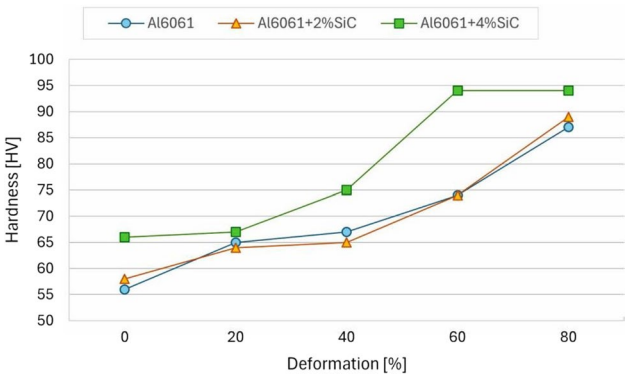

Fig. 6 Hardness of strain-hardened 6061 + SiC composites [own source]

allowable metal exit velocity (production process efficiency), as well as the die life, the amount of production scrap yield and, in the broadest sense, the quality of the product.

Porthole dies are commonly used to extrude hollow (closed) aluminium alloy sections with complex shapes and high dimensional accuracy. The design of porthole dies is a difficult process, as both the type of material to be extruded and the shape and size of the cross-section of the extruded profile must be taken into account. This information, together with the size of the extrusion press available and the diameter of the container, makes the question of whether to use single or multi-hole dies important in practice. The primary design criteria are: minimisation of high metal flow resistance, translated into lower extrusion force and higher metal exit velocity, minimisation of die elastic deflection, translated into lower risk of product dimensional inaccuracy and rapid tool wear, adjustment of metal flow during extrusion, translated into geometric shape stability and tight dimensional tolerances, improvement of the stress state in the die clearance, resulting in reduced unfavourable tensile stresses that promote tarnishing and surface cracking of the product, and maximising the strain intensity and normal compressive stresses in the welding chambers, resulting in higher quality longitudinal welds in the product. The correct choice of: the number and arrangement of the working holes in the die insert, the geometry of the die inlet channels, the geometry of the bridges (length and thickness) and mandrels and the geometry of the welding chambers (height), the pre-chambers for pre-forming the extruded material and the die clearance (length of the calibration strips) is crucial.

In the case of the extrusion of easily deformable and easily weldable aluminium alloys of the 6xxx series (AlMgSi), the design of the porthole die does not pose any major problems, even for profiles with a wall thickness of 1 mm and less. In most cases, the efforts of engineers and scientists are mainly focussed on adjusting the metal flow during extrusion by appropriate geometry of the porthole die, with the aim of improving the dimensional accuracy of complex and thin-walled profiles, or improving the surface quality of the extruded product, mainly by minimising streaking lines.

The influence of the die design and extrusion speed on the change of the wall thickness 1.25 mm of the oval profile from 6082 alloys was investigated by Borowski et al. [43]. The dimensional changes result from the complexity of the die orifice and also from the die deflection during extrusion. The original 4-hole porthole die with 2-step shaped pockets was designed and applied in industrial conditions ensuring the high metal exit speed of about 14 m/min, small dimensional deviations and good surface quality. In the study [44], the mandrel fracture behaviour through investigating elastic deformation of mandrel during the extrusion using FE analysis was examined. After optimisation with the use of HyperXtrude 13.0 software, the desired die geometry giving proper material flow at the die exit and small mandrel deflection were obtained. Xue et al. [45] applied a circular pattern of the portholes with a dart-shape inlet bridge, a buckle angle in the inlet side of the upper die, a two-step welding chamber, and a non-uniform bearing length distribution get a balanced metal flow. Work [46] reported that to obtain an uniformity of metal flow velocity at the die exit, the porthole die structure was optimised by adding baffle plates on the die insert. After optimisation, the concave defects on the extrudate were remarkably limited. Raknes et al. [47] have shown an alternative approach for reducing dimensional variations in the extruded profile by applying two mechanical calibration strategies. The first calibration strategy is based on global, longitudinal stretching in combination with local bending, while the second strategy utilises the principle of transversal stretching and local bending of the cross-section. The results for the 6082 alloy showed that both calibration strategies have proven to reduce cross-sectional variations effectively. In the work [48], the porthole die used for extrusion of a solid heatsink profile with high wall thickness variation ratio was designed using finite-element (FE) simulations. The effects of the port bridge structure, welding chamber height and the bearing length adjustment on the behaviour of the metal flow in the die were investigated. The experiment results showed that the extruded product fulfilled the requirements for dimensional tolerances. The design approach can be useful for practical implementation of die design when extruding profiles with large wall thickness variation. The paper [49] analysed porthole die extrusion processes of 7003 alloy through 3D FE simulation in the non-steady state during the entire process for following process variables: initial billet temperature, bearing length, tube thickness, and extrusion ratio. The surface state of extruded products was also examined.

The objective of study performed by Mahmoodkhani [50] was to evaluate factors contributing to the formation of PCG layers in extruded medium-strength Al–Mg–Si alloys, particularly the die bearing geometry. Optical microscopy and electron back-scattered scanning diffraction (EBSD) were used to quantify the microstructure and crystallographic texture of the extrudates. A finite-element (FE) mathematical model using the commercial software package DEFORM 2D was also developed to simulate the extrusion process to predict the loads, temperatures, and material flow patterns. The results indicate that the major factor affecting the formation of the PCG layer in AlMgSi extrudates is the local stored energy of the near surface material dependent on extrusion bearing die geometry. In turn, Zhu [51] concludes that inhomogeneous distribution of surface imperfections is a key factor for producing the surface defects on aluminium extrudates like streaking lines. He found that the surface imperfections consisting of etching pits, grain boundary grooves, grain etching steps and surface defect remains are

created in the extrudates surface during extrusion and etching processes. He analysed the effect of billet quality, extrusion process, die design and etching process on the presence of extrudates streaking lines.

A considerable number of studies are concerned with determining the effect of the porthole die geometry on the homogeneity of the structure and mechanical properties in the cross-section of the extruded product, taking into account the quality of the longitudinal and transverse welds.

Yu [52] proposed bonding criterion for hollow sections from aluminium alloys related to stress triaxiality, effective strain rate, temperature and contact time based on the plastic deformation and diffusion mechanisms for closure behaviours of micro voids on contact interfaces. It was also found that the formation of a macro-hole in the profile extruded with a shallow welding chamber is attributed to metal flow behaviour, and does not relate to solid-state bonding process. In the work [53], an algorithm for the analysis of the seam welds during the extrusion of hollow profiles from aluminium alloys has been integrated in the FE-code PF-Extrude what allows an accurate prediction of their location. Different criteria have been implemented in FEA of extrusion processes in order to quantify the quality of the seam welds in extruded profiles—Plata and Piwnik, Donati and Yu welding criterions. Kniazkin in his work [54] presents an analysis of different quality criteria of longitudinal seam welds that appear in aluminium profiles during extrusion using porthole dies. A new welding quality criterion that takes into account the unbalances of metal flow was proposed. The proposed criterion has been approved by industrial experiments for different types of profiles and particularly its numerical critical value has been found for AA 6082 alloy. In the work [55], the authors showed that increasing the lower bridge angle led to slightly higher extrusion loads and higher extrudate exit temperatures. Moreover, a dead metal zone formed under the bridge that produced higher strains near the surface of the material.

Some focus on optimising the geometry of the porthole die in order to maximise the metal exit velocity, and thus the efficiency of the extrusion process for high-component aluminium alloys of the 6xxx series.

Robbins, in his work [56], determined the effect of both the extrusion process parameters of 6xxx series aluminium alloys such using AA6063 as an example, and the die design on the extrusion process performance of thin-walled (1.6 mm) closed square sections. It was found that through die design, the efficiency of the extrusion process observed through punch travel speed can be increased from 11.7 to 17.6 mm/s. In particular, thin bridges and the opening of the inlet channels of the porthole die can increase the metal exit speed. Valberg [57], meanwhile, studied the effect of inlet channel size on the extrusion process parameters of selected 6xxx series aluminium alloys, particularly the metal flow velocity for ingots of varying lengths. The effect of porthole die inlet channel size on the extrusion speed of profiles through bridge dies was demonstrated—indicating that larger inlet channels allow an increase in the maximum punch displacement speed from 4 to 6 mm/s with an analogous value of extrusion force. Donati [58] studied the effect of porthole die design on the way metal flows during extrusion of closed profiles with varying wall thicknesses in the range of 2.3–4.8 mm in AA6082 alloy. The effects of the size of the inflow channels, varying the height of the welding chamber, the geometry of the pre-chamber and the bearing length on the value of the metal temperature during extrusion characterising the metal flow velocity were analysed. It was found that large channels and maximisation of the metal inflow volume through the use of wide pre-chambers and short bearings resulted in an increase in the metal flow velocity determined by the punch speed from 2 to 7 mm/s. It was also found that for AA6082 alloy, a higher surface quality of the extruded product is observed on dies with large inflow channels with pre-chambers. Lu [59], on the other hand, analysed the effect of die design and, in particular, bearing geometry on the process parameters of extruding 6xxx series aluminium alloys. He found that increasing the bearing length had a positive effect on the quality of longitudinal welds in the extruded profiles, while they had a simultaneous effect on reducing the metal exit speed. In his paper [60], Madura proposed an innovative porthole die for the extrusion of hollow EN AW-6005A alloy profiles with reduced wall thickness. The original design of the feeder, the maximum opening of the inlet channels and the reduction of the body surface area were used (Fig. 7).

Using a feeder (spreader) to distribute the ingot and reducing the thickness of the mandrels and bridges, the die allowed a significant reduction in surface pressure by 30 MPa compared to the current design—down to a level of 320 MPa. This translated into a reduction in mandrel deflection by 0.09–0.17 mm, particularly in the input area to a value of 0.51 mm and in the calibration area to a value of 0.44–0.50 mm (Fig. 8).

The new die design, through the use of a feeder (spreader) to distribute the ingot, a 60% increase in the area of the inlet channels and a reduction in the surface area of the body, ensured the minimisation of the stress values in the cross-section of the ingot at the entrance to the inlet channels. As a result, there was both a reduction in the stress value on the body surface by 20 MPa to a value of 340–360 MPa and a significant reduction in the entire pressure area, which reduced the value of the maximum force by almost 40% (Fig. 9).

The design which is developed has provided a reduction of the stress value in the inlet channels with respect to the standard die in corresponding areas by an average of 25 MPa in the range of 290–325 MPa, with a parallel increase in the

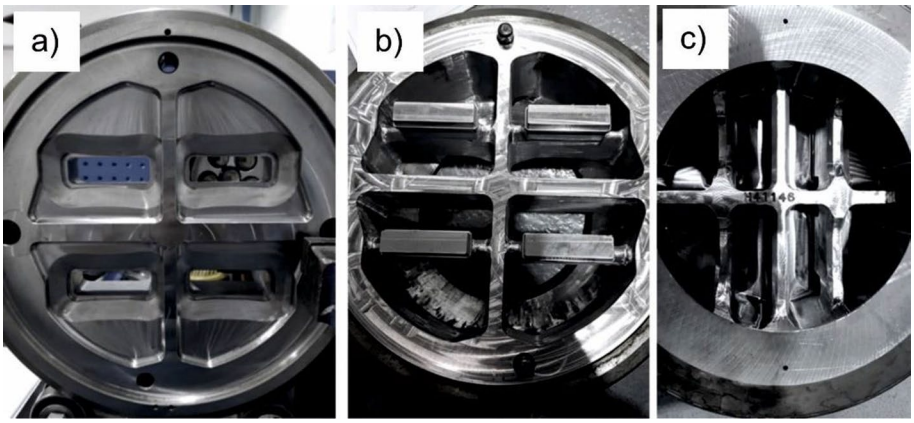

Fig. 7 Photographic documentation of an innovative porthole die for the extrusion of a hollow EN AW-6005A alloy profile [own source]: **a** die insert, **b** bridge section, **c** die assembly

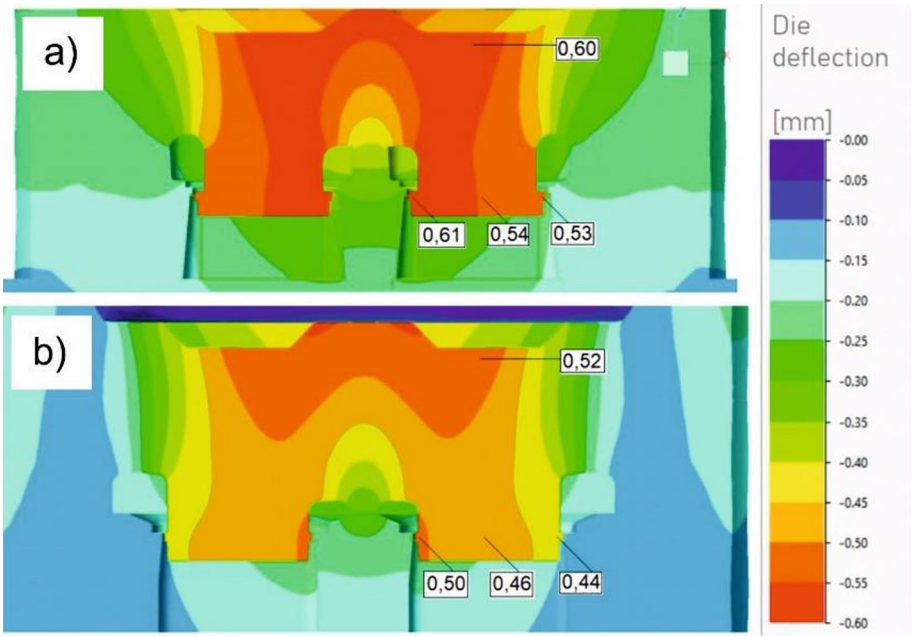

Fig. 8 Deflection distribution of porthole die for extrusion of a hollow EN AW-6005A alloy profile (in extrusion direction in perpendicular section) [own source]: **a** standard die, **b** new innovative die

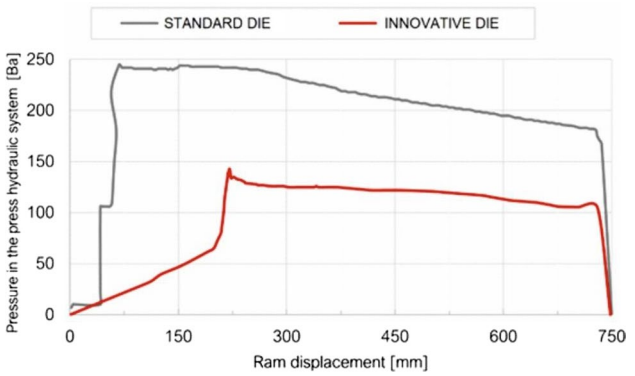

Fig. 9 Graph of the pressure variation in the press hydraulic system as a function of the punch displacement during the extrusion of a hollow EN AW-6005A alloy profile through a standard porthole die (grey line) and the innovative die design (red line) [own source]

metal flow velocity in the central inlet channels by 6 mm/s to a value in the range of 18–25 mm/s. Corresponding velocity and stress distributions in the area of the welding chamber confirm the tendency of the metal velocity in this case to increase by 30% relative to the standard die up to a value of almost 80 mm/s with a parallel reduction in stress values in the range of 5 to even 40 MPa in the area above the die clearance. The new die design provided an increase in metal flow velocity over the entire range of the tool, from the inlet channel entry area as far as to the welding chamber (Fig. 10).

The results of quality tests carried out on sections extruded at maximum velocity using the novel porthole die design showed that they met the quality requirements for mechanical properties in accordance with the PN-EN 755-2 standard [61] and the requirements for dimensional

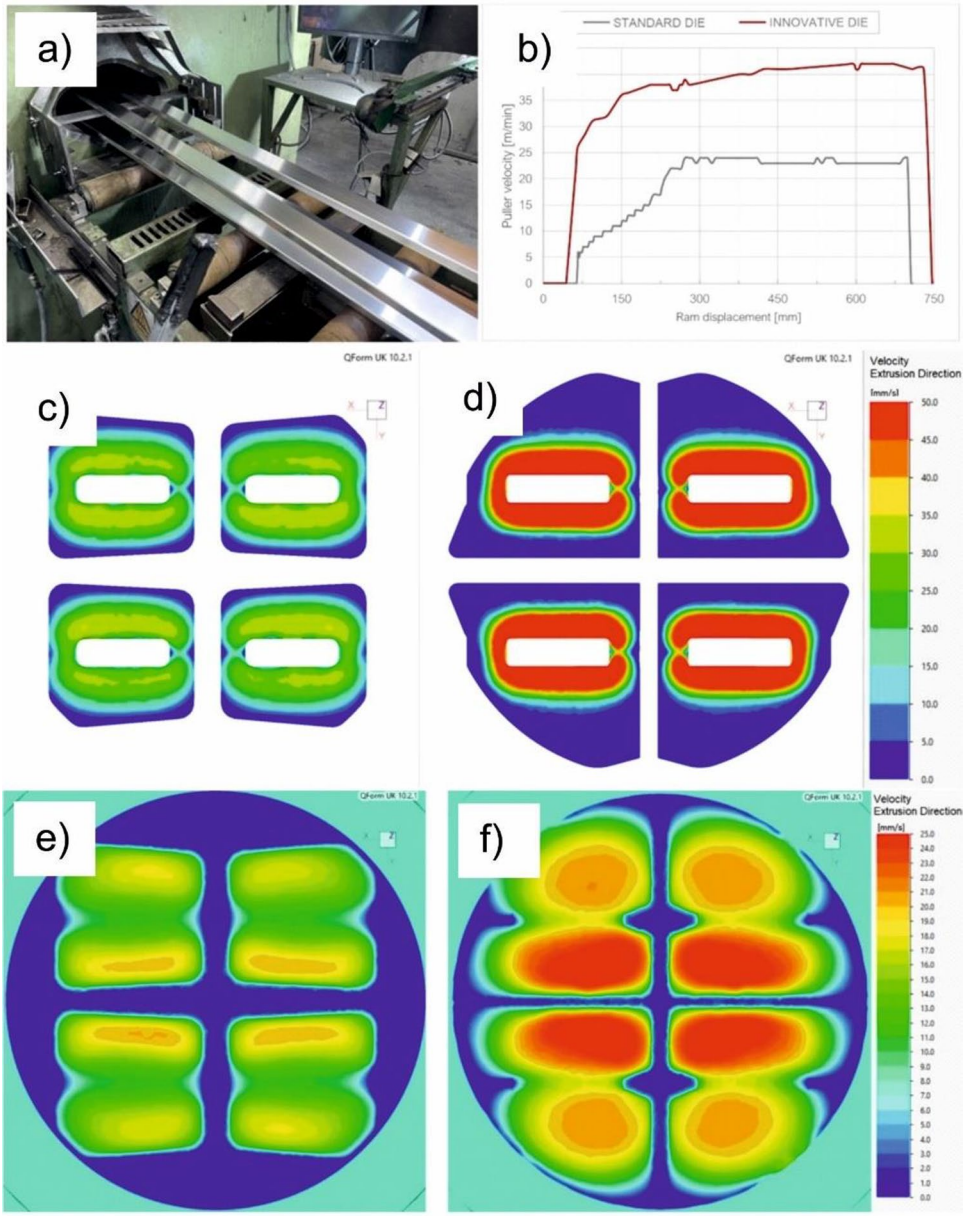

Fig. 10 Photograph of hollow EN AW-6005A alloy sections extruded by the innovative porthole die (**a**) and comparison of the metal flow velocities from the die for dies of different geometries (**b**) and the distribution of metal flow velocities in the cross-section of the die with filled inlet channels at the level of the top of the welding chamber (**c**, **d**) and at the entrance to the inlet channels (**e**, **f**) during the extrusion process by the standard die (left) and the innovative die design (right) [own source]

accuracy in accordance with PN-EN 755-9 [62]. The new die design, by ensuring uniform metal inflow through the entire die opening, eliminated geometry defects in the form of non-parallelism of the longer walls. The dimensional accuracy of the tool itself was also measured to determine any deformation of the die during the manufacturing cycle. A digital model of the new die was created using the 3D optical scanning method, and the die was rescanned after a 3.000 kg production cycle to identify potential deviations that might indicate tool deformation. It was found that no changes were observed in either the bridging part or the die insert, and the highest deviation values were in the range of − 0.02–0.04 mm, indicating high geometric stability of the die and promising a long service life (Fig. 11).

It is much more difficult to design porthole dies for the extrusion of hard-to-deform aluminium alloys of the 2xxx or 7xxx series, where there are significant frictional resistance and significant thermo-mechanical stresses on the extrusion dies, leading to major tooling problems. Here the minimum wall thickness of extruded sections is 2–3 mm at best. In this area, the key is to minimise the elastic deflection of the die, which translates into improved product dimensional tolerances and die strength/life, and to provide lower frictional resistance during extrusion, which translates into improved speed conditions (manufacturing process efficiency).

Hsu [63] analysed different welding chamber shape and bearing geometry while extruding non-symmetric hollow section from high-strength 7075 alloy. He stated that the

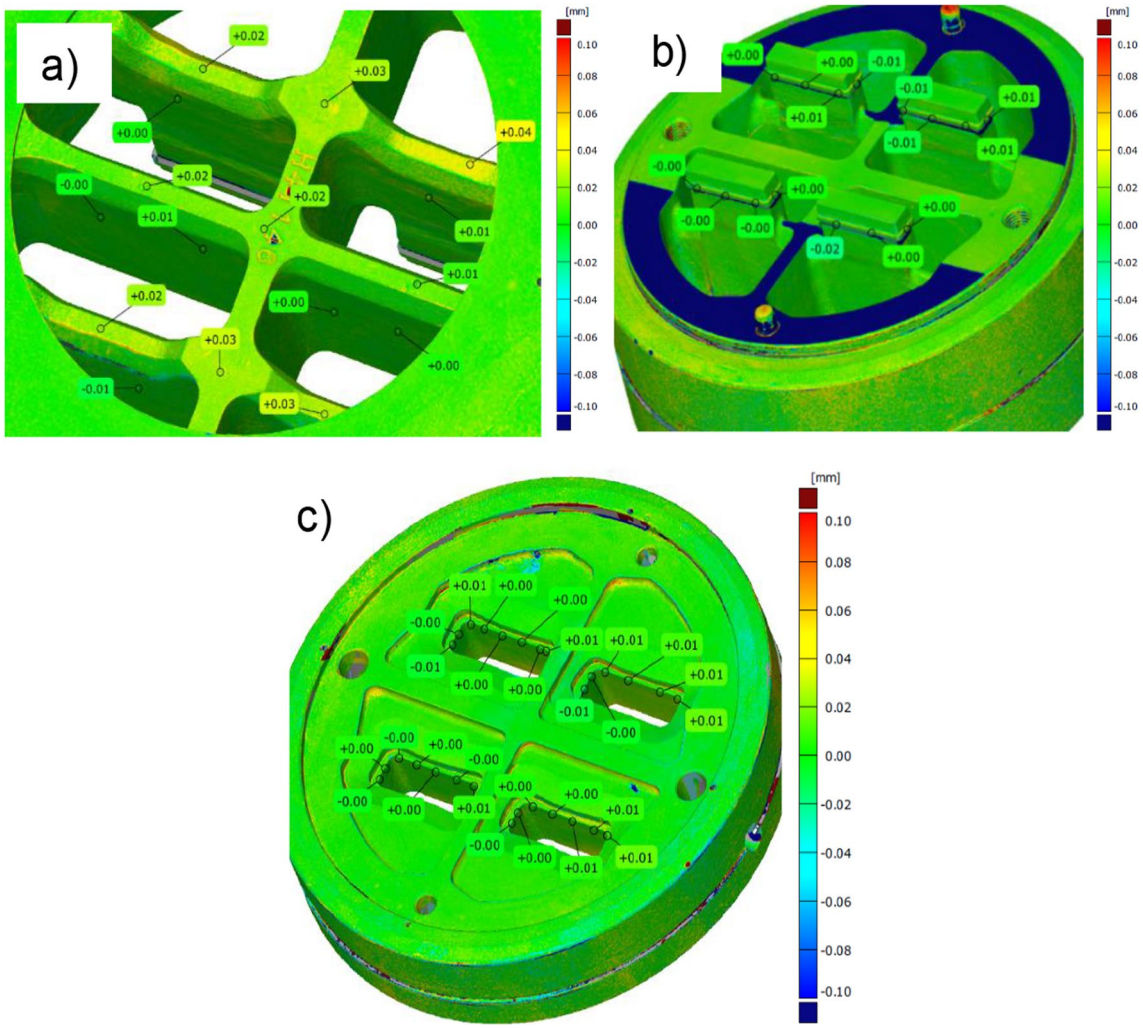

Fig. 11 Colour map of dimensional deviations on the digital model of the die after the production cycle in relation to the digital reference model of the new die in characteristic projections: **a** die entry channels with bridges, **b** bridging part, **c** die insert [own source]

minimal dead metal zone and the most uniform metal flow were found for the double arc-welding chamber and unequal bearing length. Chen [64] studied the dynamic recrystallisation (DRX) behaviour of an Al–Zn–Mg alloy during porthole die extrusion process. The volume fraction of DRX at the zones close to bridge and porthole wall is much higher than that in the other zones, and this kind of inhomogeneous DRX behaviour is mainly attributed to varying distribution of strain. Pinter in his work [65] determined the influence of die design on productivity and recovery for a 7020 hollow section. The special porthole die with the caterpillar design demonstrated a significant reduction of charge welds in extrudates compared to the butterfly type of the die. In his paper [66], Leśniak analysed the effect of the original porthole die design (Fig. 12) on the distributions of metal velocity, temperature, and mean die stress and elastic deflection during the extrusion of Ø50 × 2 mm EN AW-7021 alloy tubes on a 7-inch container diameter press using the finite-element method (FEM). An original porthole die with modified bridges and mandrels, profiling pre-chambers and a special radial-convex die inlet and special protrusions in the inlet channels (extrusion die 3) was designed and subjected to numerical analysis and experimental verification under industrial conditions. A study was carried out to evaluate the accuracy of the extruded tubes and of the dies themselves after operation using 3D optical scanning—for porthole dies of different geometries.

The results of the FEM numerical calculations show a significant improvement in the uniformity of the metal flow and a significant reduction in the elastic deflection for the proposed original design of porthole die No. 3 (Figs. 13, 14). The results of 3D optical scanning show that this translated into a significant improvement in the dimensional accuracy of the extruded tubes—there is no

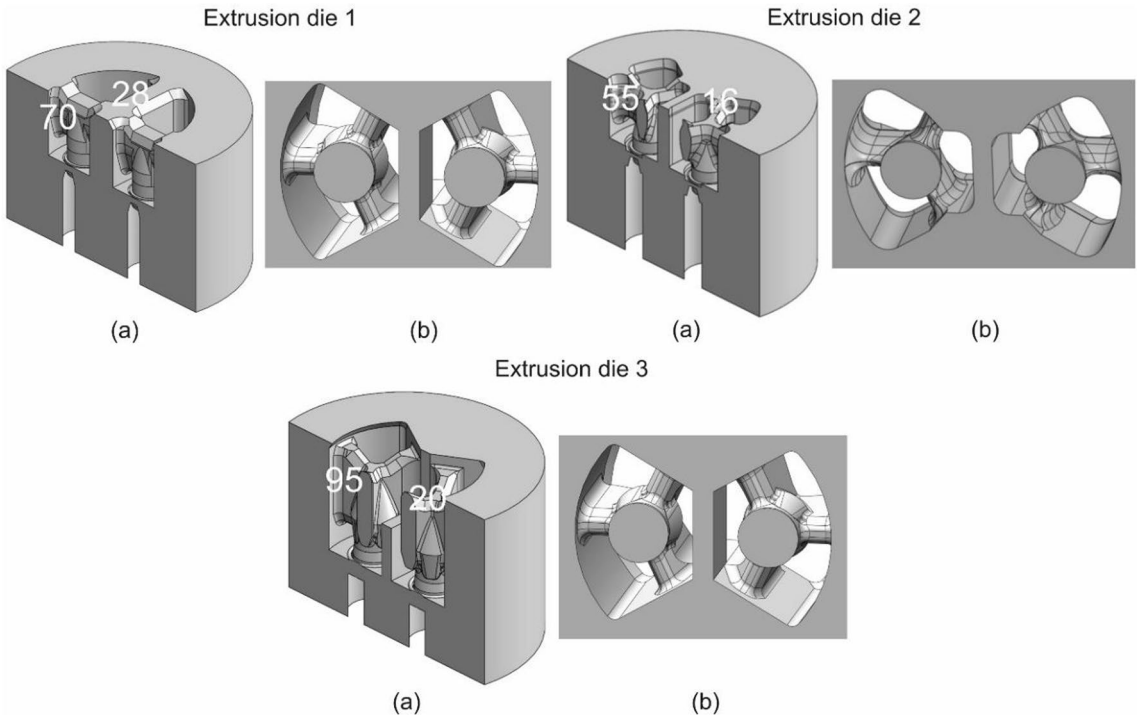

Fig. 12 Design variants of porthole dies for extrusion of Ø50 × 2 mm EN AW-7021 alloy tubes ([66] open access): **a** in the cross-sectional view and **b** in the bottom view

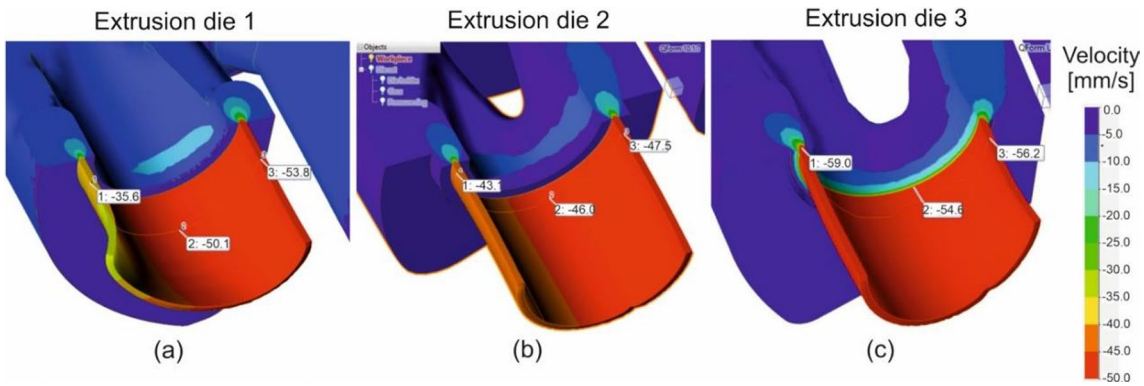

Fig. 13 Numerically calculated distributions of metal velocities during the extrusion of Ø50 × 2 mm EN AW-7021 alloy tubes for different porthole die geometries ([66] open access)

longer the very high tube eccentricity that occurred for die No. 1, or the very large deviations in tube wall thickness that occurred with die No. 2 (Figs. 15, 16). At the same time, the strength conditions of the die operation were radically improved, i.e. the axial pressures on the die bridges were significantly reduced and the phenomenon of buckling of the die mandrels was significantly reduced (Fig. 17). The appropriate design of the porthole die has eliminated the phenomenon of mandrel breakage due to unfavourable high thermo-mechanical loads applied to the die during extrusion (Fig. 18).

The authors of the paper by Lesniak et al. [66] conclude that the design of porthole dies for the extrusion of aluminium alloys of the 7xxx series requires new assumptions compared to classical dies for the extrusion of aluminium alloys of the 6xxx series. High unit pressures in the process of extrusion of Ø50 × 2 mm EN AW-7021 alloy tubes using porthole dies lead to high thermo-mechanical loads on the extrusion dies, which translates into the occurrence of permanent deformations—bridge deflection in the extrusion direction and lateral buckling of die mandrels and, consequently, to significant dimensional deviations of the extruded

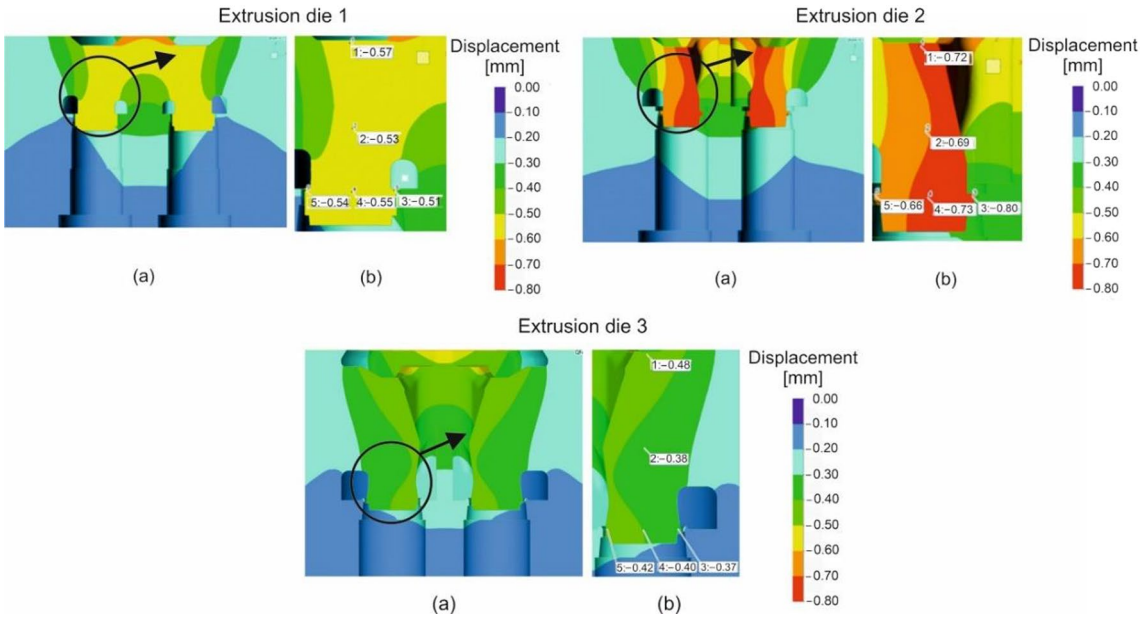

Fig. 14 Numerically calculated FEM distributions of die elastic deflection during extrusion of Ø50 × 2 mm EN AW-7021 alloy tubes for different porthole die geometries ([66] open access): a global view of mandrels and b local view of chosen part of mandrel

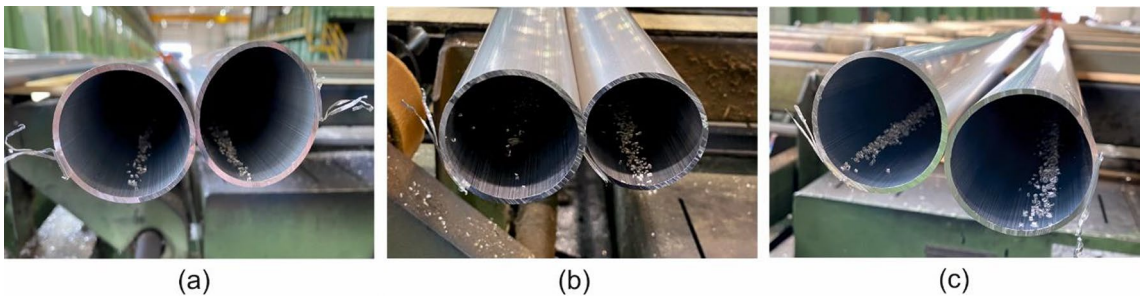

Fig. 15 Photographs of Ø50 × 2 mm tube extruded from EN AW-7021 alloy using porthole dies of different geometries ([66] open access): **a** die No. 1, **b** die No. 2, **c** die No. 3

tubes, in particular, deviations in circularity, wall thickness and product centricity, exceeding the limits of the relevant standards. Furthermore, the adjustment of the metal flow during the extrusion through die No. 1 is extremely difficult due to the obstructed metal flow in the sub-bridge regions of the die opening. The maximum opening of the inlet channels of die No. 1, together with the use of a central 2-bridge, made it possible, on the one hand, to reduce the resistance to the flow of metal during extrusion and to increase the average velocity of the metal flow from the die exit, but, on the other hand, led to an uneven distribution of the speed over the circumference of the tube and, finally, to the lateral buckling of the mandrels and the appearance of a significant ovalisation of the tube. The use of die No. 2 with a 3-point local die clearance supply (3-peak local bridges) allowed a more uniform distribution of metal particle velocities around the circumference of the tube and significantly reduced the tube ovalisation phenomenon, although it still did not provide an adequate level of tube wall thickness deviation. Only porthole die No. 3 with profiling pre-chambers, radially convex calibration bar entry and special protrusions in the die inlet channels, together with appropriate mandrel support, ensured high dimensional accuracy of the extruded tubes, in accordance with the relevant industry standard. It was also found that the potential circularity of the extruded tube is strongly related to the degree of uniformity of the plastic flow of the metal, while the potentially large dimensional deviations of the tube wall thickness are derived from the high deflection of the bridges in the extrusion direction and the deflection of the mandrels in the lateral direction.

An additional difficulty is the poor weldability of AlZnMg alloys when extruded through porthole dies, particularly those alloys containing Cu in their chemical composition. For AlCuMg, AlZnMg and AlZnMg(Cu) alloys,

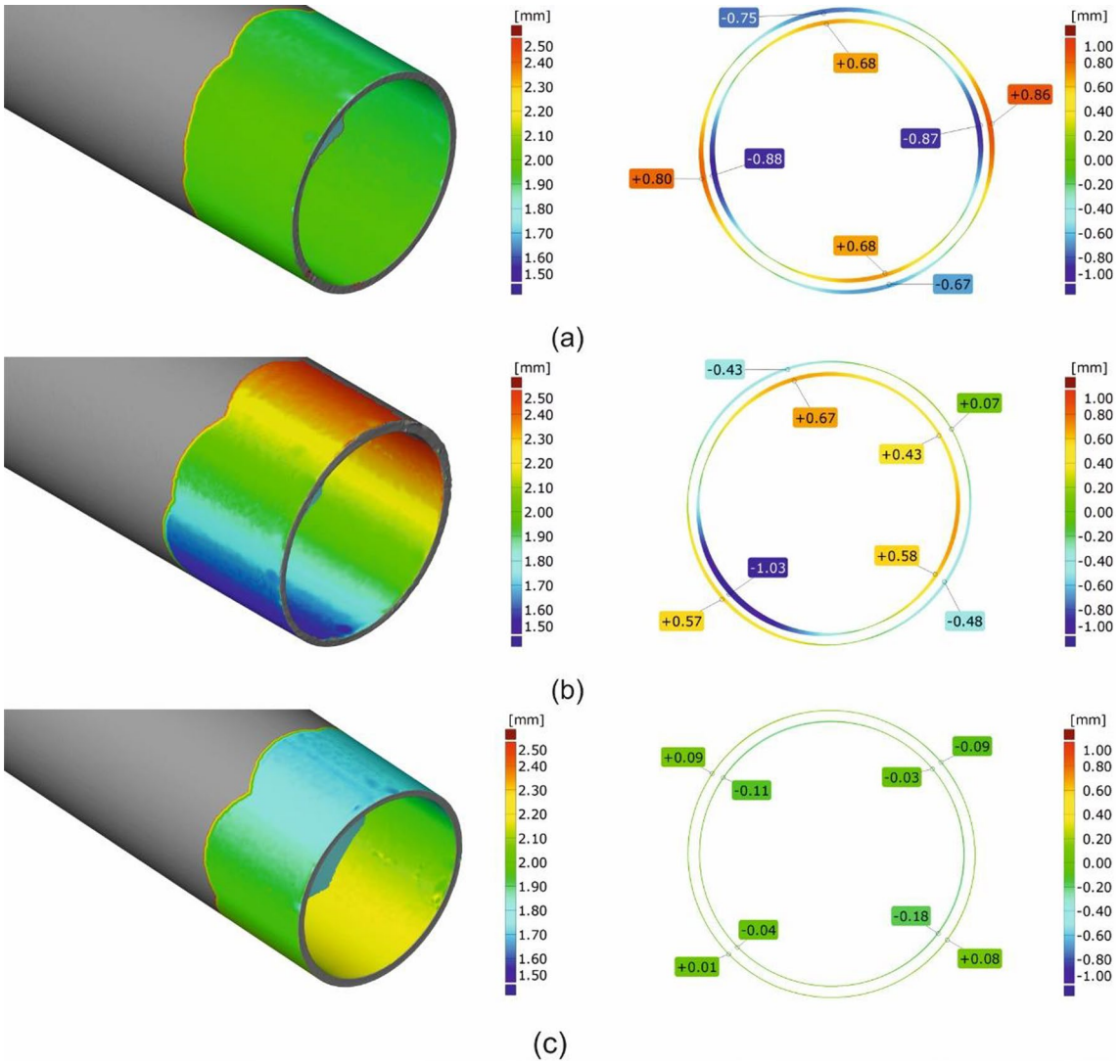

Fig. 16 Results of 3D optical scanning of Ø50×2 mm tubes extruded from EN AW-7021 alloy using porthole dies of different geometries ([66] open access): **a** die No. 1, **b** die No. 2, **c** die No. 3

above-standard stress-temperature conditions in the welding chambers of porthole dies are also important. Here a compromise in die design is required, which will ultimately allow both the quality of the extruded product and the die strength/life and process/technology parameters to be achieved.

In his paper [67], Leśniak proposed an innovative method for predicting the quality of longitudinal welds in extruded hollow profiles. The method is based on a patented laboratory [68] device for weldability testing and allows a complete mapping of the metal joining conditions in the welding chambers of a porthole die.

The cited work predicted the quality of longitudinal welds in extruded tubes of EN AW-7021 alloy with 3 different chemical compositions with varying Mg and Si contents. Numerical calculations and experimental verification under industrial conditions were carried out for the extrusion process of Ø50×2 mm tubes through a porthole die with different geometries. In the first stage, Akeret's weldability index σ_n/k was determined in weldability tests using proprietary laboratory equipment (Figs. 19, 20). In the second stage, FEM was used to verify whether the predetermined welding stress parameters could be achieved in the welding chambers of the porthole die. During stage III, the quality of the welds obtained in the extruded tubes was evaluated from a mechanical and structural point of view.

It was demonstrated that the numerically higher FEM predicted values of compressive stress in the welding chambers of porthole die No. 2 (Fig. 21) translated into higher tensile strength R_m of specimens with weld cut from Ø50×2 mm tubes extruded from 7021 alloy No. 2 using this die. In turn, the numerically higher FEM predicted values

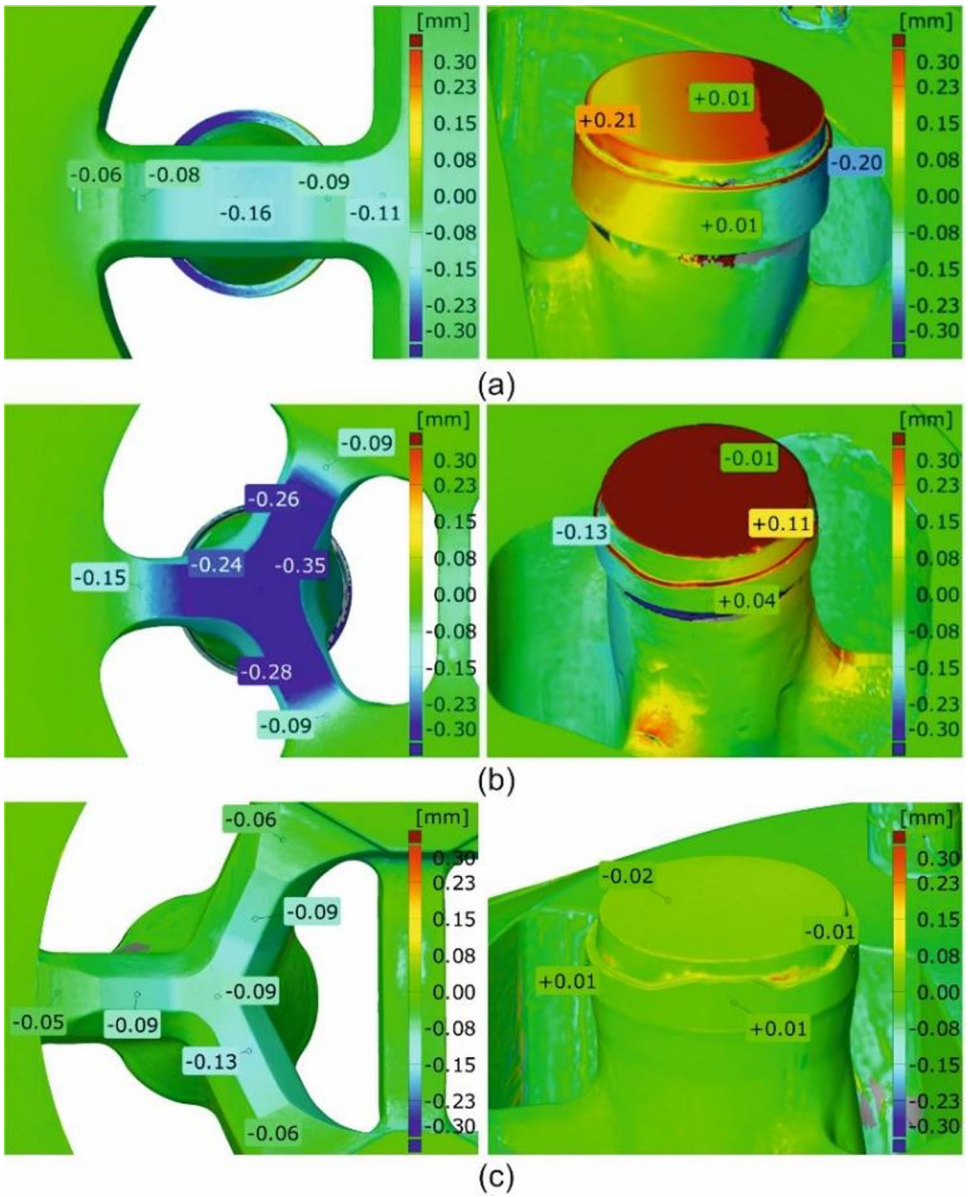

Fig. 17 Results of 3D optical scanning of the porthole dies after the operation—extrusion of a Ø50×2 mm EN AW-7021 alloy tube ([66] open access): **a** die No. 1, **b** die No. 2, **c** die No. 3

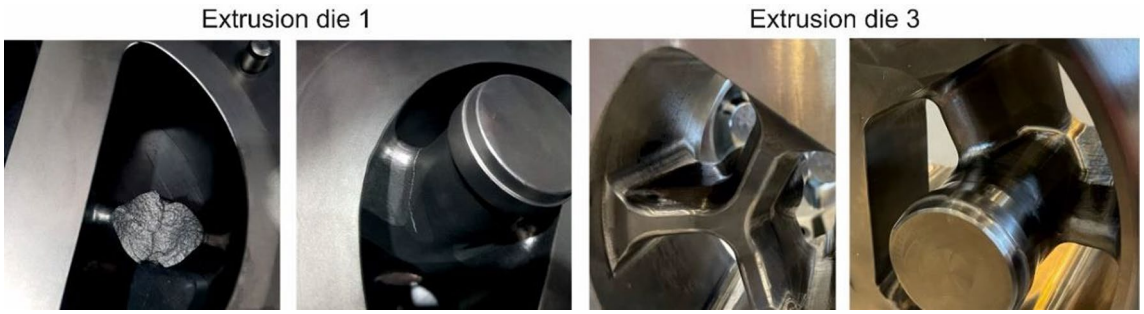

Fig. 18 Photographs of porthole dies No. 1 and No. 3 after the operation—extrusion of a Ø50×2 mm EN AW-7021 alloy tube ([66] open access)

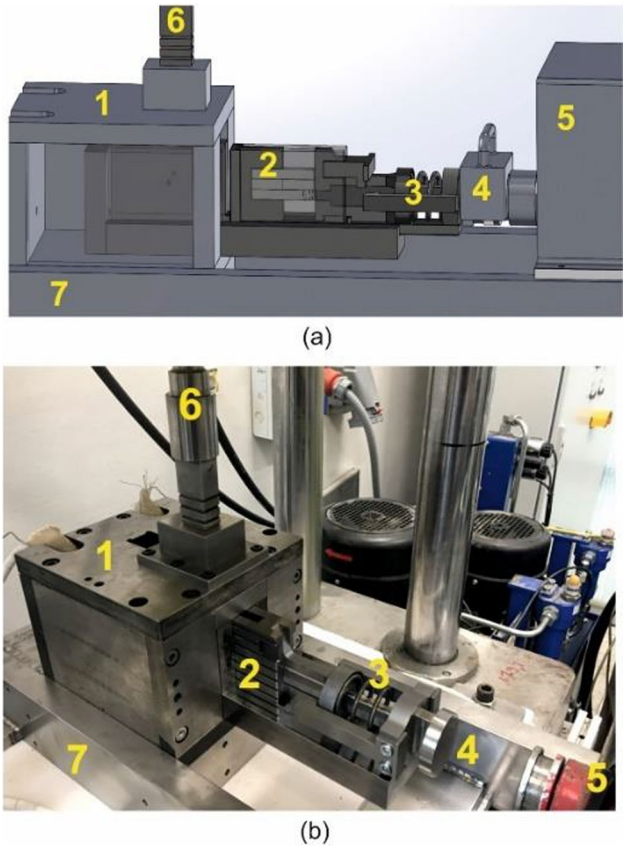

Fig. 19 Proprietary laboratory device for testing the weldability of metals and alloys: a 3D model and b physical stand ([67] open access). 1—heating chamber, 2—shearing and welding cartridge tool, 3—compression hydraulically driven stem with presser, 4—adapter of hydraulic cylinder and tool assembly holder, 5—145 hydraulic cylinder, 6—upper shearing punch, 7—main construction ram (Patent No PL230273B1, 146 AGH Krakow, 2018 [68])

of plastic strain in the welding chambers of chamber die No. 3 (Fig. 22) translated into higher percentage strain A of the specimens with welds produced from Ø50 × 2 mm tubes extruded from 7021 alloy No. 2.

When AlZnMg alloys are extruded through porthole dies, it is possible to achieve a high-quality joint and, consequently, high-strength longitudinal welds in hollow sections. The tensile strength in T5 condition for extruded Ø50 × 2 mm 7021 alloy tubes with longitudinal welds was in the range of 454–474 MPa (Fig. 23). Also noteworthy is the high ductility of the samples with welds in the analysed 7021 alloy—the percentage elongation obtained for die No. 3 was in the range of 17.5–20%. The analyses which were carried out confirmed the possibility of obtaining the predetermined ratio $\sigma_n/k = 5.88$ for both analysed dies, which was positively verified in industrial extrusion tests of Ø50 × 2 mm tubes made of 7021 alloy No. 2.

3.2 Conventional and modern methods for increasing die life in extrusion processes

Excessive tool wear is observed during the hot extrusion of aluminium, leading to the early elimination of tools from the process. Research conducted, in one of the dominant companies in the aluminium sector in 2018, presented the following reasons for the withdrawal of dies from production:

The die failure illustrated in Fig. 24 is due to the destructive mechanisms occurring in the extrusion processes. These include adhesive and abrasive wear, causing damage to the bearing surface of the die. Moreover, the bridges and mandrels are tempered at high temperatures, which leads to their cracking under the pressure of the extruded material. Additional damage is a consequence of overloading the dies in the extrusion process. An undue load may be caused

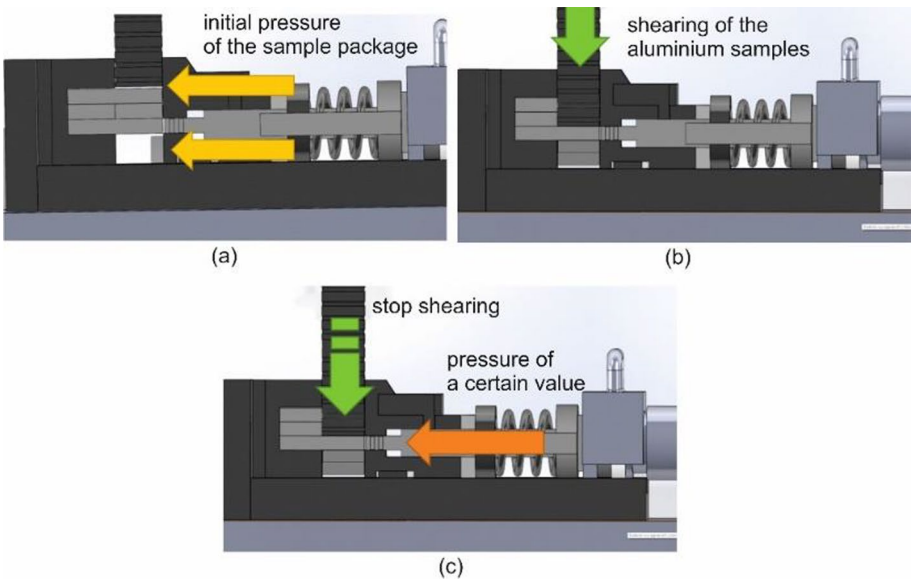

Fig. 20 Stages of the weldability test using the original proprietary device ([67] open access): **a** the tool cassette is inserted into the heating chamber and the presser presses the sample package, **b** the samples are sheared with the upper punch while holding the presser continuously, **c** the shearing punch stops and the pressing punch applies a certain pressure to the welded samples

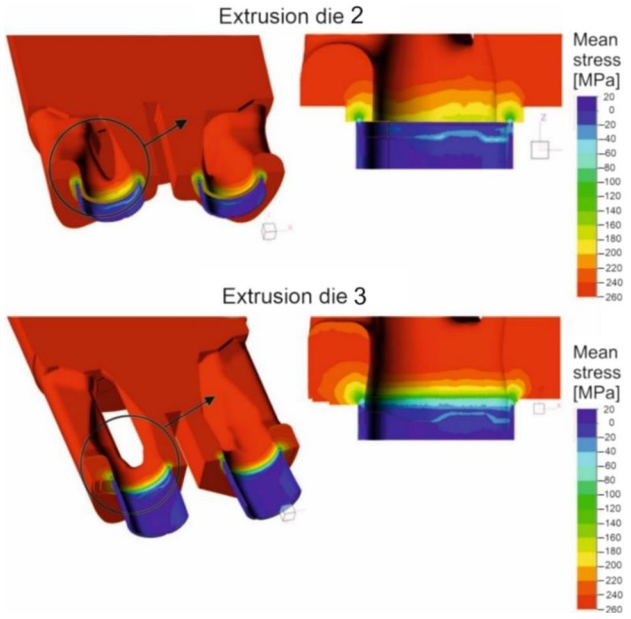

Fig. 21 Mean stress distributions for the extrusion of Ø50×2 mm EN AW-7021 alloy tubes using porthole dies No. 2 and No. 3 ([67] open access)

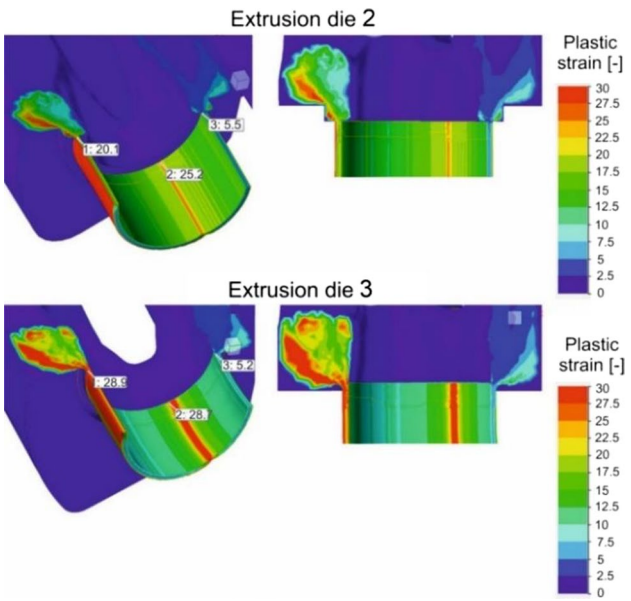

Fig. 22 Plastic strain distributions for the extrusion of Ø50×2 mm EN AW-7021 alloy tubes using porthole dies No. 2 and No. 3 ([67] open access)

by construction design errors, inadequate process preparation and technological inaccuracy. In extrusion processes, various methods are used to enhance durability of the dies. Durability is understood as the ability to resist mechanisms and destructive factors. Procedures for increasing durability are illustrated by a graph (Fig. 25) and presented below. These are conventional practices widely implemented along with new technologies that have recently been developed. The work also relates to those that are currently being tested and have not yet been extensively tried in operating conditions but demonstrate high potential.

The material from which the extrusion tools are made is crucial. To obtain a significant strength at a working temperature close to 500 °C, tool steels designed for hot work are used. Improved steel grades, are constantly being created [69], which allow to slightly extend the durability of the dies. Better results are also achieved through the development and research of existing steel grades as well as by advancing the steel remelting process [70]. Another strategy of improving tool materials is composites based on ceramics–cemented carbides. They are very beneficial for the durability increase, in tools for extruding motor valves, even up to 15 times [71]. The scientific works present a lot of evidence for the possibility of their use [72]. For several years, tool manufacturers have been employing ceramic inserts as a replaceable element, which is installed in a larger housing. Their advantage is resistance to temperatures reaching even 800–900 °C. However, there is a risk of fracturing due to low ductility. Nevertheless, ceramic materials are successfully applied in the processes of hot extrusion of aluminium [73].

The advancement of computer-assisted design and manufacturing has led to new tools for numerical analysis of extrusion processes. Computational environments have been developed to create useful models of different extrusion processes [74]. Furthermore, statistical and mathematical tools were created, which, thanks to the computational ability of servers, allow the selection of more adequate process parameters. Their optimisation can minimise the risk of excessive temperature or excessive pressure on tools in the extrusion process [75]. Modelling may be used to choose a procedure to improve wear life [76]. In addition, it can serve to determine the optimal shape of tools that will be the least susceptible to wear. Another effective way to increase durability in extrusion processes is to interfere with the tool design and process parameters to control the heat flow in the hot extrusion process. The aluminium extrusion process should be carried out in the so-called process window in terms of the temperature of the extruded material and the indirectly related temperature of the dies. Aluminium alloys possess a higher sensitivity to temperature changes than steel, which is why both the temperature range of plastic processing is narrow and the range of required tool temperature. The tools operate in environment where temperatures increase to 500 °C, which is problematic due to their tempering. However, tools not heated enough will cause material to cool down, its too low plasticity and thus excessive load on the dies. The temperature is primarily controlled using the appropriate extrusion speeds and regulating the feed temperature. Greater possibilities of process stabilisation are provided by

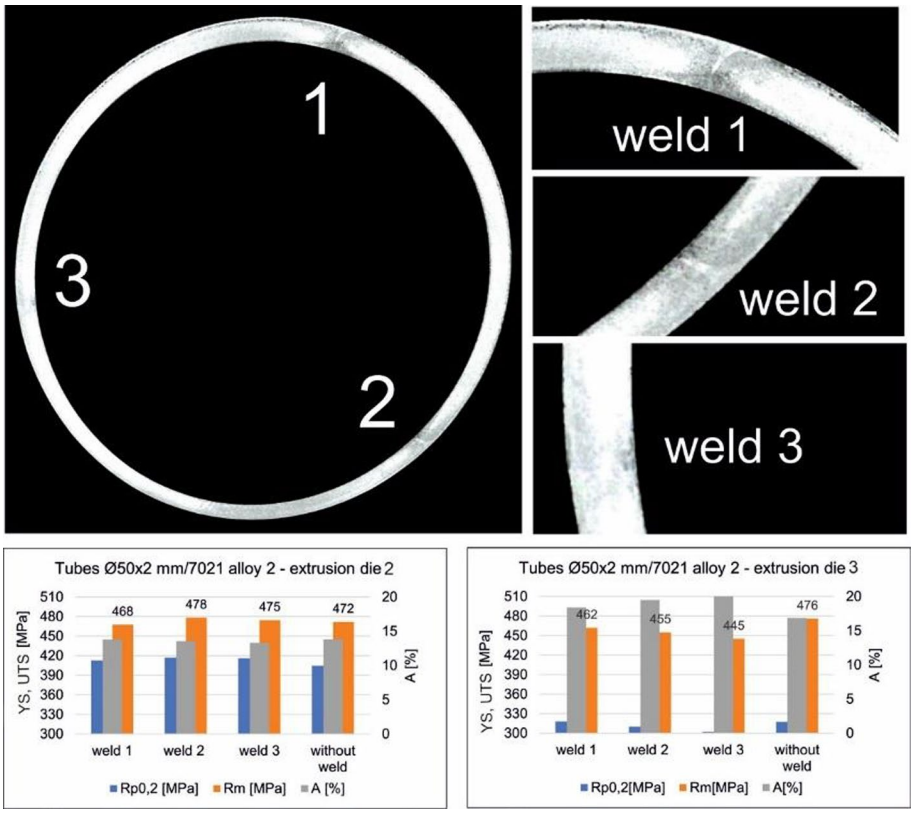

Fig. 23 Macrostructures of the extruded tube with visible welds in cross-section and mechanical properties of Ø50×2 mm tubes extruded from EN AW-7021 alloy No. 2 through porthole dies No. 2 and No. 3 in T5 condition ([67] open access)

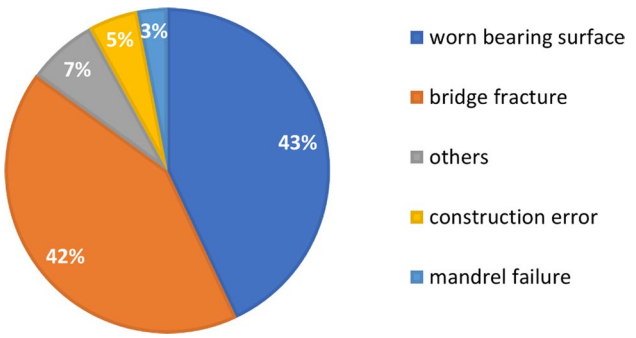

Fig. 24 Reasons for the loss of operational capability of the porthole dies from hot extrusion processes of aluminium [own source]

cooling channels, which can be performed conventionally by electro drilling and drilling of long straight-line holes in dies and milling channels in dividing planes. These channels are capable of pressing gas or coolant fluid.

In the past decade, modern methods of metal 3D printing, that provide satisfactory quality, have been discovered. Thus, so-called conformal cooling channels were developed, which can be printed in any shape and placed close to the working surface, supporting the cooling of the dies [77]. The methodology of their design was created along with guidelines for channel geometry and parameters of the manufacturing technology by laser sintering of powders [78]. In recent years, several application in extrusion dies have been presented, including porthole ones, in which such cooling channels have been built [79].

Welding techniques are an effective way to increase tool life. The bearing surface is an example of a die surface that can be rebuilt with their use in regenerative cladding. Traditional arc-welding or laser-powder-cladding methods can be employed for this objective [80]. The laser-cladding procedure creates more reproducible and accurate shapes of the welds, with a smaller melt depth. The advantage of laser coating of powders is the addition of valuable additives to the material of the padding weld [81]. Meanwhile, traditional arc welding is widely available and, therefore, has a greater potential for use. The durability of forming tools has been enhanced by the development of hybrid machining technologies that combine hard facing and nitriding, in recent years [82, 83].

The durability of extrusion dies is greatly aided by the use of surface engineering methods. The leading manner is nitriding. In industrial practice, gas and ion nitriding processes are carried out in the temperature range 450–580 °C, as a result, a thin layer of iron nitrides with a thickness of 2–10 µm and a diffusion zone with a thickness of 50–300 µm are obtained in the surface layer. During operation, iron nitrides from the working surfaces of the dies are removed, especially from the surface of the bearing surface. Moreover, extrusion dies are exposed to high temperatures during

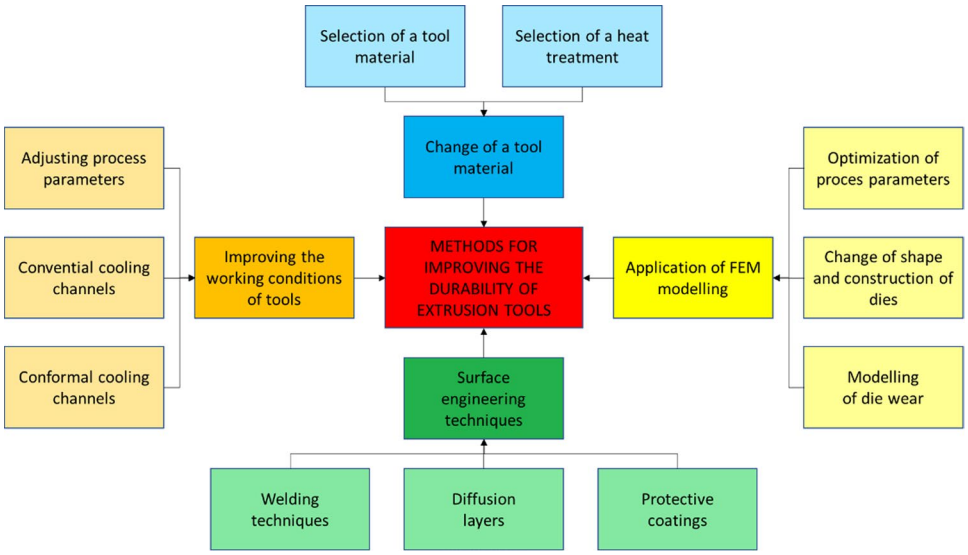

Fig. 25 Methods for extending tool life in extrusion processes [own source]

operation, which significantly affects the surface condition and hardness of the nitride layer [84]. In manufacturing, dies for extrusion of aluminium profiles are subjected to regeneration processes consisting in repeated nitriding. Most commonly, cycles between 2 and 6 regeneration are used. The study [85] of the effects of multiple nitriding revealed that it has a significant impact on the structure and hardness profile of the nitride layer. However, the number of regenerative cycles through nitriding is limited, as the key dimensions of the dies change and at some point cease to meet the quality and accuracy standards [86].

Coatings are a multifaceted group providing solution to problem of increasing the durability of extrusion tools. In recent decades, this branch of surface engineering has undergone a significant development, resulting in many progressive attempts to modify and protect the surface of tools used in metal forming, including extrusion dies. Among many deposition techniques, methods of physical deposition of coatings from the PVD (physical vapour deposition) gas phase and methods of chemical deposition of CVD gas phase coatings (the chemical vapour deposition) play an important role in industrial practice. PVD coatings can be applied to a substrate that is either cold or heated up to 200–500 °C. This allows hardened and tempered substrates like tool steels to be covered without the risk of reducing their hardness. The coating-substrate connection is adhesive or diffusion-adhesive and the stronger the better the surface was cleaned before coating. PVD techniques are diverse in many ways. They may vary in the method of obtaining metal vapours (evaporation may occur as a result of resistance, induction, electron or laser heating), in the method of applying material vapours, because the material can be sprayed (sputtering), brewed (evaporation) or sputtering (ion plating) as well as in the aspect of the process of intensification of the layer deposition.

There are at least 25 methods of manufacturing PVD coatings. In addition, PVD techniques can be supported by plasma (PAPVD), which contributes to obtaining more energy needed to activate chemical reactions. However, one of the limitations of PVD technique is the inability to cover the inner parts of the die (i.e. surface of the welding chamber), where access to the surface of the bearing surface is limited. Therefore, until recently, the usage of PVD technology was limited to several group of tools used for extrusion of hole profiles. Nevertheless, there are applications in which the effectiveness of PVD coatings, in increasing the durability of extrusion dies, has been confirmed [87]. Alternatively, CVD technology can be employed, in which deposition of coatings involves the formation of carbides and metal nitrides from gaseous atmosphere components that settle on the surface of the workpiece. Commonly, the process involves vapours of metal chemical compounds constituting the basic component of the coating and substrate components such as carbon (in the case of carbide layers) or furnace atmosphere components such as nitrogen or oxygen. The components of the atmosphere can be activated thermally (this is not beneficial due to high process temperatures) or plasma. Then, the process is referred to as PECVD (plasma-enhanced CVDs). This is a more effective method, which, due to the process temperature not exceeding 500 °C, can be used for deposition of non-equilibrium phases and allows better control over stoichiometry and purity of coatings. The use of plasma stimulates the molecules of the gas mixture, without intense heating of the substance [88], to energy levels corresponding to high-temperature conditions. It is noteworthy that modern CVD coatings are mostly multilayer systems. Combining different layered systems to achieve the best results in terms of wear rate, bonding and hardness is quintessential. An example of this

are the latest technologies developed and employed by the WEFA company (Fig. 26).

Several research centres are conducting unpublished research on the use of coatings produced by high-power pulsed magnetron sputtering (high-power impulse magnetron sputtering, HiPIMS). These are ternary coatings based on tungsten borides (WB) with additions of elements such as Ti, Zr, and Ta. They are characterised, in comparison with traditional materials, by very high hardness (depending on the phase composition $H = 20–40$ GPa) and thermal conductivity similar to steel (40 W/mK). For this reason, they can be employed to cover surfaces resistant to scratches and wear by friction. As the latest literature reports, the properties of tungsten borides can be improved by doping [89]. It is confirmed that these coatings can extend tool lifetime in comparison to traditional nitride extrusion tools. An increase in hardness, and in some cases, an improvement in the thermal stability of the proposed materials is obtained by adding the alloying element to WBx.

4 Extrusion process

4.1 Extrusion processes for metals and alloys based on severe plastic deformation

Severe plastic deformation (SPD) processes encompass a variety of methods that can be employed to refine grains to nano- or submicron-scale through the application of significant plastic deformations. These processes require the use of specialised equipment, ensuring the imposition of substantial deformations while maintaining the material's deformation coherence and dimensions. Ideally, the application of a state of uniform compression is preferred to prevent material fracture [90, 91]. In certain SPD methods, extrusion serves as the fundamental process, as seen in methods such as cyclic extrusion compression (CEC) or equal-channel angular pressing (ECAP). Other well-known methods employing severe plastic deformation include hydrostatic extrusion (HE) and KOBO. Deformation through these techniques results in a significant refinement of the microstructure in pure metals and alloys, facilitating the consolidation of powder materials. Typically, the grain size of materials deformed in this manner falls within the submicron range. The resulting grains exhibit an equiaxial shape and are separated by grain boundaries with high disorientation. The increase in the number of grain boundaries leads to a rise in stored energy, impacting the high-temperature instability of these materials. This effect can also be the catalyst for uncontrolled grain growth, particularly during the deformation process. Indeed, this is also a limiting factor for the possibility of grain refinement, especially in the case of high-purity metals [92, 93]. The utilisation of significant, intense plastic deformation is not a novel concept in metalworking; it has been practically applied since ancient times. In the case of conventional forming operations such as forging, rolling, drawing, etc., sufficiently large deformations can be achieved at both high and low temperatures. However, what is crucial is that the 'effects' stemming from deformation in SPD processes are not observed in ordinary forming operations. Some of these "effects" have been discovered precisely through the development of these processing techniques. Data presented in the literature indicate that the evolution of the microstructure during deformation strongly depends on the mechanics of the deformation. Through deformation in SPD processes, properties can be precisely controlled, resulting in materials characterised by a unique combination of properties and microstructure [94]. Substantial interest in materials with a finely divided grain structure, ongoing for several decades, contributes to the continuous development of manufacturing methods. Efforts are underway to optimise parameters, enhance process efficiency, and modify existing processes, ultimately increasing the potential for their prospective application across various industrial sectors.

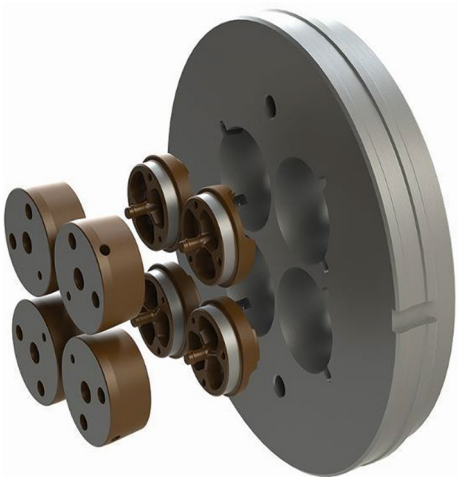

Fig. 26 CVD coated extrusion dies (CED®) for precision tubes extrusion ([89] open access)

4.1.1 Cyclic extrusion compression (CEC)

The cyclic extrusion compression (CEC) method, patented in 1979 at the Faculty of Non-ferrous Metals of AGH University of Krakow [95], operates on the principle of integrating extrusion and compression processes within a single deformation cycle (Fig. 27). The cyclic movement of metal through a die venturi, with a diameter d_m, from the upper container (diameter D_0) to the lower container (diameter D_0) leads to the accumulation of strain in the sample. In a single cycle of the CEC process, wherein the metal undergoes simultaneous extrusion and compression, a

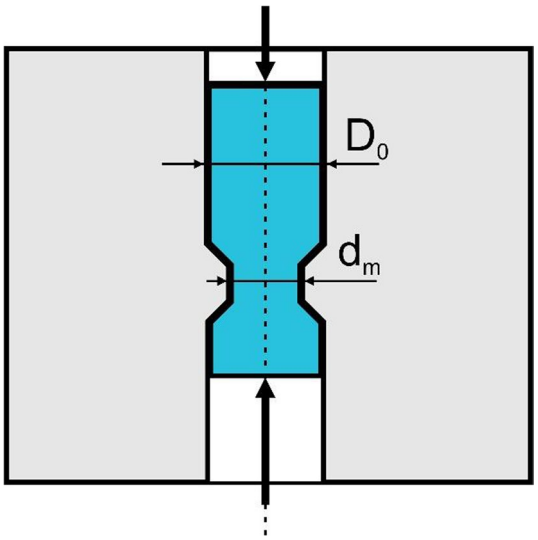

Fig. 27 Cyclic extrusion compression (CEC) scheme ([95] open access)

double deformation of equal magnitude occurs. Cumulative true strain results from the sum of strain applied in a single cycle and the total number of cycles employed. In the CEC method, both conditions for static flow are met: maintaining the full ductility of the material by applying high hydrostatic stresses to prevent material cracking, and ensuring flow stability through the use of tools that fully control the flow of the deformed material [96, 97].

In CEC processes, 90–95% of the deformation work is converted into heat, while the remaining portion of the deformation work contributes to microstructural changes and is stored in the deformed metal as plastic deformation energy. It is noteworthy that the highest concentration of stored energy occurs in areas of the highest plastic deformation, primarily within the shear bands. This stored energy then becomes the driving force behind microstructure renewal processes [97].

Extensive research conducted over many years at the Faculty of Non-Ferrous Metals of AGH University in Krakow, focussing on the deformation of metals and alloys using the CEC method, has involved materials such as copper and aluminium. The investigations have also delved into the deformation of hard-to-deform metals and the plastic consolidation of powder materials [96–98]. Microstructure observations of deformed samples reveal the presence of numerous bands and shear bands traversing significant distances, often crossing grain boundaries, and microbands in the submicron range. The microstructure is further characterised by jogs at grain boundaries and, with higher strain values, the mutual intersection of bands and microbands, leading to the division of the material into parallelograms and, consequently, its homogenisation (Fig. 28). In aluminium, the grain size after the CEC process was approximately $d = 0.6$ µm, while in copper, it was $d = 0.2$ µm. The proportion of large disorientation angles depended on the exerted deformation and ranged from 30 to 50%. The CEC process was also successfully employed for the production of Al5SiC2Cgr composites from elemental powders. These composites exhibited good cohesion and densities of 96–98% of the theoretical density.

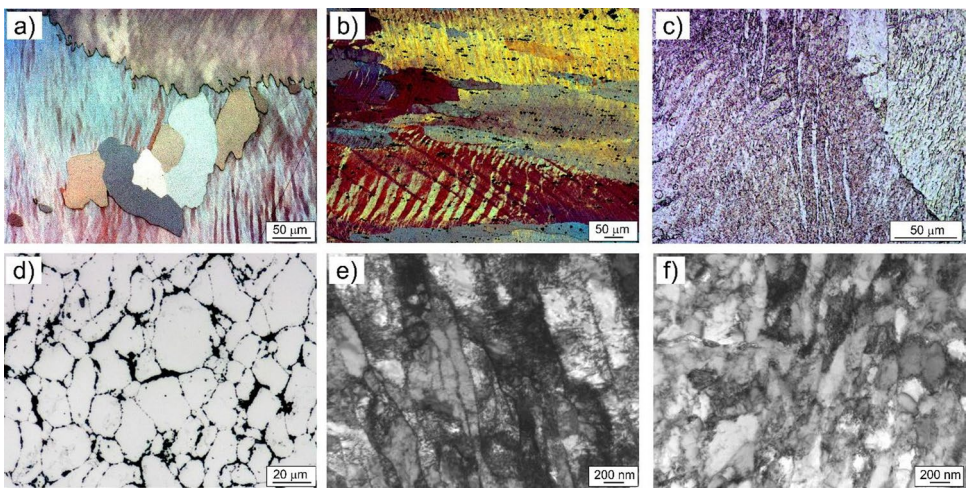

Fig. 28 Microstructure of selected materials deformed by the CEC process: **a** Al99.999, $\varepsilon = 3.37$ (8CEC)—the image displays nuclei and new grains, along with a characteristic "serrated" boundary; **b** AlMg alloy (grade 5483) $\varepsilon = 3.37$ (8CEC)—the photo shows intersecting bands and shear bands; **c** Cu99.99, $\varepsilon = 6.5$ (10CEC)—the image illustrates intersecting bands and a "serrated" boundary; **d** Al5SiC-2Cgr composite, $\varepsilon = 0.84$ (2CEC); **e** Cu99.99; $\varepsilon = 6.5$ (10CEC)—the photo shows microbands containing a high density of dislocations within their boundaries, as well as in the interior; **f** Cu99.99; $\varepsilon = 13$ (20CEC)—the image depicts cells containing a high density of dislocations within their boundaries (own source)

The SiC reinforcing phase, not exceeding 2 µm, was uniformly distributed at the grain boundaries (Fig. 28d).

The microhardness measurements of samples deformed in the CEC process demonstrate a two-stage increase. Following the initial deformation, the highest microhardness increase occurs, followed by the subsequent stabilisation of properties. The microhardness does not further increase; a so-called "plateau" is observed on the Cu hardening curves, indicating a balance between the processes of hardening and structure renewal. In the case of Al99.999 and AlMg alloy, the microhardness decreased after 8 CEC cycles, which is also characteristic of materials deformed in SPD processes (Fig. 29).

Interesting results regarding the Al-6061 alloy and Al-6061-xSiC composites ($x = 5$ and 10 wt%) are presented in the paper [99]. The authors focussed on studying the microstructure, microhardness, and abrasive wear resistance of the materials under investigation. They demonstrated microstructure refinement after the CEC process, both in grain size and SiC particles, with an increase in the amount of strain exerted during the CEC process. In addition, there was an increase in hardness and a reduction in porosity in the case of the composites, resulting in improved abrasive wear resistance, especially in the composite with 10 wt% SiC. The authors of paper [100] deformed a cast Mg–1.50Zn–0.25Gd alloy using the CEC process at temperatures of 250, 300, 350, and 400 °C. The results showed that a higher number of passes in the CEC process favours the precipitation of the secondary phase, grain refinement, and weakening of the primary texture. Deformation at moderate temperatures also promotes the precipitation of the secondary phase and weakening of the primary texture, but through particle-stimulated recrystallisation. The lower CEC deformation temperature also promotes grain refinement and an increase in the mechanical properties of the alloy under study. In the paper [101], Guo et al. presented results on Mg-1 wt% SiC nanocomposites deformed by the CEC process at 350 °C. The deformation through the CEC process resulted in increased strength of the studied composites, grain refinement, and homogenisation of the microstructure, with a rise in the number of CEC cycles. Furthermore, after deformation with 8 CEC cycles, agglomeration of nanometric particles of the SiC strengthening phase was eliminated, having a positive effect on the properties. Several results on materials deformed by the CEC process can be found in the papers of Maria and Jan Richert, e.g. [102, 103].

A significant limitation of the CEC method is the dimensions of the specimen being deformed, which obviously restricts the introduction of products manufactured by this method into the market. Siahsarani and Faraji [104, 105] proposed a modification of the CEC process, the so-called hydrostatic cyclic extrusion compression (HCEC). HCEC makes it possible to produce bars with longer lengths than the conventional CEC process. The presence of a liquid medium favours the minimisation of frictional forces and also allows for a reduction in force during the process. The results obtained by the authors appear promising for both aluminium and the AZ91 casting alloy.

The referenced research results showcase the successful application of the CEC process for deforming both pure metals and alloys. In addition, it proves feasible to produce composite materials from elementary powders and to deform hard-to-deform materials, such as the AZ91 casting alloy.

4.1.2 Equal channel angular pressing (ECAP)

The equal-channel angular pressing (ECAP) method was pioneered by Segal and co-workers in the early 1980s [106]. It is now one of the most popular severe plastic deformation (SPD) methods for refining the microstructure of various materials to sub- or even nanometric sizes. The basic principle of deformation in the ECAP process is illustrated in Fig. 30. The device matrix comprises two intersecting channels with identical cross-sections, connected at a specific angle, typically $\Phi = 90°$ [107]. The degree of deformation depends on the angle between the channels. Proper lubrication in the chamber and ram zone is crucial. This procedure minimises frictional forces and prevents the formation of a dead zone in the bending area of the angled channel [106, 107]. In addition, the ECAP process can be performed at elevated temperatures [90].

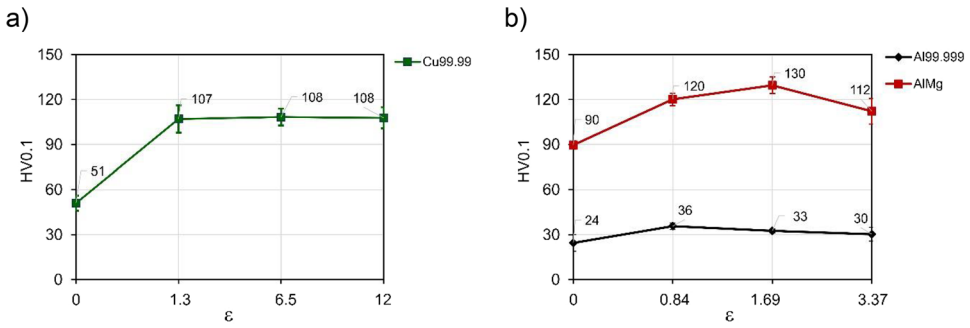

Fig. 29 Microhardness changes as a function of the strain exerted during the CEC process: **a** polycrystalline Cu99.99; **b** Al99.999 and AlMg alloy (own source)

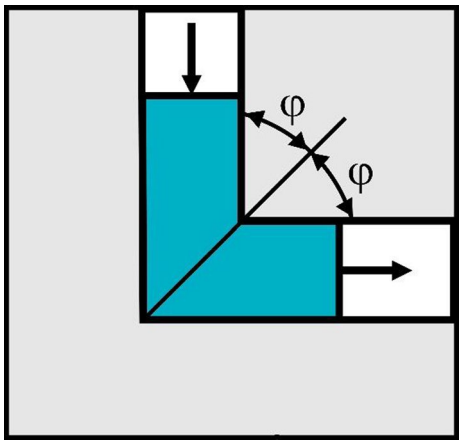

Fig. 30 Equal channel angular pressing (ECAP) scheme ([98] open access)

The extruded material possesses a cross-section similar to the channels through which it is extruded. The ingot is compressed using a punch, moving from the upper to the lower channel in subsequent operations. Moreover, it is viable to re-insert the previously extruded sample into the die, initiating another deformation cycle. When re-inserting the sample into the upper die container, a rotation of the sample is possible (often $\alpha = 90°$ or $\alpha = 180°$). This procedure facilitates a more uniform deformation over the cross-section of the specimen.

There are four ECAP deformation paths: A, B_A, B_C, and C, corresponding, respectively to situations where A—the material is not rotated between successive passes, B_A—it is rotated 90° in alternate directions between each pass, B_C—it is rotated 90° in the same direction between successive passes, and C—it is rotated 180° between passes [90, 106, 107]. The B_C path enables achieving the most homogeneous distribution of properties across the cross-section and obtaining an ultrafine-grained microstructure consisting of equiaxial grains with a large misorientation angle [97]. The deformation of the material in the ECAP process occurs through simple shearing in a very thin angular bending region (see Fig. 30). Various combinations of die container shapes are possible, including square or rectangular cross-sections, as well as circular cross-sections. Several modifications to the ECAP process exist to enhance the microstructure, such as the use of back pressure. Following the ECAP process, an ultrafine-grained material with predominantly large-angle boundaries is achieved [90, 94].

Research on ECAP deformation has encompassed numerous metallic materials, and the process has also been employed for producing composites from elementary powders. In the case of ECAP deformation, the most significant strengthening occurs in the initial stages, with subsequent changes being relatively small. However, extensive deformations promote homogenisation and the microstructure refinement. Research, conducted in collaboration with the Unipress High-Pressure Institute in Warsaw, focussed on ECAP deformation involving aluminium Al99.5 and copper Cu99.99. Samples underwent deformation through 4; 8, and 16 passes in the ECAP angle channel, resulting in deformations of 4.6; 9.2, and 18.4, respectively. The deformation amount for one passage of the specimen through the angular channel was $\varepsilon = 1.15$, with the B_C path used (the specimen was rotated 90° with respect to the previous cycle).

As with CEC-strained specimens, the microstructure after ECAP deformation also exhibited numerous bands and shear bands. In the range of smaller deformations, these bands were mostly limited to single grains, whereas at larger deformations, they extended over considerable distances, sometimes reaching several hundred micrometres. The shear bands traversing the grain boundaries created distinctive jogs on the grain boundaries, indicating substantial plastic deformation (see Fig. 31). Characteristic of materials deformed by the ECAP process is the presence of two families of intersecting bands and shear bands. The intersection of these bands results in the division of the material into parallelograms, and as the number of intersecting bands increases in further stages of deformation, it contributes to the homogenisation of the microstructure. The formation of jogs in the intersecting bands provides evidence of significant shear deformation in the band, leading to a distortion of its straight path and, among other effects, the distortion of grain boundaries [97]. After 16 passes through the ECAP angular channel, grains in the microstructure were similar in shape to equiaxial grains. The grain size, approximately $d = 0.57$ μm in aluminium and $d = 0.3$ μm in copper, resembled that observed after CEC deformation. Following the most substantial deformation ($\varepsilon = 18.4$), the proportion of large misorientation angles was in the range of 75–80%. In the submicron range of aluminium, grains/subgrains and microbands consisting of elongated subgrains were present, all free of dislocations. Increasing the number of passes through the ECAP angular channel results in a change in the shape of grains towards nearly equiaxial, indicating that the microstructure composed of microbands becomes unstable. A different type of microstructure was observed in copper. The observed microbands were predominantly composed of dense dislocation tangles, and the dislocation density varied depending on the level of deformation. The dislocation density varied with the level of deformation. Similar to aluminium, locally observed were the intersections of microbands leading to the division of the material into micro- and nano-volumes. Equally characteristic were the cellular arrangements observed in the vicinity of microbands and within microbands.

Similarly to the CEC process, microhardness increases in two stages after ECAP. The most significant increase

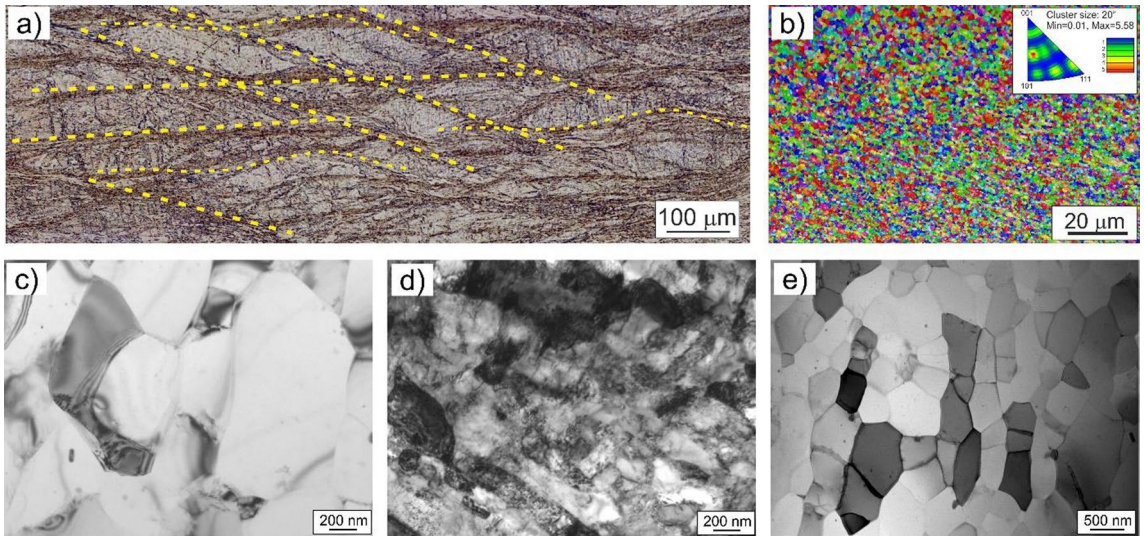

Fig. 31 Microstructure of selected metals deformed in the ECAP process; **a** Cu99.99, $\varepsilon = 4.6$ (4ECAP)—the photo shows intersecting shear bands and grain boundary deflections; **b** Cu99.99 $\varepsilon = 18.4$ (16ECAP)—the photo shows EBSD map and basic triangle [98]; **c** Al99.5, $\varepsilon = 4.6$ (4ECAP)—the image shows dislocation-free subgrains; **d** Cu99.99, $\varepsilon = 4.6$ (4ECAP)—the image shows cellular arrangements and microbands with high dislocation density; **e** Al99.5; $\varepsilon = 9.2$ (8ECAP)—the image shows dislocation-free subgrains (own source)

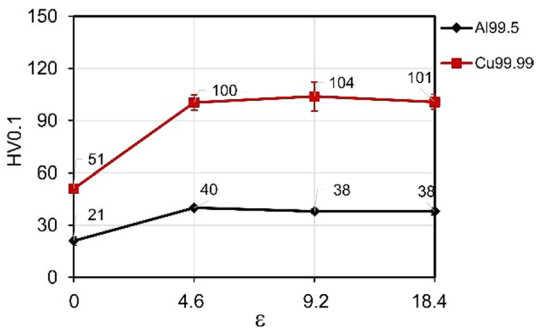

Fig. 32 Microhardness changes depending on the level of deformation applied in the ECAP process for Cu99.99 and Al99.5 ([98] open access)

occurs initially, and further deformation does not cause substantial changes in microhardness; it remains relatively constant (see Fig. 32). In both aluminium and copper, microhardness doubled after the smallest applied strain compared to the initial state, reaching 40 HV0.1 for aluminium and 100 HV0.1 for copper, respectively. The strengthening curves exhibit a 'plateau' phenomenon.

The obtained results indicate that a satisfactory level of properties was achieved already after 4 passes through the ECAP angular channel. Further deformation does not cause changes in microhardness levels but contributes to the homogenisation of the microstructure. More extensive results regarding the deformation of aluminium and copper in the ECAP process are presented in [98].

The research results regarding the AlZnMg alloy deformed through the ECAP process at temperatures of 150 and 200 °C, presented in paper [108], demonstrate an enhancement in the alloy's properties after the ECAP process. Notably, the alloy deformed at a lower temperature exhibited higher property levels. The improvement in properties is associated with grain refinement as well as the precipitation of the $MgZn_2$ phase. Interesting results concerning the AlMgScZr alloy are discussed in the study [109]. The authors presented findings on the evolution of the alloy's microstructure after deformation through ECAP and FSP (friction stir processing). The ECAP process was carried out at 300 °C with 6 passes through the angular channel using the Bc path. Significant microstructure refinement was achieved, with grain size below 1 µm after the ECAP process. However, larger grains were still present in the microstructure, accompanied by a change in the morphology and distribution of $Al_3(ScZr)$ phase precipitates. In comparison to the FSP process, higher property levels were obtained—the ultimate tensile strength (UTS) was 418 MPa, yield strength (YS) was 322 MPa, and elongation reached 20%.

Liu et al., in their study [110], presented results on a biodegradable ZnCuMg alloy deformed through the ECAP process (4, 8, and 12 passes). Two alloys with different Cu content in the as-cast state were investigated. The authors focussed on the evolution of the $CuZn_5$ and Mg_2Zn_{11} phases. Deformation resulted in the refinement of the eutectic structure, with fine precipitates of Mg_2Zn_{11} in the microstructure. In addition, dynamic precipitation of the $CuZn_5$ phase was observed in both alloys. The grain size after 12 passes

through the ECAP angular channel was approximately $d = 0.63$ µm for the Zn3Cu0.5 Mg alloy and $d = 0.99$ µm for the Zn1Cu0.5 Mg alloy. The matrix rearrangement occurred through dynamic recrystallisation (DRX).

The equal-channel angular pressing (ECAP) method stands out as one of the most popular severe plastic deformation (SPD) methods, with extensive research conducted by various centres both in Poland and internationally. Investigations into the application of ECAP methods for the deformation of metals and alloys are undertaken at ambient temperatures as well as elevated temperatures. Researchers are also exploring modifications to the ECAP process to induce greater plastic deformation and achieve a more uniform microstructure across the cross-section, particularly when dealing with hard-to-deform materials. While this paper references only a subset of these studies, existing literature consistently demonstrates a substantial microstructure refinement following the ECAP process, accompanied by an increase in mechanical properties corresponding to the deformation size. Furthermore, an increase in the number of passes through the angular channel leads to the homogenisation of the microstructure.

4.1.3 Hydrostatic extrusion (HE)

In the hydrostatic extrusion method (Fig. 33), the billet material in the container is surrounded by a liquid medium, effectively minimising frictional forces. This allows for achieving significant plastic deformation with a simultaneous high strain rate (even exceeding 10^4 s^{-1}), resulting in a more homogeneous microstructure on the cross-section of the extruded ingot [111, 112]. The punch does not have direct contact with the ingot. The extrusion of the ingot material through the die occurs due to the high pressure of the surrounding liquid. A fundamental condition for the efficient operation of the press is the proper sealing of the liquid-filled space. Through the hydrostatic extrusion (HE) process, it is possible to obtain highly uniform microstructures with diverse shapes and cross-sections, such as rods, wires, and small tubes [113]. It is also an effective method leading to a significant increase in mechanical properties and substantial grain size reduction in many metals and alloys, including aluminium and aluminium alloys, copper, titanium, and steels [113–115]. The results presented in numerous studies demonstrate the high efficiency of the hydrostatic extrusion process and suggest the possibility of achieving similar results as with SPD methods using much higher plastic deformation.

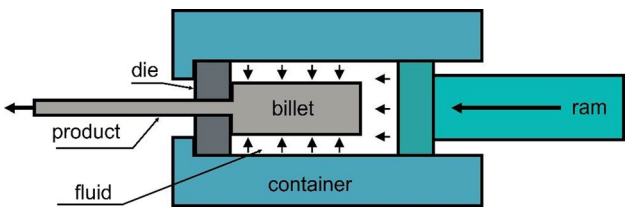

Fig. 33 Hydrostatic extrusion (HE) scheme ([98] open access)

Research carried out at the Faculty of Non-ferrous Metals in collaboration with the Unipress Institute of High Pressure Physics Polish Academy of Sciences in Warsaw focussed on the hydrostatic extrusion of aluminium (Al99.5) and copper (Cu99.99). Microstructural studies of these materials revealed the presence of elongated grains in the direction of extrusion, along with numerous bands and shear bands cutting through several grains and forming distinct jogs at the boundaries (see Fig. 34). The shear bands extend over considerable distances, reaching several hundred micrometres. Noticeable features include characteristic 'zigzags' and 'wavy' grain boundaries, providing evidence of significant shear deformations transmitted through the bands. Equally noteworthy is the intersection of bands and microbands, which occupy substantial volumes of the sample and proceed at different angles to the extrusion direction.

In the submicron range, microbands are present in the microstructure of aluminium and copper, exhibiting different types of dislocation structures. In aluminium, microbands appear against a background of subgrains, with the majority of interior microbands containing minimal or no dislocations. This absence of dislocations in aluminium suggests the occurrence of intensive microstructural renewal processes, likely taking place during or just after deformation. In copper, microbands were observed against a background of cellular dislocation structure. The cell walls were composed of dense dislocation tangles, while the interior of these cells was nearly free of dislocations. Notably, in copper deformed by hydrostatic extrusion, microbands tend to group into 'bundles' consisting of several microbands, running over considerable distances. The measured grain/subgrain size in aluminium averages $d = 0.6$ µm, while in copper, it ranges from $d = 0.2 \div 0.3$ µm. The proportion of large misorientation angles falls within the range of 40–90%, depending on the applied deformation. This considerable variation in the microstructure of aluminium and copper stems from a notable temperature increase in the microband region during hydrostatic extrusion at high strain rates. Under such conditions, adiabatic shear microbands can form, leading to dynamic recrystallisation phenomena. The basic triangles shown in Fig. 34b, e demonstrate that in both aluminium and copper, the intensity distributions concentrate around the <112> poles. The texture intensity maxima are 8.38 for aluminium and 11.50 for copper, respectively. Microhardness measurements revealed a twofold increase after the hydrostatic extrusion process in both aluminium and copper. The most significant changes in properties occurred at the initial stages of deformation, with subsequent changes

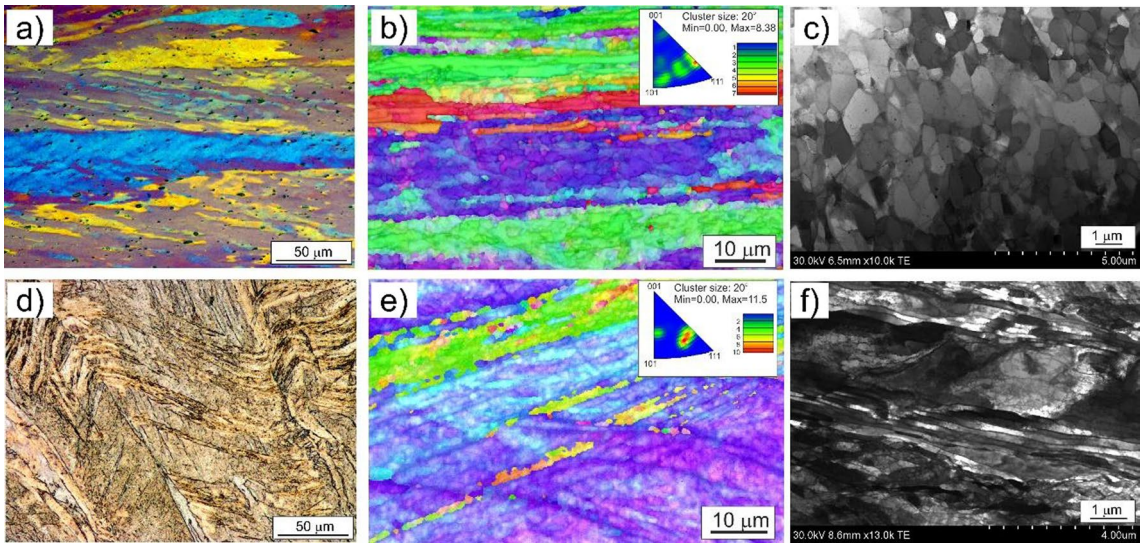

Fig. 34 Microstructure of Al99.5 and Cu99.99 deformed by hydrostatic extrusion (HE) process: **a** Al99.5, $\varepsilon = 1.44$: the image displays elongated grains in the extrusion direction, along with numerous bands and shear bands; **b** Al99.5, $\varepsilon = 2.68$: the image features an electron backscatter diffraction (EBSD) map and a basic triangle; **c** Al99.5, $\varepsilon = 3.18$: the image showcases dislocation-free subgrains; **d** Cu99.99, $\varepsilon = 1.88$: the image reveals numerous bands and jogs on the boundaries formed by shear bands passing through them; **e** Cu99.99, $\varepsilon = 2.24$: the image presents an EBSD map and a basic triangle; **f** Cu99.99, $\varepsilon = 3.68$: the image shows microbands in the vicinity of cellular structures ([98] open access)

being marginal. Tensile strength more than doubled after the hydrostatic extrusion process. In aluminium, a characteristic decrease in elongation with increasing strain rate is observed—at a strain rate of 10^4 s^{-1}, it is about 3%. In copper, elongation remains at a similar level throughout the entire deformation range (see Fig. 35).

In Poland, research on the hydrostatic extrusion process is primarily concentrated at the UNIPRESS Institute of High Pressure Physics Polish Academy of Sciences in Warsaw and the Warsaw University of Technology. Notably, scientists in South Korea have also contributed significantly to this field. Over the past few decades, numerous papers have been published on a variety of materials, including aluminium alloys, titanium alloys, niobium, and steel. In their paper [116], Lee et al. presented results on Al7.5 Mg alloys. Prior to the hydrostatic extrusion process, these alloys were produced from elementary powders milled at cryogenic temperatures and subsequently sintered using the hot isostatic pressing (HIP) method. The samples underwent extrusion with a cross-section reduction ratio of 9:1 at 400 °C. Following the hydrostatic extrusion process, porosity was nearly eliminated, and the grain size of the produced materials reached approximately $d = 0.3$ μm. In addition, a notable increase in mechanical properties and improved ductility

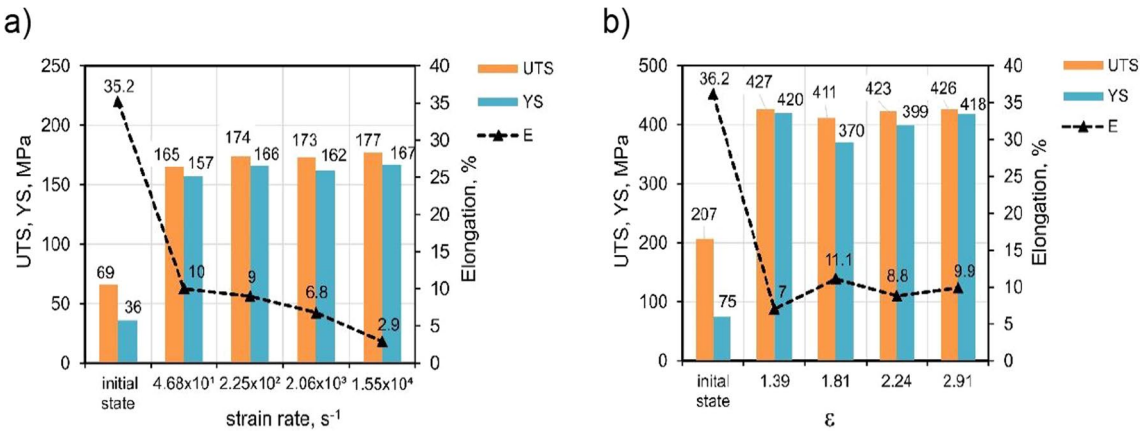

Fig. 35 Comparison of the mechanical properties of aluminium and copper after hydrostatic extrusion deformation: **a** Al99.5 deformed with a strain rate in the range of $10^1 \div 10^4$ s^{-1}; **b** Cu99.99 deformed with a constant strain rate of 3.68×10^2 s^{-1} ([98] open access)

were observed. The authors of paper [117] investigated the impact of hydrostatic extrusion combined with artificial ageing on the microstructure, mechanical, and electrical properties of the 6101 alloy (AlMgSi). The study revealed that the applied thermo-plastic processing was an effective method for producing wires with a grain size of 0.3–0.4 μm, characterised by high tensile strength (> 330 MPa) and increased electrical conductivity (up to 58% IACS). The mechanical properties of the alloy were notably influenced by the hydrostatic extrusion (HE) process parameters. In another study [118], results were presented for Niobium tubes extruded through hydrostatic extrusion with extrusion coefficients of 3.1 and 3.6, respectively. The authors focussed on texture, microstructure, and microhardness studies. The paper demonstrated an increase in the proportion of large misorientation angle fractions after the HE process, along with a proven elevation in microhardness. The relationship between grain size and Vickers hardness was consistent with the Hall–Petch relationship. The application of the hydrostatic extrusion process to the extrusion of titanium and titanium alloys has also garnered interest, as evidenced by results presented in papers [119–121], among others. Thanks to the application of the hydrostatic extrusion process, it is possible to obtain products characterised by small grain size and high mechanical properties. In the case of hydrostatic extrusion, it is feasible to produce items with dimensions that allow for further processing, and in the case of titanium, there are possibilities for medical applications. Considerable attention in the context of hydrostatic extrusion is dedicated to the deformation of various steel grades. Results related to the deformation of steel can be found, among others, in works [122–124].

In summary, based on the above considerations, it can be concluded that in materials deformed by severe plastic deformation (SPD) methods, the increase in mechanical properties results, among other factors, from grain refinement. Another common phenomenon is the occurrence of the so-called "softening" after exceeding a certain level of deformation, as confirmed by the research results mentioned above. The tensile strength of materials with a highly refined grain is significantly higher compared to their coarse-grained counterparts, suggesting changes in deformation mechanisms during deformation with high plastic deformation values. However, this high strength is associated with relatively low ductility in nanocrystalline materials [125–127]. Grain size influences mechanical properties, especially the yield stress. For polycrystalline materials with a grain size above 1 μm, this relationship is captured by the Hall–Petch equation:

$$\sigma_y = \sigma_0 + kd^{-\frac{1}{2}} \tag{1}$$

where σ_y is the yield strength, σ_0 and k are the constants, and d is the average grain size.

For grains smaller than 1 μm, the strength parameters are less dependent on grain size, and there is often a reversal of the Hall–Petch relationship. It is also possible to observe a "plateau" on the strengthening curves, as well as softening of the material due to grain refinement to nanometric or submicron sizes [125, 128].

Both the CEC and ECAP methods are conducted under conditions of low strain rates ranging from 10^{-3} to 10^{-2} s^{-1}. On the other hand, the application of hydrostatic extrusion allows for the deformation of materials at high strain rates, reaching up to 10^4–10^5 s^{-1}. At low strain rates ($10^{-4} \div 10^{-1}$ s^{-1}), as observed in the CEC and ECAP methods, heat is dissipated to the surroundings, and the deformation process can be treated as isothermal. Conversely, at high strain rates ($10^1 \div 10^5$ s^{-1}), such as in the case of the hydrostatic extrusion method, the deformation process is treated as adiabatic. In such cases, the heat generated leads to an increase in temperature, facilitating the acceleration of energy release stored in the material and consequently promoting microstructure renewal processes [98, 115].

A characteristic feature shared by materials deformed using methods such as CEC, ECAP, HE, and other forms of intense plastic deformation described in the literature is the formation of a microstructure comprised of nano- and ultrafine grains with significant misorientation. The saturation state also emerges after surpassing a specific deformation value, unique to each process. Sometimes, material softening is also observed. The size and shape of the formed nano-grains depend on the type of material being deformed. In pure metals, the resulting microstructural elements are larger due to the more favourable conditions for microstructure renewal processes compared to alloys, where the presence of precipitates may hinder the development of renewal processes. Moreover, both the material's strengthening level and grain size are influenced by additional factors such as the magnitude of the stacking fault energy (SFE), which dictates the plastic deformation mechanism, the kinetics of deformational strengthening, and the dislocation structure. Other significant factors include the presence of atoms in solution (solution strengthening) or the existence of particles (solution or dispersion strengthening). The final degree of strengthening in metals and alloys is determined only by the combined influence of all these factors.

4.2 KOBO extrusion process of metals and alloys

4.2.1 KOBO extrusion

The search for methods of obtaining advanced materials, the possibilities of their shaping, and achieving desired properties of products in economically justified processes

is the basis of modern engineering approach based on the latest achievements of scientific research. The KOBO extrusion process, classified as a part of the SPD (Severe Plastic Deformation) processes (Fig. 36), represents an innovative and attractive way of plastic shaping of various types of products, allowing for achieving very favourable deformation results both in terms of product properties and the costs of their production.

The KOBO extrusion method was developed and patented by its inventors: Andrzej Korbela and Włodzimierz Bochniak. This method of extruding metals and alloys, known from patent descriptions PL 168018, PL 174474, and U.S. Patent 5,737,959 (1998); European Patent 0.711.210 (2000) [129–131], involves periodically forcing a variable twisting in the shearing zone, due to the oscillatory, bidirectional rotation of the die along with the adjoining part of the extruded material. This adhesion is caused by irregularities made on the frontal surface of the die. This method allows for a reduction in the force required for extrusion, thus the power of the press, the possibility of extrusion without preheating the billet, increased degree of processing, and acceleration of the extrusion process. The extrusion parameters with twisting include temperature, speed, degree of processing, and primarily the angle and frequency of bidirectional twisting of the die, which also determine the mechanical properties of the products obtained in this way. According to scientific publications, e.g. 132, 133, the reason for the beneficial behaviour of metals and alloys during their extrusion with oscillatory twisting and achieving extraordinarily high-strength properties in the products made this way is the generation and therefore the permanent presence in the structure of point defects that exceed their equilibrium concentration by over ten orders of magnitude. This results in a drastic reduction in the viscosity coefficient of materials subjected to extrusion with twisting, down to the level of 10^6 [Pa s], justifying the reduced level of their strength properties during this process. On the other hand, an increase in these properties in the product occurs as a result of the

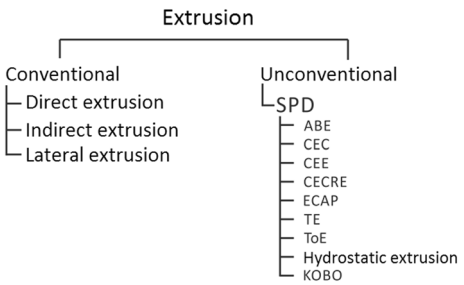

Fig. 36 Severe plastic deformation (SPD) methods (own source). ABE—Accumulative back extrusion, CEC—cyclic extrusion compression, CEE—cyclic expansion extrusion, CECRE—C-shape equal-channel angular extrusion, ECAP—equal-channel angular pressing, TE, twist extrusion, ToE, torsion extrusion

immediate formation of hardening clusters of point defects in the material leaving the die. Despite the attractive effects achieved by metals and alloys as a result of extrusion with twisting, initiating this process, understood as the start of plastic flow of material through the die, usually has to be preceded by a period of multiple, bidirectional twisting of the material, in order to acquire a sufficiently high concentration of point defects. The strong generation of point defects as a result of cyclic, bidirectional twisting of the material, followed by their diffusion to further parts of the billet, including those near the die, lowers the material's viscosity. Therefore, since the twisting affects the entire cross-section of the extruded material, in the initial stage of the process, it is accompanied by a high torque, which causes a strong load on the mechanical system of the press, high energy consumption, and increased wear of the press's working elements. Another innovative patent solution (PL 237 369 B1 from 2021 [134]) related to the KOBO process allows for a significant reduction in the time required to initiate the KOBO process, reduction of the initial high torque of the die, as well as the maximum extrusion force occurring in its initial stage. This results in lower energy consumption of the process and reduced wear of the press's working tools.

The effects induced by the plastic deformation of metal through axially symmetric extrusion using an oscillating die in the KOBO process are a result of changing the plastic deformation scheme, leading to a different state of stress than in conventional extrusion.

In the study [135], the possibility of controlling the localisation of plastic flow (shear bands) and the mechanical properties of metals (viscosity) during the plastic deformation process, which is suitably modified, was experimentally determined. This confirms the questioning of the nature of shear bands, mechanisms of their existence, and their morphological form. It was indicated that there are possibilities and certain conditions under which a layered plastic flow similar to rigid (lesser displacement) shearing deformation in metallic crystals can occur. The possible dominant role of point defects in structural processes (diffusion) and their impact on the mechanical properties of crystals (viscosity) was documented.

The results of research presented in the literature (e.g. [133, 136, 143]) also indicate that deformation by the KOBO method, under the same parameters, can lead to different microstructural responses, depending on the type and condition of the deformed metal. The suitability of using the KOBO extrusion process for metallic materials with different structures and properties, either to obtain a final product or to precede its further plastic processing, has been experimentally verified multiple times, as documented in many scientific papers [136, 137].

The main characteristic parameters for the KOBO extrusion process are room temperature of the billet and the

frequency and angle of oscillation of the die (Fig. 37). Different values for these parameters are provided in the literature. Typically, frequencies from 2 to 10 Hz and oscillation angles from 2 to 8 degrees are used.

The appropriate selection of these values for a given type of input material (ingot) allows for achieving the desired effect of plastic deformation, distinguished by a favourable microstructure and high mechanical properties close to uniformity.

KOBO extrusion offers possibilities for plastic shaping of metallic material inputs such as solid ingots, chips, or layered material (Fig. 38a–c) into rods or profiles.

Research on the effects of the process at various stages: at the front (F), in the middle (M), and at the end (E), as well as in the butt (Fig. 39), allows for the assessment of the uniformity of the internal structure and mechanical properties (strength, ductility, microhardness).

A characteristic feature is the appearance of the surface of products extruded by the KOBO method, revealing the texture of the surface resulting from the rotational movement of the shaping tool, i.e. the die (Fig. 40).

An important issue in designing the KOBO process for obtaining a specific type of product is not only the appropriate selection of process parameters but also the geometry of the die, as demonstrated in work [138]. Different geometric features of the frontal surface of the die induce different

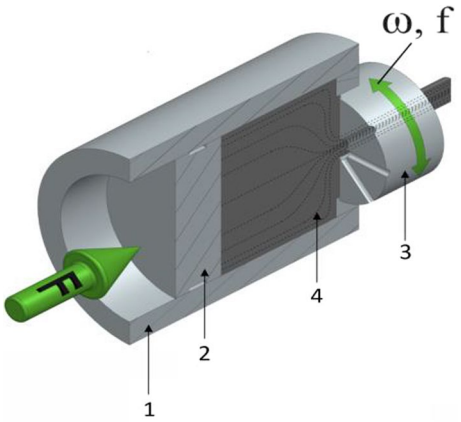

Fig. 37 Scheme of KOBO extrusion process: 1—container sleeve, 2—dummy billet, 3—die, 4—billet, ω, die oscillation angle, *f*, die oscillation frequency (own source)

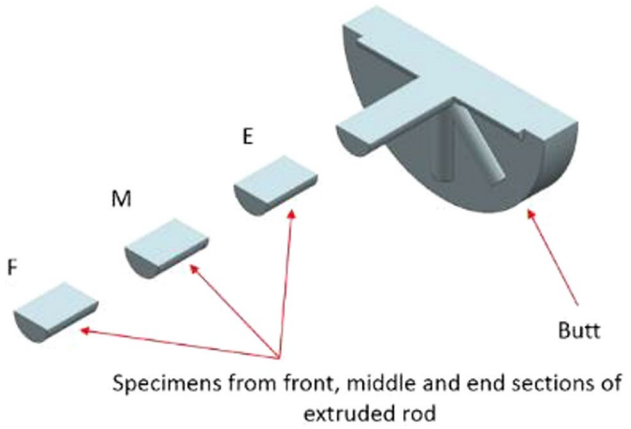

Fig. 39 Scheme showing the locations of specimens to analyse the structure and properties of products after the KOBO process (own source)

levels of extrusion force, which justifies the choice of a variant more favourable from the point of view of the expected reduction in maximum extrusion force (example shown in Fig. 41).

The maximum extrusion force in the KOBO process and the mechanical properties depend on the working parameters of the tool, namely the angle of deflection and primarily the frequency of oscillation of the die (Fig. 42).

The state of work shows that based on experimental results, the possibility of recycling waste chips from mechanical processing (e.g. of hard-to-deform aluminium alloys of the 2xxx and 7xxx series) into solid products without passing through a liquid phase has been demonstrated, using the low-temperature KOBO extrusion process. Research on the geometrical, mechanical, and structural characteristics of the products/pressings has confirmed their full consolidation and compliance with the requirements set for products extruded from ingots. Compared to other recycling methods, low-temperature extrusion of chips using the KOBO method represents a fully innovative, energy-efficient, and technologically attractive solution ("cold" process).

Based on experimental data in works [139, 140], the possibility of consolidating by-products of turning, milling, and drilling of aluminium alloys into the form and properties of solid metals using low-temperature KOBO extrusion was presented. Research on the mechanics and structural

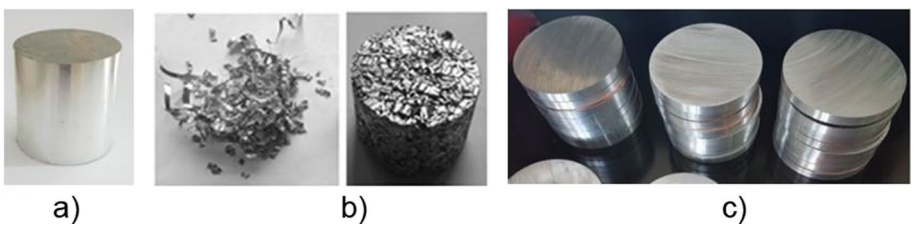

Fig. 38 Examples of input materials (ingots) for extrusion in the KOBO process: **a** solid ingot, **b** compacted chips, **c** layered ingot (e.g. Al/Cu) (own source)

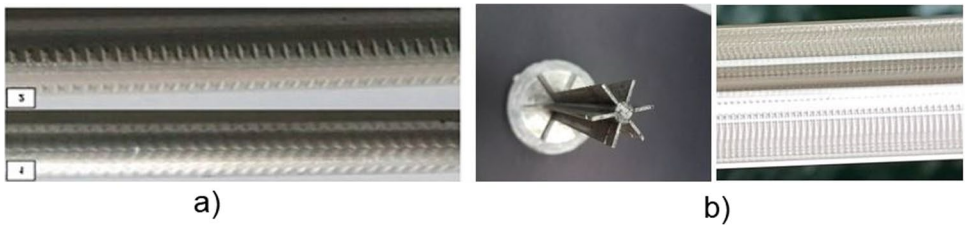

Fig. 40 View of the surface of products after extrusion by the KOBO method with characteristic texture due to the oscillation of the die (own source): **a** rods: 1—rod from solid ingot material, 2—rod obtained from scrap chips; **b** profile

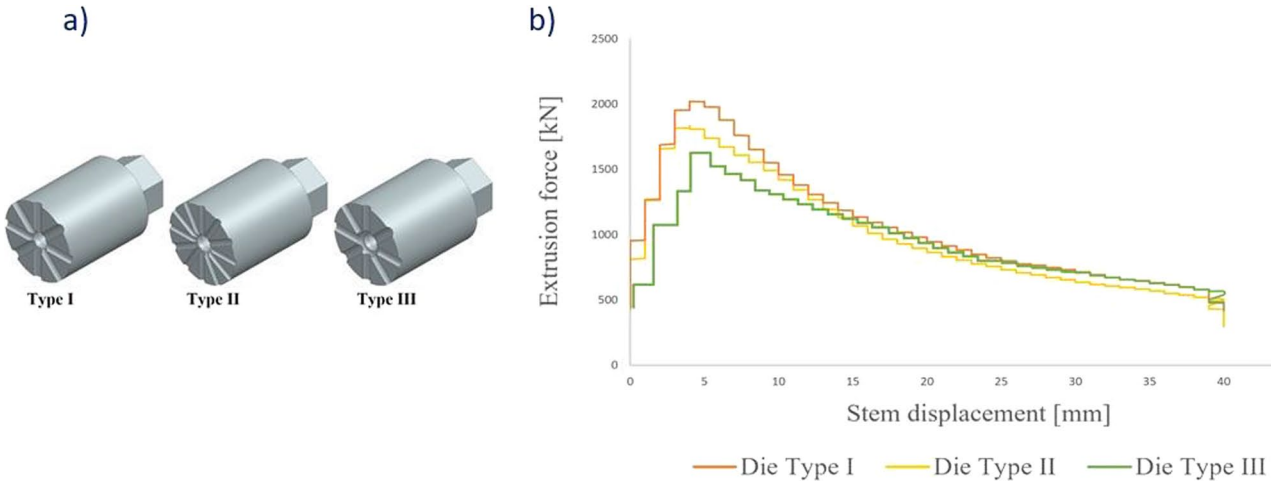

Fig. 41 Influence of die geometry on the KOBO extrusion force: **a** examples of dies type I, II, III, **b** extrusion force—stem displacement relationships ([138] open access)

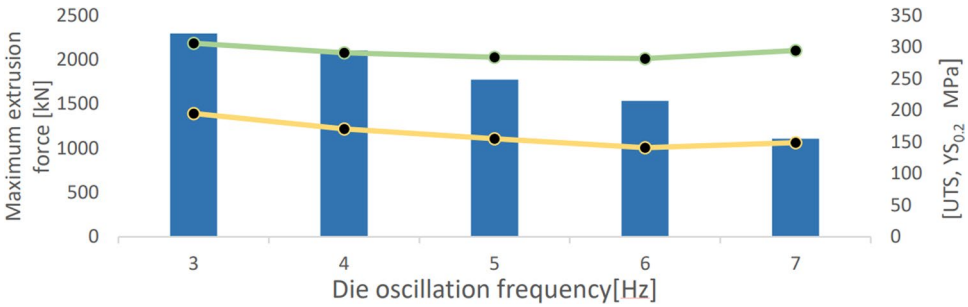

Fig. 42 The impact of the frequency of die oscillation on the value of the maximum KOBO extrusion force and the values of the yield strength YS and tensile strength UTS ([138] open access)

properties of the final products revealed their complete consolidation and proved their compliance with the requirements for products made from solid ingots. Importantly, the consolidation process does not require high or even elevated temperatures, which significantly reduces the costs of the process.

Some recycling technologies can also act as a reinforcement process, leading to improved mechanical properties of the recycled materials. The authors of work [141] provided an example that, compared to the raw material, a titanium sample that was processed and recycled exhibited a higher yield strength (from 355 to 375 MPa).

The parameters of the concurrent extrusion process of metals and alloys using the KOBO method (oscillating die with a specific frequency and angle of deflection) and the effects of the specific mechanical loading on structural phenomena indicate their distinctiveness compared to those occurring during conventional extrusion. This is especially true considering the impact of the geometric and material characteristics of the die, as well as the conducted analysis of the effectiveness of controlling process parameters in order to achieve the predetermined mechanical and structural properties of extruded products from input materials (ingots) of varying structure (solid material, composite layered material, chips).

Obtaining products in the KOBO process with functional properties, particularly strength and ductility, and essentially superplastic properties, positions this issue as highly

attractive with anticipation for solutions that will advance scientific research and technological applications. The matter concerning the design of dies for the KOBO extrusion process is particularly important and has not yet been sufficiently developed. This highlights the potential for innovation and improvement in this area, suggesting that further research and development could lead to significant advancements in the field of plastic processing of metals and alloys.

4.2.1.1 Microstructure The transformation of the microstructure of plastically deformed metallic materials under the conditions of the KOBO extrusion process ("cold" with oscillation of the die) depends on the type of metallic material (alloy), its form (cast metal, compacted chips, layered composite).

An example of the evolution of the structure of AZ91 magnesium alloy ingots, which were extruded using the KOBO method, is presented in paper [142]. This paper demonstrates grain refinement, a banded effect involving the elongation of individual structural elements such as the solid solution, the γ $Mg_{17}Al_{12}$ phase, eutectic and pre-eutectic, correlated with the direction of extrusion and revealing characteristic swirling flow lines resulting from the cyclic twisting of the extruded alloy. The use of the KOBO method allows for the plastic deformation of products made from the casting alloy ($MgAl_9Zn_1$) without homogenisation and preheating of the charge, i.e. at room temperature. The KOBO method enables us to drastically improve the mechanical properties (UTS, YS, A) of the AZ91 alloy ($MgAl_9Zn_1$) compared to the properties of sand casting.

The effects caused by the plastic deformation of metal through axisymmetric extrusion using an oscillating die in the KOBO process [143] result from a change in the plastic deformation scheme, leading to a different state of stress than in conventional extrusion. The results of research presented in the literature also indicate that deformation by the KOBO method, under the same parameters, can lead to different microstructural responses, depending on the type and condition of the deformed metal.

The analysis of the microstructure in different areas of the KOBO extruded product (Fig. 43) shows very fine grain and uniformity of structure on both the cross-sectional and longitudinal sections. The identified in KOBO extrusion superplastic type of metal flow enables to obtain a high-quality product, even with complex shapes. Low flow stress and lack of strain hardening under high strain conditions, which characterises superplastic flow, allows for deformation of hard alloys at low temperature. Modification of the

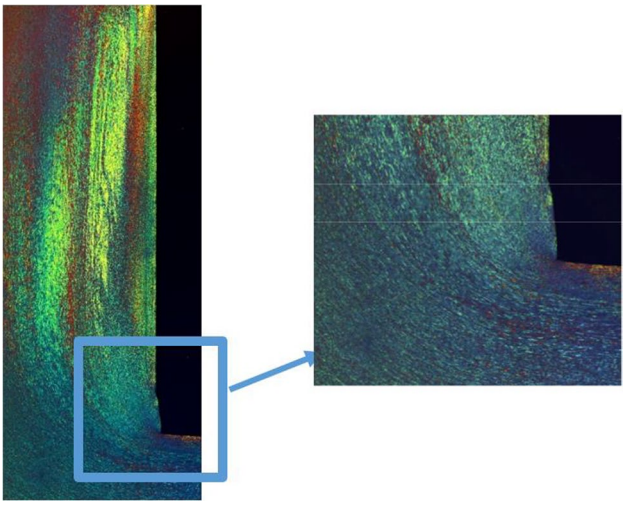

Fig. 44 Identification of the zone of intense plastic deformation of Al7075 in the KOBO extrusion process ([144] open access)

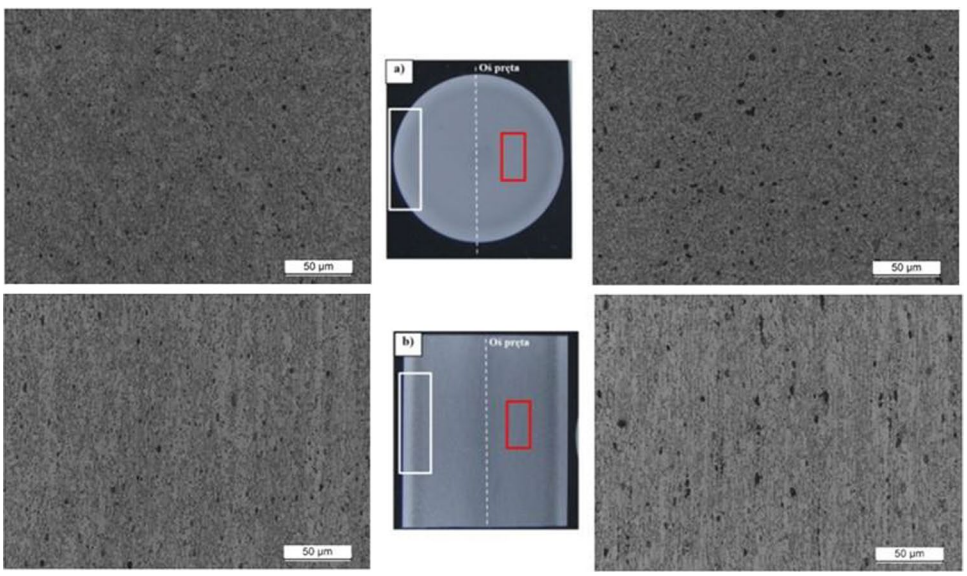

Fig. 43 Microstructure of the Al 7075 product extruded in the KOBO process in the surface area and inside the billet ([144] open access)

die geometry (with grooves) affects the extrusion forces making them lower. Characteristic metal flow in KOBO process is presented on Fig. 44. The geometric features of KOBO extrusion dies with different geometries have influence on the nature of plastic flow of the billet material and final structural, mechanical and geometrical characteristics of the extruded product and the level of extrusion force.

The KOBO extrusion using different die geometries showed significant differences in the flow scheme depending on the type of die. From the dies tested, the most preferred flow pattern was obtained using a Type III die, which is confirmed by the lowest extrusion force. The properties are the same in the entire volume of the product, there is no difference between front, middle and end part of the profiles**.** (Fig. 45).

4.2.2 Modelling

Due to the complexity of the plastic flow mechanics in the KOBO extrusion process, adequate modelling is difficult, and effects close to real results are achieved when the issue is formulated within a selected, narrowed range of analysis of the impact of a given factor, with assumptions formulated for this range, usually simplifying the problem.

In papers [145, 146], a modelling approach to predicting texture development in KOBO extrusion—an unconventional extrusion process assisted by cyclic twisting of the matrix—was proposed. The deformation field and trajectories of material points were determined for non-hardening material using the finite-element method. Subsequently, the evolution of the crystallographic texture was modelled along these trajectories. For this purpose, a micromechanical model combining a model of crystal plasticity and a coherent scheme of transition from grain scale to polycrystal was utilised.

The authors of paper [147] proposed a method for modelling an innovative and effective technique for manufacturing a bimetallic composite tube using the KOBO extrusion technique with an oscillating die. Compared to traditional extrusion, KOBO extrusion enabled the induction of high-frequency deformation path changes under the combined action of extrusion force and twisting moment. Numerical simulations of KOBO extrusion were conducted at extrusion speeds of 1, 2, 3 and 4 $mm \cdot s^{-1}$ and rotation frequencies of 2.5, 5, 8 and 10 Hz. It was demonstrated that through comprehensive analysis of the impact of rotational frequency and extrusion speed on reducing total energy consumption and increasing power conversion efficiency, it is advantageous to perform KOBO extrusion with a lower rotation frequency and higher extrusion speed, assuming the quality of forming the bimetallic concentric composite tube is guaranteed.

The impact of the characteristic plastic zone constituted in KOBO extrusion on the final properties of the product and the maximum extrusion force was illustrated, among others, in paper [148]. It presented numerical results of stress and strain distribution in the extruded material, as well as temperature increase caused by plastic work and friction. The shape of the plastic deformation zones was experimentally verified (Fig. 46). The approach presented constitutes a promising numerical tool for simulating the KOBO process.

4.3 Plastic consolidation in the hot extrusion process

4.3.1 Introduction

The development of modern materials engineering, due to the implementation of new manufacturing and material processing techniques, provides some opportunities to produce new material variants with new or modified functional properties. These materials are often based on the chemical composition of typical metal alloys, but because of a different processing technology, they are characterised by a modified structure, which causes a significant change in the mechanical and functional properties of the components manufactured from them. The processing technologies in question are plastic consolidation of loose materials (powders, flakes, chips), which fall under the broad field of powder metallurgy (PM).

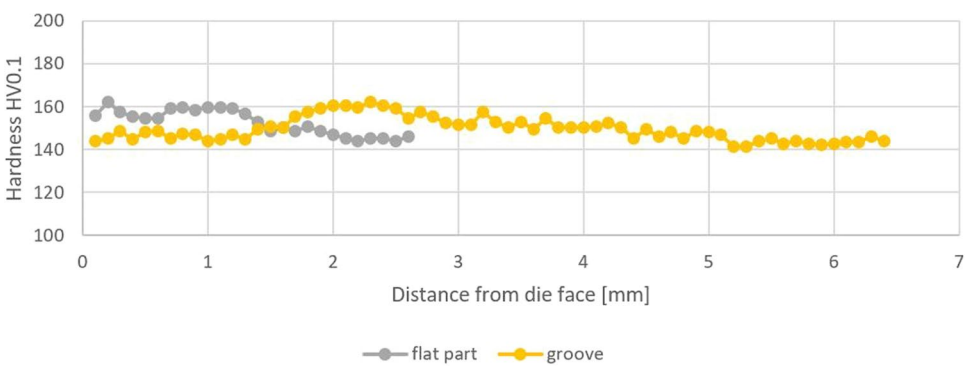

Fig. 45 Distribution of microhardness in the area of the plastic zone after extrusion using a die with grooves, extrusion of aluminium 2024 in the KOBO process: $V = 0.1$ mm/s, $\omega = \pm 8°, = 7$ Hz ([144] open access)

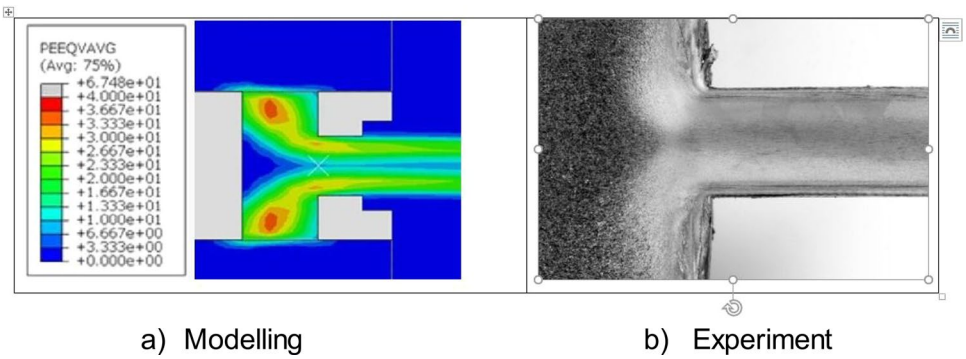

Fig. 46 Plastic deformation zone of M1E copper: **a** in the KOBO process model, **b** in experimental studies ([148] open access)

Methods of traditional powder metallurgy enable making new materials susceptible to plastic forming from materials with specific physical properties with the technology of pressing and sintering of powders/flakes. Currently, powder metallurgy methods are used to produce a variety of machine and equipment parts, including bearing materials, friction components, electrical contacts, indexable inserts and composites. The process of manufacturing materials/components by traditional powder metallurgy consists of three basic technological operations: production of output components, forming of shapes (pressing), and sintering.

Powder making involves a set of mechanical or physico-chemical processes aimed at obtaining a complex substance, mixture or chemical compound in powdered form. Those processes may consist in mechanical or physic-chemical grinding of a solid material, or obtaining a powder through chemical reactions [149].

On the one hand pressing is a way of combining loose powder particles, but on the other hand, a way of giving a suitable shape to the compact. During pressing, particles are regrouped, deformed (elastic, plastic deformation) or crushed [149].

The next stage is the sintering process. It is an important operation since it gives the right strength and density to a sinter. The main driving force behind the sintering process is the free energy of the powder surface and the stored strain energy, accumulated in lattice defects. Both of them are reduced during sintering, which leads to significant structural changes: spheroidisation of pores and their volumetric reduction, formation of necks between powder particles, polygonisation and recrystallisation within the volume of powder particles, which in turn, is associated with a significant reduction in lattice defects. Those phenomena, closely related to diffusive mass transport, can only take place under conditions of high atomic mobility, and therefore, at sufficiently high temperatures [149, 150].

In traditional powder metallurgy, the second (middle) stage, i.e. pressing, is usually carried out in single- or double-action dies (Fig. 47), where the densification of the powder material is determined by the amount of pressure applied

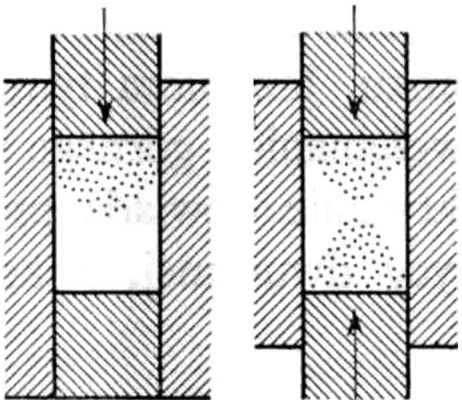

Fig. 47 Differences in density of a compact for one-sided and two-sided pressing (own source)

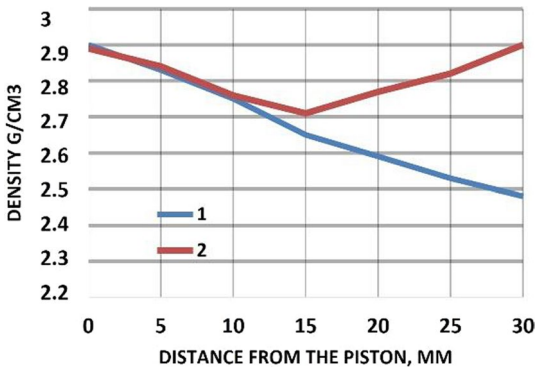

Fig. 48 A diagram of single-sided and double-sided pressing of powder AlCu6.5%—relation between the density and the distance from the piston. 1—powder pressed on one side, 2—powder pressed on both the sides (own source)

and the properties of the powder itself, e.g. granulation. This constitutes the major limitation in terms of both achievable densities and tool strength. With single-sided and double-sided pressing, there are some differences in the density of the compact obtained (Figs. 47, 48). Therefore, in order to achieve the same density throughout the entire volume of

the material, the most optimal technology is always being sought, i.e. a technology that could produce materials almost solid and with the properties desired.

Powder metallurgy technologies—which often have a better economic effect compared to other processing technologies—can provide high formability and a non-standard structure, and thus unique functional properties for the materials and products made. Thus, the use of powders/ribbons as feedstock creates new opportunities for the traditional aluminium industry, especially in the aerospace, engineering and automotive industries [151, 152].

4.3.2 Research

In recent years, various research initiatives have been undertaken so as to develop aluminium as well as aluminium alloys through powder metallurgy (APM). Some works focussed only on classical methods in the field of sintering technology for aluminium and its alloys [153, 154]. Other studies concerned the issues of more complicated processes, for example combined sintering processes and plastic processing with additional heat treatment of 2xxx and 7xxx series alloys [155], or research into the production of composites using powder metallurgy methods [156]. The main problem to be solved for the used aluminium powders and aluminium alloys is their passivation, a tough oxide layer on the powder surface which hinders fabrication and leads to poorer quality of APM products.

Any modification to any of those three PM stages allows obtaining materials with different functional properties. Within the issues aforesaid, various studies are under way now, for example, on different mixtures of elements or combinations of alloys as feedstock for powder processing. Research has been conducted using several combinations of pre-alloys such as Al–Cu, Al–Mg, Al–Si, Si–Mg, Cu–Si, and Cu–Mg in combination with aluminium powders of known oxide content [163]. This study was aimed at influencing the change in the material density after sintering, which, in turn, is strongly influenced by the aluminium oxide content and the chemical composition of the powders. It was shown that significantly better sintering effects with a smaller volume change are observed rather for alloy powders, not for mixtures of metal powders. Metallurgy of aluminium powders still constitutes a major challenge due to the presence of permanent oxide layers on aluminium particles. Unlike other metal oxides, especially of copper and iron, aluminium oxides do not undergo reduction during the sintering process. Solving the problem of the aluminium oxide layer is more difficult due to its stability, which causes the problem of wetting of particles by liquid phases and severely disrupts bridging between powder particles during the sintering process [157]. Nevertheless, there is a growing interest in sintered materials/composites made from naturally alumina-reinforced aluminium alloys, since this significantly increases the strength of the material itself or components made therefrom.

Another study under analysis evaluated the coupled effects of vacuum, pressure and temperature of the sintering process on the microstructure and mechanical properties of an APM aluminium alloy. Research was done for AA2024 alloy sputtered with nitrogen with an average particle sizes for three subgroups, respectively: Dv10 = 23.2 µm, Dv50 = 53.4 µm and Dv90 = 90.2 µm [158]. The morphology and the microstructure of the powder cross-section are shown in Fig. 49. Most of powder grains were almost spherical in shape with a rough surface, and the powder grain structure was typically dendritic. An analysis of the powder structure proved that alloying elements, such as Cu and Mg, were mainly concentrated at the dendritic boundaries.

The investigated aluminium alloy powder was pressed into $\varphi 40 \times 2$ mm disks at 450 MPa using a hydraulic press, and then hot sintered in graphite dies at 10 MPa under vacuum. The sintering process parameters were established basing upon previous studies [159, 160] and after differential scanning calorimetry (DSC) studies. Pressing temperatures of 500 °C and 575 °C were adopted, at low (LV) and high

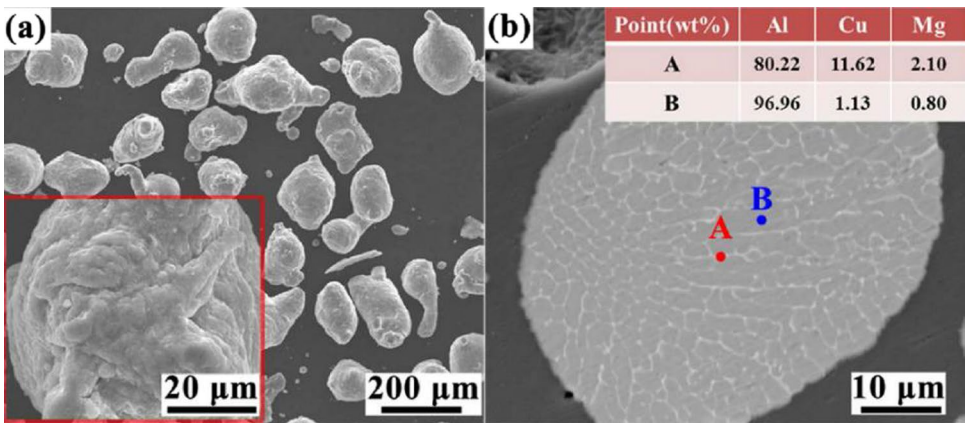

Fig. 49 AA2024 alloy powder: **a** grain morphology, **b** grain cross-sectional structure with a microanalysis of chemical composition [158]

(HV) vacuum [158]. The effect of the resulting density of materials and oxygen content in them is shown in Fig. 50.

It can be seen from the results in Fig. 50 that the density obtained at high vacuum was always higher than at low vacuum, whereas the oxygen content was the opposite. This can prove that pressure-assisted sintering had actually a positive effect on aluminium powders. An increase in temperature from 500 to 575 °C no longer improved the density obtained. At the same time, the oxygen content changed with increasing temperature, but still in accordance with the relationship that the oxygen content of aluminium sintered in low vacuum was higher than that of aluminium sintered in high vacuum [159]. Thus, the paper [160] showed that the quality of powder densification depends primarily on the plastic deformation of the powder during hot pressing, but also on the vacuum used. This arises from the fact that at high vacuum the oxide layers on the grains break more easily and the grains bond together better than at low vacuum.

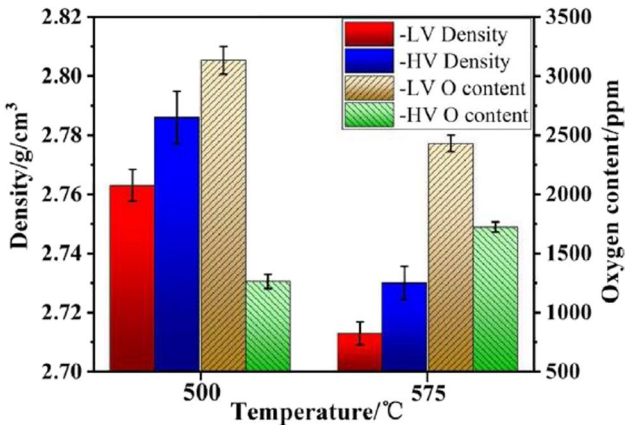

Fig. 50 Density and oxygen content of AA2024 alloy produced from powder as a function of temperature and vacuum value during the sintering process [158]

Sintering issues have been addressed in studies on pressure selection for this process. In paper [161], a novel low-pressure sintering process was proposed and its effectiveness investigated. The material studied was AA2024 alloy, whose powders were compacted at 400 MPa into 40 × 2 mm diameter compacts. Those compacts, placed in a graphite mould, were then sintered in a precision vacuum hot-press furnace. Three different sintering pressures were used, respectively: 0 MPa, 0.1 MPa and 10 MPa. The temperatures values chosen for sintering were: 525 °C and 575 °C. The results showed that in the case of non-pressure sintering (0 MPa), it was difficult to densify the compact and pores were still visible in the compacts. Low-pressure sintering (0.1 MPa) at 575 °C gave very good results where the material achieved a density of 2.732 g/cm^3, a tensile strength of 226 MPa and an elongation which provides a good equilibrium between workability and strength—Fig. 51 [162]. The authors assume that those results will bring new insights into the industrialisation of powder metallurgy of aluminium alloys.

Research into PM issues is also done for other, more modern methods, like spark plasma sintering. Spark plasma sintering (SPS) is a material processing technology in which powdered materials are assembled into parts by means of pressure and electric current applied simultaneously. In conventional powder metallurgy (PM), the densification and sintering processes are separate operations [149]. Atomised aluminium powders and aluminium with 0.4% Mg were processed using SPS and conventional PM steps. The tests carried out for both materials and technologies showed that the higher density of the materials obtained was the higher were the pressing pressure, temperature and sintering time. On the other hand, high temperature and long sintering time were unfavourable from the in view of hardness and the oxygen and hydrogen content in the material obtained [162]. An examination of the mechanical properties of the produced PM and SPS samples showed that both strength and ductility were significantly higher for the materials produced

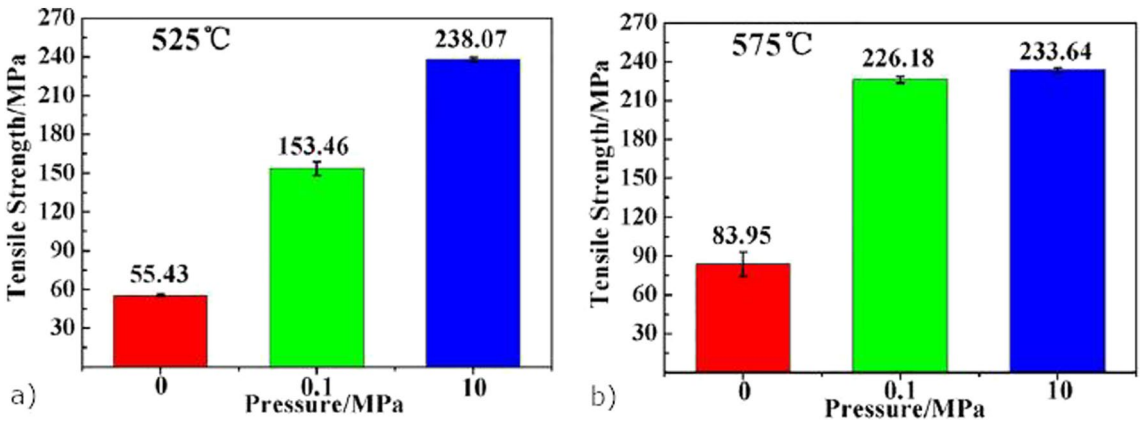

Fig. 51 Tensile properties of aluminium alloys that were sintered under different pressure states: **a** at temp. 525 °C; **b** at temp. 575 °C [162]

from Al and Al + 0.4 Mg powders using SPS technology—Fig. 52. The results of the measurement of residual oxygen and hydrogen content showed significantly lower contents in the SPS samples compared to their conventional PM counterparts [162].

The examples discussed demonstrate how various modifications of classical powder metallurgy (PM) processes affect the final properties of products. For this reason, many scientists and research centres are still conducting research so as to develop the most effective technologies for manufacturing materials and products from powders with defined properties. One of very popular technologies offering very good results is plastic consolidation of materials through hot extrusion [163, 164]. At the Institute of Non-Ferrous Metals, a number of studies have been conducted on the plastic consolidation of materials by means of hot extrusion. This process falls within the scope of traditional powder metallurgy whose methods, improved and modified over the years, have led to the isolation of a new way of producing materials. The process of plastic consolidation consists in extruding a pre-compacted material (formed into a compact so that it could be heated) at a specific temperature in a system of co-rotating or counter-rotating hot extrusion. The process essentially combines compaction and sintering with addition of plastic deformation of the material, which favours achieving higher densities and ultimately higher mechanical properties. Extruded sections or profiles, made of powder materials, can be either semi-finished products for further plastic forming or already are the final product [165]. Materials from Rapid Solidification processes (atomisation and melt-spinning) or even recycled materials can be used for plastic consolidation, which enables manufacturing alloys with a chemical composition that is impossible to obtain with classical metallurgical methods. This, in turn, creates conditions to produce materials with a set of new features.

The research dealt with AlCuMg alloys from the same 2xxx series of aluminium alloys as analysed in the works previously discussed. A new AlCuMg(ZrSc) alloy (Table 3) was obtained using the rapid solidification method in powder form by liquid-phase atomisation and in ribbon form by melt-spinning (Fig. 53a). The prepared materials were then subjected to plastic consolidation by hot extrusion process. This process consisted in cold pre-pressing (compaction), the purpose of which was to degas the powder, to maximise its initial compaction and to form a compact (Fig. 53b) that could be heated up to the pre-set temperature and loaded into the press container for further plastic consolidation in the hot extrusion process [163, 165]. Flowsheets of the processes discussed are shown in Fig. 53c.

For the plastic consolidation process in discussion, aluminium alloys of the 2xxx series were prepared with traditional methods (casted), as a comparative basis for materials

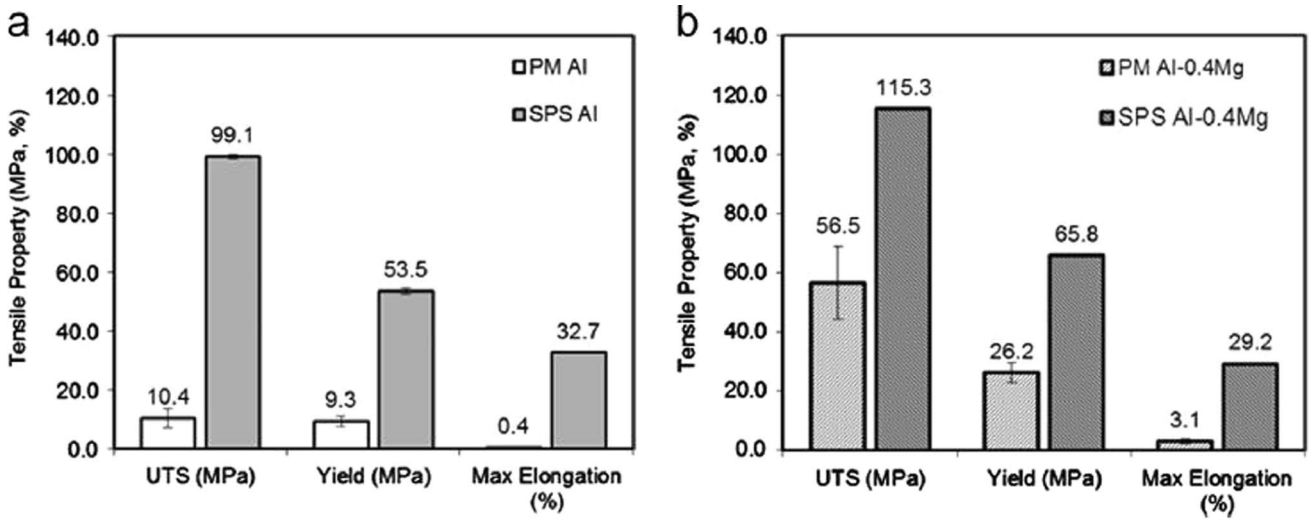

Fig. 52 Comparison of the tensile properties measured for materials prepared through conventional PM and SPS processing. **a** Al and **b** Al–0.4 Mg powders [162]

Table 3 Chemical compositions of alloys: AlCuMg and AlCuMgMn(ZrSc)

Alloy	Si	Fe	Cu	Mg	Zn	Ti	V	Sc	Zr
AlCuMg + ZrSc casted	0.04	0.13	6.41	0.25	0.02	0.08	0.11	0.23	0.34
AlCuMg(ZrSc) powder	0.03	0.06	6.5	0.35	0.03	0.08	0.12	0.25	0.36
AlCuMg(ZrSc) ribbons	0.03	0.06	6.42	0.30	0.03	0.08	0.12	0.25	0.36

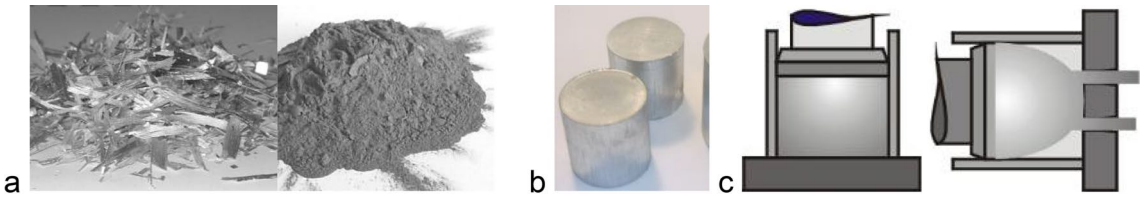

Fig. 53 Materials for the plastic consolidation process and its stages: **a** ribbons and powder, **b** pre-compacted materials, **c** pre-compaction and plastic consolidation (hot extrusion) [own source]

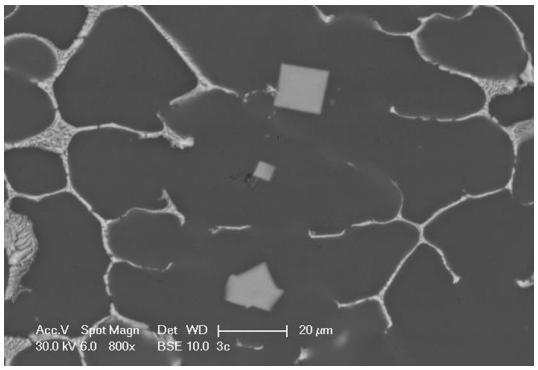

Fig. 54 Structure of extruded bars from alloy AlCu + ZrSc—SEM [own source]

produced by means of rapid solidification (atomisation and melt-spinning) methods—the respective chemical compositions are given in Table 3 [166].

The new reference alloy AlCu (classic) and AlCuMg(ZrSc) produced by rapid solidification methods in the form of powder and ribbons was characterised in terms of structure. The study was aimed at characterising the initial structure of rapidly crystallised materials, identifying and determining the dispersion of the Zr and Sc phases. In the study on the morphology, powder grains were found to be mostly spherical in shape. The obtained materials in the form of powders and ribbons have an ultrafine, homogeneous structure in which no large precipitations of zirconium or zirconium-scandium phases are observed, as found in materials produced with traditional methods (Fig. 54). A more extensive study of the structure was performed for bars extruded from the alloys under investigation after plastic consolidation (Figs. 55, 56). A series of transmission electron microscope images of the microstructure were analysed in special software for grain size. This resulted in obtaining grain size distribution histograms for the material after consolidation and in different heat treatment tempers, which

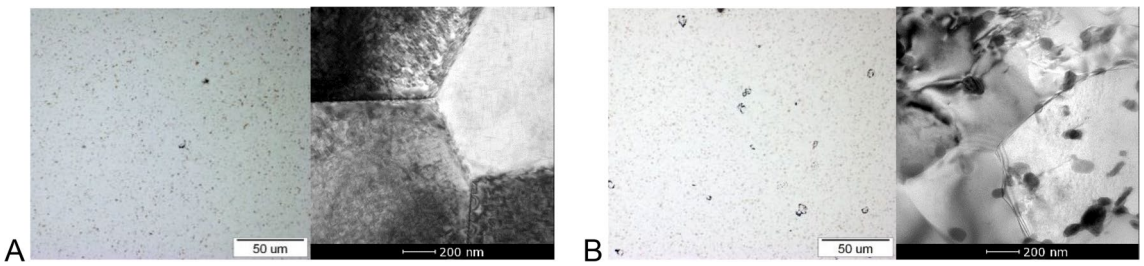

Fig. 55 Structures of extruded bars (temper F) from alloy AlCuMg(ZrSc) by optical microscope and TEM—**a** powder, **b** ribbons [own source]

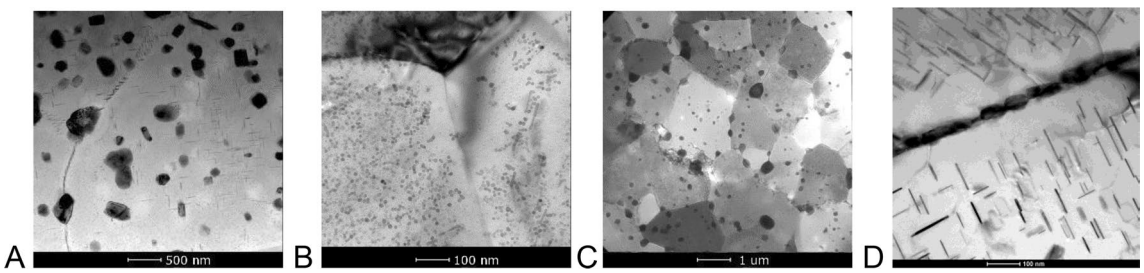

Fig. 56 Structures of extruded bars by TEM (temper T6) from alloy AlCuMg(ZrSc). **a**, **b** Powder, **c**, **d** ribbons [own source]

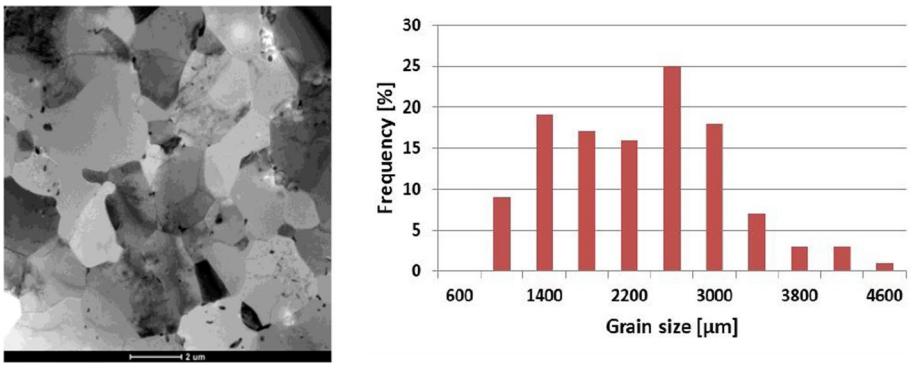

Fig. 57 An exemplary (TEM) microstructure of bars extruded from AlCuMg + ZrSc alloy produced with traditional methods in the temper *F* and a histogram of grain size distribution (average grain size 2400 nm) [own source]

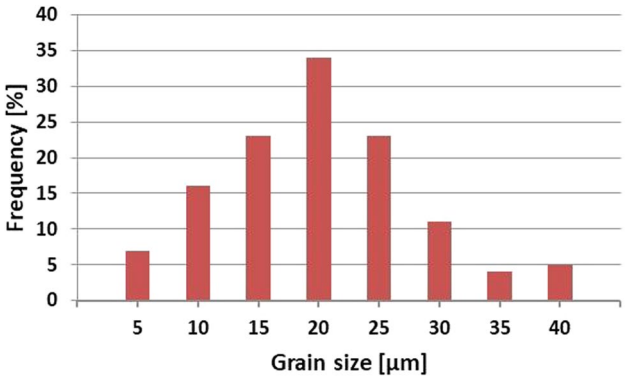

Fig. 58 Histogram of grain size distribution at bars extruded from AlCuMg + ZrSc alloy produced with traditional methods in the temper T6—average grain size 22 µm [own source]

were also compared with materials produced with traditional methods (Figs. 57, 58, 59, 60, 61, 62) [166].

The optical microscope images of the microstructure (Fig. 55) show individual pores in the material (mainly for the ribbon-consolidated material), but no large material defects. Large Zr or Sc precipitates that occur as cubes or needles for material produced by the classic casting method (Fig. 54) are not observed. Such large Zr or Sc separations eliminate such a material from the possibility of proper further plastic working. Therefore, this can prove that materials with such unusual chemical compositions cannot be produced in the classical way. Figures 55 and 56 with TEM show that in powders and ribbons of this type Zr and Sc separations are very fine, of nanometric size.

In the structure of the AlCuMg + ZrSc alloy produced by the traditional method (Fig. 57), observed are equiaxial grains, slightly elongated only locally. There is a high density of dislocations within the grains and at the boundaries, and a small number of large Zr/Sc precipitates < 500 um. After heat treatment to the temper T6, a finely dispersed Al_2Cu phase is observed inside the grains. Fine precipitates within grain boundaries and larger dispersed ones within and across the grain boundaries can be seen. A wide zone free of precipitates—approx. 150 nm. Average grain size, temper T6—22 µm.

For the new AlCuMg(ZrSc) alloy produced from ribbons (Fig. 58) in the extruded temper (F), equiaxial grains with low dislocation density inside are observed on the microstructures. Very fine phase separations with Cu content inside and at the grain boundaries. After heat treatment to temper T6, the grains are equiaxial with a large size dispersion. Fine dispersed Al_2Cu reinforcing phase within the grains. Numerous < 500 nm precipitates located at boundaries, along boundaries and within grains.

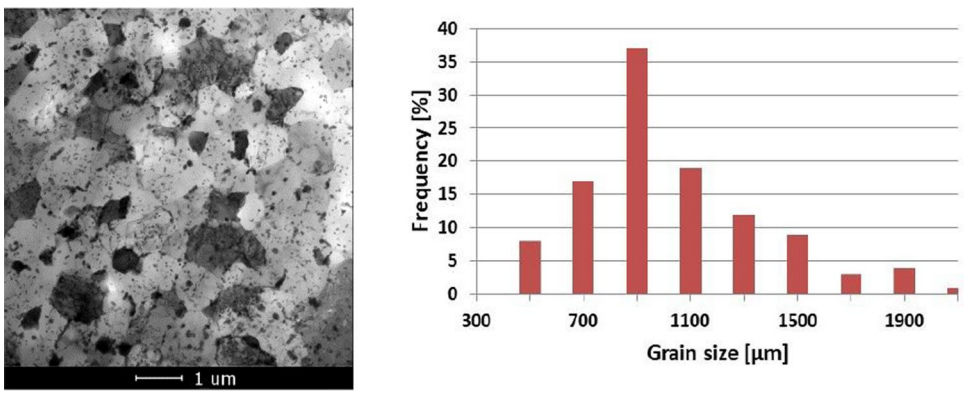

Fig. 59 An exemplary (TEM) microstructure of bars extruded from ribbons (AlCuMg(ZrSc) alloy) in the temper *F* and a histogram of grain size distribution (average grain size 940 nm) [own source]

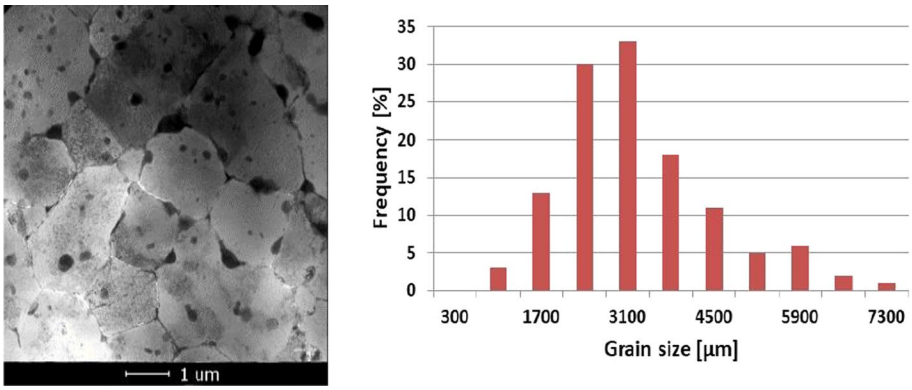

Fig. 60 An exemplary (TEM) microstructure of bars extruded from ribbons (AlCuMg(ZrSc) alloy) in the temper T6 and a histogram of grain size distribution (average grain size 3000 nm) [own source]

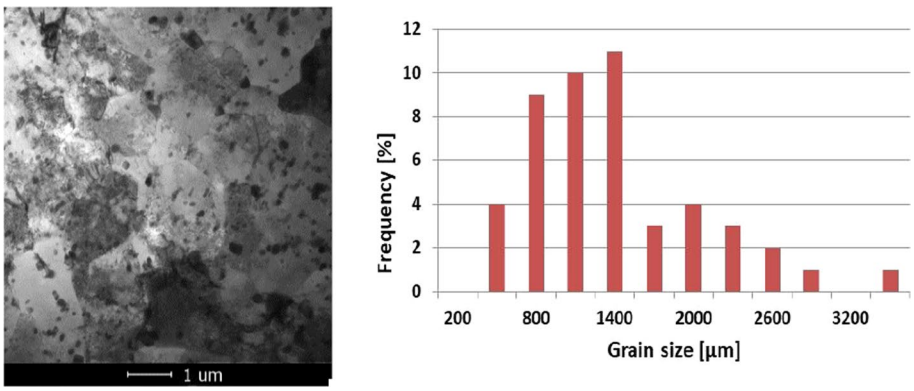

Fig. 61 An exemplary (TEM) microstructure of bars extruded from powder (AlCuMg(ZrSc) alloy) in the temper *F* and a histogram of grain size distribution (average grain size 1200 nm) [own source]

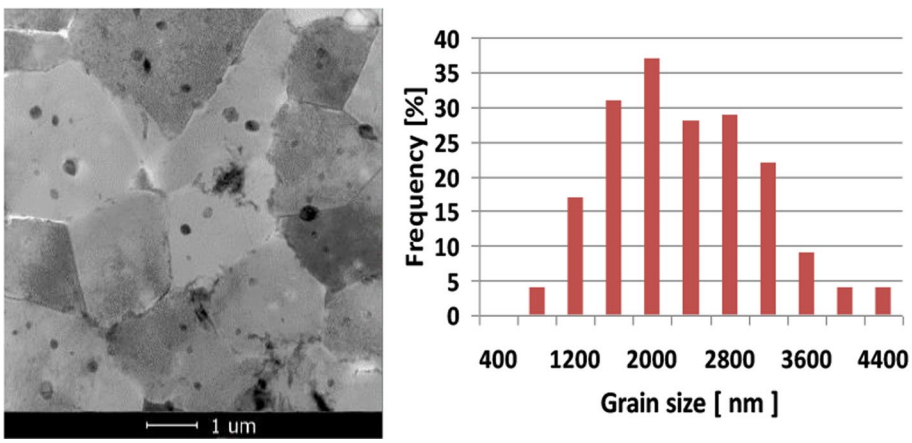

Fig. 62 An exemplary (TEM) microstructure of bars extruded from powder (AlCuMg(ZrSc) alloy) in the temper T6 and a histogram of grain size distribution (average grain size 2100 nm) [own source]

A precipitation-free zone in the range from approx. 100 to 200 nm. Average grain size, temper T6—3000 nm.

As far as AlCuMg(ZrSc) material produced from the powders (Fig. 59) in the extruded temper is concerned, observed are equiaxial grains with a high density of dislocations within and across the boundaries. Numerous large precipitates were observed on the analysed surface of the sample which contained GP zones as well as fine Al–Cu precipitates with Sc, Fe, and Zr content. Precipitates under 50 nm in shape, resembling coffee beans with Al, Zr and Sc content, were also noticed. After heat treatment to temper T6, equiaxial grains with a finely dispersed Al_2Cu phase inside and a narrow zone free of precipitates are observed. Precipitates occur along the grain boundaries as well as being coagulated and dispersed within the grains. In addition to the GP zones, the samples contained finely dispersed θ'-Al_2Cu precipitates formed into elongated disks (their occurrence confirms the heat treatment done). A large number of phases containing Mg, Fe, Sc, Zr, Ti,

V, Mn, Cr, and Ni, in addition to Al–Cu, were observed in the sample. Average grain size, temper T6—2100 nm.

An important part of the study was an evaluation of the mechanical properties of the bars in the extruded temper, after plastic consolidation and heat treatment. The results of those tests are shown in Table 4.

The results of the mechanical properties corroborate that, due to the presence of large Zr or Sc precipitates, the mechanical properties of a classically produced AlCuMg + ZrSc alloy are lower than those of an alloy of identical chemical composition, but produced by plastic consolidation in the hot powder extrusion procedure. On the one hand, this is due to the large precipitates, and on the other—to larger grains; Zr and Sc do not act as grain grinders.

5 Summary

On the basis of presented results, it may be stated that the current research works on homogenisation of precipitation hardenable aluminium alloys focus on designing of tailored process parameters for given composition. Often it is combined with selection of most favourable concentrations of main components. The advantages of such approach are maximisation of utilisation of additions taking part in precipitation hardening as well as reduction of consequences of transition elements microsegregation present in as-cast billets. The continuously growing requirements regarding extruded products properties as well as extrusion process efficiency, allow to expect that similar research will be continued for existing and new alloys. The advances in alloys composition design as well as in billets casting processes, changing current limitations of homogenisation parameters, will create the need for re-designing of previous homogenisation schedules. It may be expected that mathematical models of microstructure transformations, getting more and more advanced and reliable, will enable achieving this with reduced efforts spent on time- and cost consuming experimental work.

Magnesium alloys are lightweight materials and demonstrate the unique properties which are attractive for many applications, including aerospace crafts, automotive and sporting goods and others. The major factor in the widespread use of these alloys is their low density, which is noticeable lower than that of aluminium alloys. For example, the Mg–Li alloys are the lightest industrial metallic materials. On the other hand, the magnesium alloys containing rare-earth elements (WE), because of their superior corrosion resistance, are used in the aerospace engines instead of the aluminium alloys. The magnesium alloys can be successfully deformed by extrusion and forging. The future magnesium alloys applications are driven by the innovations in their metal forming. The first example can be the extrusions and forgings from the alloys containing rare-earth elements, which improve their mechanical and functional properties including corrosion resistance. The alloys with addition of lithium are also very attractive, as they create the lightest industrial metallic materials of about 1.4 g/cm^3. The crucial is also development of the new extrusion products of complex shape, such as hollow profiles produced with the use of the porthole dies, which are applicable in the aerospace and transport industry, the sports equipment and others.

Among the new development directions in the field of aluminium matrix composites, it is worth noting the work on recognising and mastering the technology of hot welding extrusion of hollow sections from aluminium matrix composites with the use of porthole dies. The use of porthole dies in the technology of extrusion of composites on an aluminium matrix creates new possibilities for the production of products of various shapes and properties. An important direction of development enabling the maximisation of strength properties of products from aluminium matrix composites is the use of deformation hardening in the production process.

Table 4 Exemplary mechanical properties of the tested classical and plastic-consolidated materials for different heat and thermo-mechanical treatment parameters

Alloy	Temper/type of heat or thermo-mechanical treatment	Yield [MPa]	UTS [MPa]	A [%]
AlCuMg + ZrSc	F—fabricated/extruded	202	274	18.2
	T6—solution heat treated and artificially aged	309	431	10.8
AlCuMg(ZrSc) powder	F—extruded/hot consolidated	207	293	16.1
	T6—solution heat treated and artificially aged	390	490	15.5
	T3—solution heat treated, 5% cold worked and naturally aged	354	404	8.2
	T8510—solution heat treated, cold annealing with controlled deformation 3% and artificial ageing	422	545	17.5
	T8—solution heat treated, 4% cold worked and then artificially aged	394	530	14.8
	T9—solution heat treated, artificially aged and then 3% cold worked	426	566	17.0

More and more innovative porthole dies for the extrusion of hollow high-component 6xxx alloy profiles with reduced wall thickness are proposed. The original design of the feeder, the maximum opening of the inlet channels and the reduction of the body surface area are used. This is the way to radical increase in metal exit speed from the die opening and the same to improve the effectiveness of manufacturing process using the cracking models of Cockroft–Latham and others. In case of hard deformable AlZnMg and AlZnMgCu alloys where we meet huge tools problems as a result of significant frictional resistance and also weldability problems of the alloy, here a compromise in die design is required, which will ultimately allow both the quality of the extruded product and the die strength/life and process/technology parameters to be achieved. One of the development directions is to introduce die inserts from the better steels produced by the technology of 3D printing.

The methods currently used in industry to increase the durability of aluminium extrusion tools, taking into account both conventional and innovative approaches, were discussed. An analysis of research on new technologies and solutions for improving tool durability shows that there is a real possibility of significantly extending tool life. Although developing new technologies and conducting research on them involves high costs and requires advanced expertise, the potential economic and operational benefits are obvious. Increasing tool life translates into more efficient production processes, which is key to remaining competitive in the market. Therefore, investment in scientific and technological development of new tool materials and processing methods is the basis for future progress and optimisation in the production of aluminium extrusion. The development of new protective coatings, 3D-printing technology for creating conformal cooling channels, and advanced surface engineering methods such as laser surfacing are opening up new perspectives for increasing tool life. Investment in R&D and scientific-industrial cooperation, is key to further development and innovation in light metal processing.

The characteristic feature that unites severe plastic deformation methods, especially those based on the extrusion process, is the formation of a microstructure consisting of nano- and ultrafine grains with a high misorientation. This occurs when a certain strain value, specific to each process, is exceeded, leading to the emergence of a saturated state. The size and shape of the nano-grains formed depend on the type of material being deformed. In pure metals, the microstructure elements formed are larger than in alloys, where the presence of precipitates may inhibit the development of microstructure renewal processes due to the greater ease of microstructure renewal. In materials deformed by SPD methods, it is important to determine the fraction of high angle boundaries, which significantly affects properties. In most cases, the fraction of high angle boundaries exceeds 50%. The level of mechanical properties obtained is related to the microstructure formed after deformation, and this is influenced, among other things, by the deformation method used. It is definitely impacted by the homogeneity of the microstructure, which usually increases with an increasing degree of deformation.

Since the inception of research on severe plastic deformation (SPD) methods, there has been an avalanche of publications, and conferences dedicated to this field have been organised. However, it must be acknowledged that technological development is still in its early stages. The focus of the work primarily revolves around fundamental microstructural research. Despite the extensive studies, no industrial sector has successfully implemented materials produced through SPD processes. The deciding factors for this include economic considerations and the relatively small dimensions of the manufactured products, making them less practical for industrial applications. This has prompted the search for new solutions, both in terms of tools and alternative processes that would allow for significant refinement of the microstructure in materials with larger dimensions, ultimately enabling their practical use. The use of a combination of deformation in a chosen SPD method, for example, with the hydrostatic extrusion process or solely the hydrostatic extrusion process, allows for the production of a final product in the form of rods, pipes, or other profiles with various end cross-sections and lengths depending on the size of the input material. Undoubtedly, this will facilitate the potential application of materials produced in this way, characterised by ultrafine grain size and high-strength properties, making them competitive with products manufactured using traditional plastic processing methods.

The use of the KOBO process, characterised by the oscillation of the tool, i.e. the die generating a variable deformation path, indicates a high potential for producing various types of products (rods, wires, profiles, etc.) with desired mechanical and structural properties. A comparison of this process in terms of energy expenditure with conventional methods clearly indicates the enormous potential of the process both in terms of lower energy levels, i.e. competitive lower implementation costs (a process with significantly lower energy requirements, lower extrusion force), and the quality of the shaped products (high uniformity of properties across the cross-section and along the length of the extruded product).

The initial structure of the investigated alloys, obtained from hot plastic consolidation of materials produced in the rapid solidification processes is ultrafine-grained. The grain size is twice as small as when the alloy is produced by the classic method (billet casting, extrusion). After heat treatment (solution and artificial ageing) to the temper T6, the grain size increases to an average size of 2–3 μm, but is then an order of magnitude smaller than for a standard

alloy. According to preliminary assumptions for the new AlCuMg(ZrSc) alloy plastically consolidated by hot extrusion from rapid solidification (powder) materials after thermo-mechanical treatment, obtained are higher mechanical properties than for typical AlCuMg + ZrSc alloys produced with conventional methods. The highest mechanical properties, while maintaining relatively high ductility, are obtained in this material for temper T8510 and T9 at a cold deformation of 3%. Compared to classical powder metallurgy as well as its various modifications as described, the process of plastic consolidation by hot extrusion enables manufacturing materials of almost any chemical composition, high density, very fine structure and high properties. It is, therefore, a future-proof technology for producing materials with new, non-standard properties.

Funding This study was funded by the National Centre for Research and Development in Poland (NCBR) Grant No. TECHMATSTRATEG-III/0017/2019—New coatings to increase tool life in forging and extrusion processes and Grant No. TECHMATSTRATEG2/406439/10/NCBR/2019—Extrusion welding of high-strength sections from 7xxx series aluminium alloys.

Declarations

Conflict of interest The authors declare no conflict of interest.

References

1. Wang Y, Hou L, Su H, Tian Q, Yu K, Eskin D, Katgerman L, Zhuang L. Tuning homogenization of high-strength aluminum alloys through thermodynamic alloying approach. Mater Des. 2022;221:110975. https://doi.org/10.1016/j.matdes.2022.110975.
2. Shu WX, Hou LG, Liu JC, Zhang C, Zhang F, Liu JT, Zhuang LZ, Zhang JS. Solidification paths and phase components at high temperatures of high-Zn Al–Zn–Mg–Cu alloys with different Mg and Cu contents. Metall Mater Trans A. 2015;46:5375–92. https://doi.org/10.1007/s11661-015-3050-x.
3. Priya P, Johnson DR, Krane MJM. Modeling phase transformation kinetics during homogenization of aluminum alloy 7050. Comput Mater Sci. 2017;138:277–87. https://doi.org/10.1016/j.commatsci.2017.06.043.
4. Woźnicki A, Leszczyńska-Madej B, Włoch G, Grzyb J, Madura J, Leśniak D. Homogenization of 7075 and 7049 aluminium alloys intended for extrusion welding. Metals (Basel). 2021;11:338. https://doi.org/10.3390/met11020338.
5. Woźnicki A, Leszczyńska-Madej B, Włoch G, Madura J, Bogusz M, Leśniak D. Homogenization of extrusion billets of a novel Al–Mg–Si–Cu alloy with increased copper content. Materials. 2023;16:2091. https://doi.org/10.3390/ma16052091.
6. Lin H, Zhu K, Liu Q, Chen L, Wang Z, Li X. Microstructural characterization of the as-cast and homogenized Al–Cu–Mg–Ag alloy. Materials. 2023;16:433. https://doi.org/10.3390/ma16010433.
7. Deng Y, Zhang Y, Wan L, Zhu AA, Zhang X. Three-stage homogenization of Al–Zn–Mg–Cu alloys containing trace Zr. Metall Mater Trans A. 2013;44:2470–7. https://doi.org/10.1007/s11661-013-1639-5.
8. Shan Z, Liu S, Ye L, Liu X, Dong Y, Li Y, Tang J, Deng Y, Zhang X. Effect of three-stage homogenization on recrystallization and fatigue crack growth of 7020 aluminum alloy. J Mark Res. 2020;9:13216–29. https://doi.org/10.1016/j.jmrt.2020.09.066.
9. Zhou H, Ding L, Liu M, Zeng Y, Lei X, Weng Y, Wang K, Jia Z. The effects of double-step homogenization on precipitation behavior of Al_3Zr dispersoids and microstructural evolution in 2196 aluminum alloy. Metals (Basel). 2023;13:1018. https://doi.org/10.3390/met13061018.
10. Li Z, Qin J, Zhang H, Wang X, Zhang B, Nagaumi H. Improved distribution and uniformity of α-Al(Mn, Cr)Si dispersoids in Al–Mg–Si–Cu–Mn (6xxx) alloys by two-step homogenization. Metall Mater Trans A. 2021;52:3204–20. https://doi.org/10.1007/s11661-021-06243-3.
11. Røyset J, Bauger Ø, Reiso O, Tundal U. Innovations in billet casting and homogenization. In: Proceedings of the 11th international aluminum extrusiontechnology seminar (ET'16), Chicago, IL, USA, n.d. p. 115–15.
12. Bayat N, Carlberg T, Cieslar M. In-situ study of phase transformations during homogenization of 6005 and 6082 Al alloys. J Alloys Compd. 2017;725:504–9. https://doi.org/10.1016/j.jallcom.2017.07.149.
13. Kumar S, Grant PS, O'Reilly KAQ. Evolution of Fe bearing intermetallics during DC casting and homogenization of an Al–Mg–Si Al alloy. Metall Mater Trans A. 2016;47:3000–14. https://doi.org/10.1007/s11661-016-3451-5.
14. Qin J, Nagaumi H, Yu C, Liu F, Li Y, Wang L. Coarsening behavior of Mg2Si precipitates during post homogenization cooling process in Al–Mg–Si alloy. J Alloys Compd. 2022;902:162851. https://doi.org/10.1016/j.jallcom.2021.162851.
15. Zeng Z, Stanford N, Davies CHJ, Nie J-F, Birbilis N. Magnesium extrusion alloys: a review of developments and prospects. Int Mater Rev. 2019;64:27–62. https://doi.org/10.1080/09506608.2017.1421439.
16. Pan F, Jiang B, Wang J, Hu Y, Luo S, Nie F, Birbiis N. High plasticity magnesium alloys. London: Elsevier; 2022.
17. Liu Z, Li L, Yi J, Li S, Wang G. Influence of extrusion speed on the seam weld quality in the porthole die extrusion of AZ31 magnesium alloy tube. Int J Adv Manuf Technol. 2017;92:1039–52. https://doi.org/10.1007/s00170-017-0200-x.
18. Negendank M, Sanabria V, Müller S, Reimers W. Extrusion of magnesium alloy hollow profiles with axial variable wall thickness; 2019: p. 030002. https://doi.org/10.1063/1.5112530.
19. Li L, Cao H, Qi F, Wang Q, Zhao N, Liu Y, Ye X, Ouyang X. Effect of heat treatment on microstructure and mechanical properties of Mg–5Zn–1Mn alloy tube. Metals (Basel). 2020;10:301. https://doi.org/10.3390/met10030301.
20. Zhong L, Wang Y, Dou Y. On the improved tensile strength and ductility of Mg–Sn–Zn–Mn alloy processed by aging prior to

extrusion. J Magn Alloys. 2019;7:637–47. https://doi.org/10.1016/j.jma.2019.07.007.
21. Calado LM, Carmezim MJ, Montemor MF. Rare earth based magnesium alloys—a review on WE series. Front Mater. 2022. https://doi.org/10.3389/fmats.2021.804906.
22. Gusieva K, Davies CHJ, Scully JR, Birbilis N. Corrosion of magnesium alloys: the role of alloying. Int Mater Rev. 2015;60:169–94. https://doi.org/10.1179/1743280414Y.0000000046.
23. Ghorbanpour S, McWilliams BA, Knezevic M. Effect of hot working and aging heat treatments on monotonic, cyclic, and fatigue behavior of WE43 magnesium alloy. Mater Sci Eng A. 2019;747:27–41. https://doi.org/10.1016/j.msea.2019.01.056.
24. Wu X, Xu C, Kuan J, Zhang Z, Zhang J, Yang W. Effects of hot extrusion temperature on mechanical and corrosion properties of Mg–Y–Zn–Zr biological magnesium alloy containing W phase and I phase. Materials. 2020;13:1147. https://doi.org/10.3390/ma13051147.
25. Xu W, Birbilis N, Sha G, Wang Y, Daniels JE, Xiao Y, Ferry M. A high-specific-strength and corrosion-resistant magnesium alloy. Nat Mater. 2015;14:1229–35. https://doi.org/10.1038/nmat4435.
26. Wang Y, Zhao G. Hot extrusion processing of Al–Li alloy profiles and related issues: a review. Chin J Mech Eng. 2020;33:64. https://doi.org/10.1186/s10033-020-00479-7.
27. Chen L, Zhao G, Chen G, Liang Z, Zhang C. Numerical simulation and experimental study on porthole die extrusion process of LZ91 Mg–Li alloy. Acta Metall Sin. 2018;54:339–46.
28. Ewa Śliwa R. Metal forming of magnesium alloys for various applications. In: Magnesium alloys structure and properties, IntechOpen; 2022. https://doi.org/10.5772/intechopen.101034.
29. Mussatto A, Ahad IU, Mousavian RT, Delaure Y, Brabazon D. Advanced production routes for metal matrix composites. Eng Rep. 2021. https://doi.org/10.1002/eng2.12330.
30. Nturanabo F, Masu L, Baptist Kirabira J. Novel applications of aluminium metal matrix composites. In: Aluminium alloys and composites. IntechOpen; 2020. https://doi.org/10.5772/intechopen.86225.
31. Bhoi NK, Singh H, Pratap S. Developments in the aluminum metal matrix composites reinforced by micro/nano particles—a review. J Compos Mater. 2020;54:813–33. https://doi.org/10.1177/0021998319865307.
32. Mistry JM, Gohil PP. Research review of diversified reinforcement on aluminum metal matrix composites: fabrication processes and mechanical characterization. Sci Eng Compos Mater. 2018;25:633–47. https://doi.org/10.1515/secm-2016-0278.
33. Feijoo I, Merino P, Pena G, Rey P, Cabeza M. Microstructure and mechanical properties of an extruded 6005A Al alloy composite reinforced with TiC nanosized particles and strengthened by precipitation hardening. Metals (Basel). 2020;10:1050. https://doi.org/10.3390/met10081050.
34. Zasadzińska M, Strzępek P, Mamala A, Noga P. Reinforcement of aluminium-matrix composites with glass fibre by metallurgical synthesis. Materials. 2020;13:5441. https://doi.org/10.3390/ma13235441.
35. Yi L-F, Kunimoto S, Ishii T, He L, Onda T, Chen Z-C. Improved mechanical properties of mechanically milled Mg2Si particles reinforced aluminum-matrix composites prepared by hot extrusion. Mater Sci Eng A. 2023;871:144904. https://doi.org/10.1016/j.msea.2023.144904.
36. Babu JSS, Lee CH, Kang CG. Study of the mechanical and workability properties of extruded aluminium (Al6061) based composites reinforced with MWCNTs. J Market Res. 2020;9:5278–92. https://doi.org/10.1016/j.jmrt.2020.03.054.
37. Li Z, Chen L, Zhang X, Zhao G, Zhang C. Strengthening mechanism and anisotropy of mechanical properties of Si3N4p/Al–Mg–Si composites fabricated by sintering and extrusion. Mater Des. 2021;210:110111. https://doi.org/10.1016/j.matdes.2021.110111.
38. Li Z, Chen L, Zhang X, Que B, Zhao G, Zhang C. Effects of TiB2 particle and local aspect ratio on microstructure and mechanical properties of an I-shaped TiB2/6061Al composite profile. Mater Sci Eng A. 2022;846:143284. https://doi.org/10.1016/j.msea.2022.143284.
39. Nittala A, Smith J, Gwalani B, Silverstein J, Kraft FF, Kappagantula K. Simultaneously improved electrical and mechanical performance of hot-extruded bulk scale aluminum–graphene wires. Mater Sci Eng B. 2023;293:116452. https://doi.org/10.1016/j.mseb.2023.116452.
40. Wu B, Peng Y, Tang H, Zhan Y, Zhang F. Microstructural evolution of nanodiamond-reinforced aluminum matrix composites during the process of hot extrusion. Ceram Int. 2023;49:9355–70. https://doi.org/10.1016/j.ceramint.2022.11.103.
41. Zasadziński J. Technological diagrams of manufacturing products of 6061 + SiC aluminum alloy composites, Rudy i Metale Nieżelazne 64; 2019.
42. DWA Aluminium Composites USA Inc. http://www.dwa-usa.com (n.d.).
43. Borowski J, Płaczek G, Jurczak H, Leśniak D, Libura W, Zasadziński J, Rękas A. Analysis of mechanical properties and dimensional accuracy of hollow thin-walled shapes extruded from AW6082 alloy. Metal Forming XXVI. 2016;I:7–20.
44. Liu Z, Li L, Li S, Yi J, Wang G. Simulation analysis of porthole die extrusion process and die structure modifications for an aluminum profile with high length-width ratio and small cavity. Materials. 2018;11:1517. https://doi.org/10.3390/ma11091517.
45. Xue X, Vincze G, Pereira A, Pan J, Liao J. Assessment of metal flow balance in multi-output porthole hot extrusion of AA6060 thin-walled profile. Metals (Basel). 2018;8:462. https://doi.org/10.3390/met8060462.
46. Yi J, Wang Z, Liu Z, Zhang J, He X. FE analysis of extrusion defect and optimization of metal flow in porthole die for complex hollow aluminum profile. Trans Nonferrous Met Soc China. 2018;28:2094–101. https://doi.org/10.1016/S1003-6326(18)64853-8.
47. Raknes CA, Welo T, Paulsen F. Dimensional accuracy of aluminium extrusions in mechanical calibration; 2018: p. 160024. https://doi.org/10.1063/1.5035050.
48. Donati L, Segatori A, Gamberoni A, Reggiani B, Tomesani L, Benchmark E. Effect of die design on profile quality and distortions of thin C-shaped hollow profiles. Mater Today Proc. 2017;10(2019):171–84. https://doi.org/10.1016/j.matpr.2018.10.394.
49. Truong TT, Hsu Q-C, Tong V-C, Sheu J-J. A design approach of porthole die for flow balance in extrusion of complex solid aluminum heatsink profile with large variable wall thickness. Metals (Basel). 2020;10:553. https://doi.org/10.3390/met10050553.
50. Mahmoodkhani Y, Wells MA, Parson NC, Chen J, Poole WJ. Influence of extrusion die bearing geometry on surface grain. In: ET'16: a clear vision for the future: proceedings of the twelfth international aluminium extrusion technology seminar & exposition; 2016.
51. Zhu H, Zhang X, Couper MJ, Dahle AK. The formation of streak defects on anodized aluminum extrusions. JOM. 2010;62:46–51. https://doi.org/10.1007/s11837-010-0077-8.
52. Yu J, Zhao G, Chen L. Analysis of longitudinal weld seam defects and investigation of solid-state bonding criteria in porthole die extrusion process of aluminum alloy profiles. J Mater Process Technol. 2016;237:31–47. https://doi.org/10.1016/j.jmatprotec.2016.05.024.

53. Crosio M, Hora D, Hora P. Experimental and numerical analysis of bonding criteria for seam welds during aluminium extrusion processes of hollow profiles, Zurich; 2019.
54. Kniazkin I, Vlasov A. Quality prediction of longitudinal seam welds in aluminium profile extrusion based on simulation. Proc Manuf. 2020;50:433–8. https://doi.org/10.1016/j.promfg.2020.08.079.
55. Wang Y, Wells MA. The effect of the bridge's angle during porthole die extrusion of aluminum AA6082. Metals (Basel). 2023;13:605. https://doi.org/10.3390/met13030605.
56. Robbins PH, Mahmoodkhani Y, Jowett C, Dickson R. Extrusion productivity: ram speed/die design/container. In: Proceedings of the ET'22 extrusion technology conference and exhibition, Orlando US; 2022.
57. Valberg H, Nolte D, Yawar K. Metal flow conditions in porthole channels of different size. Key Eng Mater. 2014;611–612:1005–12. https://doi.org/10.4028/www.scientific.net/KEM.611-612.1005.
58. Donati L, Ben Khalifa N, Tomesani L, Tekkaya AE. Effect of porthole design and welding chamber dimensions on material flow and weld deformability of extruded aluminium profiles. Key Eng Mater. 2012;504–506:523–8. https://doi.org/10.4028/www.scientific.net/KEM.504-506.523.
59. Lu FL, Song JS, Zhang J. Numerical simulation analysis on porthole dies extrusion of aluminum mini-thin harmonica-shaped tube. Appl Mech Mater. 2013;457–458:156–9. https://doi.org/10.4028/www.scientific.net/AMM.457-458.156.
60. Madura J. Analysis of extrusion of profile from 6005A alloy by using innovative porthole die constructions. Doctoral Thesis, AGH; 2023.
61. EN 755-2; Aluminium and aluminium alloys—extruded rod/bar, tube and profiles—part 2: mechanical properties.
62. 755-9; Aluminium and aluminium alloys—extruded rod/bar, tube and profiles—part 9: profiles, tolerances on dimensions and form.
63. Hsu Q-C, Chen Y-L, Lee T-H. Non-symmetric hollow extrusion of high strength 7075 aluminum alloy. Proc Eng. 2014;81:622–7. https://doi.org/10.1016/j.proeng.2014.10.050.
64. Chen G, Chen L, Zhao G, Zhang C, Cui W. Microstructure analysis of an Al–Zn–Mg alloy during porthole die extrusion based on modeling of constitutive equation and dynamic recrystallization. J Alloys Compd. 2017;710:80–91. https://doi.org/10.1016/j.jallcom.2017.03.240.
65. Pinter T. The influence of die design on productivity and recovery for an AA7020 hollow section. Light Metal Age; 2020.
66. Leśniak D, Zasadziński J, Libura W, Żaba K, Puchlerska S, Madura J, Balcerzak M, Płonka B, Jurczak H. FEM numerical and experimental study on dimensional accuracy of tubes extruded from 6082 and 7021 aluminium alloys. Materials. 2023;16:556. https://doi.org/10.3390/ma16020556.
67. Leśniak D, Libura W, Leszczyńska-Madej B, Bogusz M, Madura J, Płonka B, Boczkal S. FEM numerical and experimental work on extrusion welding of 7021 aluminum alloy. Materials. 2023;16:5817. https://doi.org/10.3390/ma16175817.
68. Leśniak D, Rekas A, Libura W, Zasadzinski J, Latos T, Jurczak H. Method for testing ability of metals or alloys and the device for producing welded samples for testing weldability of metals or alloys. Patent No PL230273B1, AGH Krakow; 2018.
69. Krumphals F, Wlanis T, Sievert R, Wieser V, Sommitsch C. Damage analysis of extrusion tools made from the austenitic hot work tool steel Böhler W750. Comput Mater Sci. 2011;50:1250–5. https://doi.org/10.1016/j.commatsci.2010.04.022.
70. Berrais A, Boudebane A, Labaiz M, Montagne A, Lemboub S, Touhami MZ, Ourdjini A. Analysis of wear of a nitrided AISI H13 hot work tool steel in an aluminium hot extrusion process. Wear. 2023;514–515:204587. https://doi.org/10.1016/j.wear.2022.204587.
71. Painter B, Shivpuri R, Altan T. Prediction of die wear during hot-extrusion of engine valves. J Mater Process Technol. 1996;59:132–43. https://doi.org/10.1016/0924-0136(96)02294-7.
72. Janus P. Surface modification of hydrostatic extrusion dies; 2004.
73. https://www.morgantechnicalceramics.com/en-gb/products/zirconia-ceramic-components/copper-and-brass-extrusion-dies/ (2022).
74. Lin Z, Juchen X, Xinyun W, Guoan H. Optimization of die profile for improving die life in the hot extrusion process. J Mater Process Technol. 2003;142:659–64. https://doi.org/10.1016/S0924-0136(03)00686-1.
75. He Y, Huang T, Wang Y, Nie Y, Li Y, Wang Y. A new lightweight design method integrating shape optimization with life cycle assessment for extrusion dies. J Clean Prod. 2017;150:47–57. https://doi.org/10.1016/j.jclepro.2017.02.186.
76. Qamar SZ, Sheikh AK, Arif AFM, Younas M, Pervez T. Monte Carlo simulation of extrusion die life. J Mater Process Technol. 2008;202:96–106. https://doi.org/10.1016/j.jmatprotec.2007.08.062.
77. Pelaccia R, Negozio M, Donati L, Reggiani B, Tomesani L. Efficiency of conformal cooling channels inserts for extrusion dies. Proc Manuf. 2020;47:209–16. https://doi.org/10.1016/j.promfg.2020.04.181.
78. Bertoli C. Optimization of hybrid extrusion dies with internal cooling channels, ETH; 2020.
79. Hölker R, Haase M, Ben Khalifa N, Tekkaya AE. Hot extrusion dies with conformal cooling channels produced by additive manufacturing. Mater Today Proc. 2015;2:4838–46. https://doi.org/10.1016/j.matpr.2015.10.028.
80. Appiah ANS, Bialas O, Żuk M, Czupryński A, Sasu DK, Adamiak M. Hardfacing of mild steel with wear-resistant Ni-based powders containing tungsten carbide particles using powder plasma transferred arc welding technology. Mater Sci Pol. 2022;40:42–63. https://doi.org/10.2478/msp-2022-0033.
81. Lu H, Cai J, Luo K, Xing F, Zhang Q, Yao J, Lu J. Thermal fatigue life and improvement mechanism of Fe-based coatings on H13 extrusion die by laser additive remanufacturing. Surf Coat Technol. 2021;408:126808. https://doi.org/10.1016/j.surfcoat.2020.126808.
82. Gronostajski Z, Widomski P, Kaszuba M, Zwierzchowski M, Hawryluk M. Influence of both hardfaced and nitrided layers on the durability of hot forging tools. Surf Innov. 2018;6:301–10. https://doi.org/10.1680/jsuin.18.00021.
83. Kaszuba M, Widomski P, Białucki P, Lange A, Boryczko B, Walczak M. Properties of new-generation hybrid layers combining hardfacing and nitriding dedicated to improvement in forging tools' durability. Arch Civ Mech Eng. 2020;20:78. https://doi.org/10.1007/s43452-020-00080-8.
84. Hubicki R, Richert M, Łebkowski P. Influence of operating temperature on the service life of aluminum extrusion dies. Materials. 2022;15:6656. https://doi.org/10.3390/ma15196656.
85. Pachutko B, Borowski J, Jurczak H. Studies of the wear processes of dies for aluminum profile extrusion with prototyped nitrided layers. Metal Forming-Obróbka Plastyczna Metali XXV (2014) 201–213.
86. Lukaszkowicz K, Dobrzanski LA, Kokot G, Ostachowski P. Characterization and properties of PVD coatings applied to extrusion dies. Vacuum. 2012;86:2082–8. https://doi.org/10.1016/j.vacuum.2012.04.025.
87. Maier J. Long term wear investigation on CVD coated extrusion dies; 2019.
88. https://wefa.com/en/coated-dies/ (2022).
89. Moscicki T, Psiuk R, Słomińska H, Levintant-Zayonts N, Garbiec D, Pisarek M, Bazarnik P, Nosewicz S, Chrzanowska-Giżyńska

J. Influence of overstoichiometric boron and titanium addition on the properties of RF magnetron sputtered tungsten borides. Surf Coat Technol. 2020;390:125689. https://doi.org/10.1016/j.surfcoat.2020.125689.
90. Valiev RZ, Islamgaliev RK, Alexandrov IV. Bulk nanostructured materials from severe plastic deformation. Prog Mater Sci. 2000;45:103–89. https://doi.org/10.1016/S0079-6425(99)00007-9.
91. Valiev RZ, Estrin Y, Horita Z, Langdon TG, Zechetbauer MJ, Zhu YT. Producing bulk ultrafine-grained materials by severe plastic deformation. JOM. 2006;58:33–9. https://doi.org/10.1007/s11837-006-0213-7.
92. Lowe TC, Valiev RZ. The use of severe plastic deformation techniques in grain refinement. JOM. 2004;56:64–8. https://doi.org/10.1007/s11837-004-0295-z.
93. Furukawa M, Horita Z, Nemoto M, Langdon TG. The use of severe plastic deformation for microstructural control. Mater Sci Eng A. 2002;324:82–9. https://doi.org/10.1016/S0921-5093(01)01288-6.
94. Segal V. Review: modes and processes of severe plastic deformation (SPD). Materials. 2018;11:1175. https://doi.org/10.3390/ma11071175.
95. Richert J, Richert M, Zasadziński J, Korbel A. Mode of plastic deformation of metals and alloys and the equipment for plastic deformation of metals and alloys. PL 181 693; 1979.
96. Richert M. Engineering of nanomaterials and ultrafine-grained structures. Kraków: AGH University Press; 2006.
97. Richert J. Innovative methods of metal forming. Kraków: AGH University Press; 2010.
98. Leszczyńska-Madej B. Methods of grain refinement by intensive plastic deformation methods. Kraków: Wzorek Press; 2013.
99. El-Garhy G, El Mahallawy N, Shoukry MK. Effect of grain refining by cyclic extrusion compression (CEC) of Al-6061 and Al-6061/SiC on wear behavior. J Market Res. 2021;12:1886–97. https://doi.org/10.1016/j.jmrt.2021.03.114.
100. Huang H, Tang Z, Tian Y, Jia G, Niu J, Zhang H, Pei J, Yuan G, Ding W. Effects of cyclic extrusion and compression parameters on microstructure and mechanical properties of Mg–1.50Zn–0.25Gd alloy. Mater Des. 2015;86:788–96. https://doi.org/10.1016/j.matdes.2015.07.155.
101. Guo W, Wang Q, Ye B, Li X, Liu X, Zhou H. Microstructural refinement and homogenization of Mg–SiC nanocomposites by cyclic extrusion compression. Mater Sci Eng A. 2012;556:267–70. https://doi.org/10.1016/j.msea.2012.06.086.
102. Richert M, Stüwe HP, Zehetbauer MJ, Richert J, Pippan R, Motz Ch, Schafler E. Work hardening and microstructure of AlMg5 after severe plastic deformation by cyclic extrusion and compression. Mater Sci Eng A. 2003;355:180–5. https://doi.org/10.1016/S0921-5093(03)00046-7.
103. Richert MW, Richert J, Leszczyńska-Madej B, Kuczek Ł, Wzorek Ł. AgSnBi powder consolidated by CEC reciprocal extrusion. Arch Civ Mech Eng. 2014;14:580–5. https://doi.org/10.1016/j.acme.2014.04.002.
104. Siahsarani A, Faraji G. Hydrostatic cyclic extrusion compression (HCEC) process; a new CEC counterpart for processing long ultrafine-grained metals. Arch Civ Mech Eng. 2020;20:108. https://doi.org/10.1007/s43452-020-00115-0.
105. Siahsarani A, Faraji G. Processing and characterization of AZ91 magnesium alloys via a novel severe plastic deformation method: hydrostatic cyclic extrusion compression (HCEC). Trans Nonferrous Met Soc China. 2021;31:1303–21. https://doi.org/10.1016/S1003-6326(21)65579-6.
106. Segal VM. Severe plastic deformation: simple shear versus pure shear. Mater Sci Eng A. 2002;338:331–44. https://doi.org/10.1016/S0921-5093(02)00066-7.
107. Segal VM. Materials processing by simple shear. Mater Sci Eng A. 1995;197:157–64. https://doi.org/10.1016/0921-5093(95)09705-8.
108. Injor OM, Daramola OO, Adewuyi BO, Adediran AA, Ramakokovhu MM, Sadiku RE, Akinlabi ET. Grain refinement of Al–Zn–Mg alloy during equal channel angular pressing (ECAP). Results Eng. 2022;16:100739. https://doi.org/10.1016/j.rineng.2022.100739.
109. Jiang J, Jiang F, Zhang M, Yi K. Microstructure evolution and tensile property of deformed Al–Mg–Sc alloy: comparison of ECAP and FSP. J Mark Res. 2023;22:2612–26. https://doi.org/10.1016/j.jmrt.2022.12.109.
110. Liu H, Ye L, Ren K, Sun C, Zhuo X, Yan K, Ju J, Jiang J, Xue F, Bai J. Evolutions of CuZn5 and Mg2Zn11 phases during ECAP and their impact on mechanical properties of Zn–Cu–Mg alloys. J Mark Res. 2022;21:5032–44. https://doi.org/10.1016/j.jmrt.2022.11.095.
111. Jeong HG, Yoon DJ, Kim EZ, Park HJ, Na KH. The influence by hydrostatic extrusion on the microstructure and extrudability of the IM processed hypereutectic Al–Si–X alloys. J Mater Process Technol. 2002;130–131:438–43. https://doi.org/10.1016/S0924-0136(02)00714-8.
112. Lewandowska M. Mechanism of grain refinement in aluminium in the process of hydrostatic extrusion. Solid State Phenom. 2006;114:109–16. https://doi.org/10.4028/www.scientific.net/SSP.114.109.
113. Widlicki P, Garbacz H, Lewandowska M, Pachla W, Kulczyk M, Kurzydlowski KJ. The influence of hydrostatic extrusion on the microstructure of 6082 aluminium alloy. Solid State Phenom. 2006;114:145–50. https://doi.org/10.4028/www.scientific.net/SSP.114.145.
114. Lewandowska M, Kurzydlowski KJ. Recent development in grain refinement by hydrostatic extrusion. J Mater Sci. 2008;43:7299–306. https://doi.org/10.1007/s10853-008-2810-z.
115. Lewandowska M. Kształtowanie mikrostruktury i właściwości stopów aluminium metodą wyciskania hydrostatycznego, Oficyna Wydawnicza Politechniki Warszawskiej, Warszawa; 2006.
116. Lee S, Yoon CY, Park HJ, Kim SS, Kim EJ, Choi TH, Rhee KY. A study of hydrostatic extrusion as a consolidation process for fabricating ultrafine-grained bulk Al–Mg alloy. J Mater Process Technol. 2007;191:396–9. https://doi.org/10.1016/j.jmatprotec.2007.03.085.
117. Majchrowicz K, Pakieła Z, Chrominski W, Kulczyk M. Enhanced strength and electrical conductivity of ultrafine-grained Al–Mg–Si alloy processed by hydrostatic extrusion. Mater Charact. 2018;135:104–14. https://doi.org/10.1016/j.matchar.2017.11.023.
118. Lee J, Jeong H, Park S. Effect of extrusion ratios on hardness, microstructure, and crystal texture anisotropy in pure niobium tubes subjected to hydrostatic extrusion. Trans Nonferrous Met Soc China. 2021;31:1689–99. https://doi.org/10.1016/S1003-6326(21)65608-X.
119. Moreno-Valle EC, Pachla W, Kulczyk M, Savoini B, Monge MA, Ballesteros C, Sabirov I. Anisotropy of uni-axial and bi-axial deformation behavior of pure Titanium after hydrostatic extrusion. Mater Sci Eng A. 2013;588:7–13. https://doi.org/10.1016/j.msea.2013.08.044.
120. Garbacz H, Semenova I, Zherebtsov S, Motyka M. Nanocrystalline titanium. 1st ed. London: Elsevier; 2018.
121. Topolski K, Pachla W, Garbacz H. Progress in hydrostatic extrusion of titanium. J Mater Sci. 2013;48:4543–8. https://doi.org/10.1007/s10853-012-7086-7.
122. Maj P, Adamczyk-Cieślak B, Mizera J, Pachla W, Kurzydłowski KJ. Microstructure and mechanical properties of duplex stainless steel subjected to hydrostatic extrusion. Mater Charact. 2014;93:110–8. https://doi.org/10.1016/j.matchar.2014.03.017.

123. Pachla W, Skiba J, Kulczyk M, Przybysz S, Przybysz M, Wróblewska M, Diduszko R, Stępniak R, Bajorek J, Radomski M, Fąfara W. Nanostructurization of 316L type austenitic stainless steels by hydrostatic extrusion. Mater Sci Eng A. 2014;615:116–27. https://doi.org/10.1016/j.msea.2014.07.069.
124. Zdunek J, Maj P, Kulczyk M, Mizera J. Texture, residual stresses and mechanical properties analysis in the commercial 1.4462 duplex stainless steel subjected to hydrostatic extrusion. Arch Civ Mech Eng. 2019;19:525–34. https://doi.org/10.1016/j.acme.2018.12.008.
125. Valiev RZ, Alexandrov IV, Zhu YT, Lowe TC. Paradox of strength and ductility in metals processed bysevere plastic deformation. J Mater Res. 2002;17:5–8. https://doi.org/10.1557/JMR.2002.0002.
126. Pozdnyakov VA. Ductility of nanocrystalline materials with a bimodal grain structure. Tech Phys Lett. 2007;33:1004–6. https://doi.org/10.1134/S1063785007120061.
127. Zhu YT, Wu XL. Ductility and plasticity of nanostructured metals: differences and issues. Mater Today Nano. 2018;2:15–20. https://doi.org/10.1016/j.mtnano.2018.09.004.
128. Meyers MA, Mishra A, Benson DJ. Mechanical properties of nanocrystalline materials. Prog Mater Sci. 2006;51:427–556. https://doi.org/10.1016/j.pmatsci.2005.08.003.
129. Korbel A, Bochniak W. Method of extruding materials, PL168018; 1995.
130. Korbel A, Bochniak W. Method of extrusion of products especially metallic, PL174474; 1998.
131. Korbel A, Bochniak W. Method of plastic forming of materials, 5.737.959; 1998.
132. Korbel A, Bochniak W. Lüders deformation and superplastic flow of metals extruded by KOBO method. Phil Mag. 2013;93:1883–913. https://doi.org/10.1080/14786435.2013.765977.
133. Korbel A, Bochniak W, Ostachowski P, Błaż L. Visco-plastic flow of metal in dynamic conditions of complex strain scheme. Metall Mater Trans A. 2011;42:2881–97. https://doi.org/10.1007/s11661-011-0688-x.
134. Śliwa RE, Bochniak W, Korbel A. Method of lowering the die torque in the initial stage of the extrusion process with oscillatory twisting of metallic materials. PL237369; 2021.
135. Korbel A, Bochniak W. Stratified plastic flow in metals. Int J Mech Sci. 2017;128–129:269–76. https://doi.org/10.1016/j.ijmecsci.2017.04.006.
136. Gronostajski Z, Pater Z, Madej L, Gontarz A, Lisiecki L, Łukaszek-Sołek A, Łuksza J, Mróz S, Muskalski Z, Muzykiewicz W, Pietrzyk M, Śliwa RE, Tomczak J, Wiewiórowska S, Winiarski G, Zasadziński J, Ziółkiewicz S. Recent development trends in metal forming. Arch Civ Mech Eng. 2019;19:898–941. https://doi.org/10.1016/j.acme.2019.04.005.
137. Bochniak W. Theoretical and practical aspects of plastic forming of metals. KoBo method, AGH, Kraków; 2009.
138. Zwolak M, Śliwa RE, Pawłowska B, Wędrychowicz A. Possibility of deformation of billet with various internal structure in KOBO extrusion. Key Eng Mater. 2022;926:511–22. https://doi.org/10.4028/p-32j6m1.
139. Pawłowska B, Śliwa RE, Zwolak M. Possibilities to obtain products from 2024 and 7075 chips in the process of consolidation by KoBo extrusion. Arch Metall Mater. 2019. https://doi.org/10.24425/amm.2019.130083.
140. Korbel A, Bochniak W, Śliwa R, Ostachowski P. Low-temperature consolidation of chips from hard-to-deform aluminium alloys. Metal Forming Obróbka Plastyczna Metali. 2016;XXVII:133–51.
141. Topolski K, Bochniak W, Łagoda M, Ostachowski P, Garbacz H. Structure and properties of titanium produced by a new method of chip recycling. J Mater Process Technol. 2017;248:80–91. https://doi.org/10.1016/j.jmatprotec.2017.05.005.
142. Długosz P, Bochniak W, Ostachowski P, Molak R, Duarte Guigou M, Hebda M. The influence of conventional or KOBO extrusion process on the properties of AZ91 (MgAl9Zn1) alloy. Materials. 2021;14:6543. https://doi.org/10.3390/ma14216543.
143. Koprowski P, Bieda M, Boczkal S, Jarzębska A, Ostachowski P, Kawałko J, Czeppe T, Maziarz W, Łagoda M, Sztwiertnia K. AA6013 aluminium alloy deformed by forward–backward rotating die (KoBo): microstructure and mechanical properties control by changing the die oscillation frequency. J Mater Process Technol. 2018;253:34–42. https://doi.org/10.1016/j.jmatprotec.2017.10.043.
144. Zwolak M, Śliwa RE, Pawłowska B, Wędrychowicz A, Szawara P. The effect of microstructure transformation of light alloy products in the co-extrusion and KOBO processes. In: Prace XII Konferencja PLASTMET; 2021.
145. Kowalczyk-Gajewska K, Sztwiertnia K, Kawałko J, Wierzbanowski K, Wronski M, Frydrych K, Stupkiewicz S, Petryk H. Texture evolution in titanium on complex deformation paths: experiment and modelling. Mater Sci Eng A. 2015;637:251–63. https://doi.org/10.1016/j.msea.2015.04.040.
146. Kowalczyk-Gajewska K, Stupkiewicz S. Modelling of texture evolution in kobo extrusion process/Modelowanie Rozwoju Tekstury W Procesie Wyciskania Metoda Kobo. Arch Metall Mater. 2013;58:113–8. https://doi.org/10.2478/v10172-012-0160-y.
147. Qian L, Cui Z, Sun C, Geng S, Sun Z. Investigation of deformation compatibility and power consumption during KOBO extrusion of bimetallic composite tube. Int J Adv Manuf Technol. 2022;118:3477–86. https://doi.org/10.1007/s00170-021-08608-9.
148. Wójcik M, Skrzat A. Coupled thermomechanical Eulerian–Lagrangian analysis of the KOBO extrusion process. Arch Metall Mater. 2021. https://doi.org/10.24425/amm.2022.139719.
149. German RM. Powder metallurgy and particulate materials technology, MPIF, Princeton, USA; 2005.
150. Kim KT, Lee SC, Ryu HS. Densification behavior of aluminum alloy powder mixed with zirconia powder inclusion under cold compaction. Mater Sci Eng A. 2003;340:41–8. https://doi.org/10.1016/S0921-5093(02)00175-2.
151. Jang GB, Hur MD, Kang SS. A study on the development of a substitution process by powder metallurgy in automobile parts. J Mater Process Technol. 2000;100:110–5. https://doi.org/10.1016/S0924-0136(00)00426-X.
152. Wang T, Zhang B, Chen G, Feng J. High strength electron beam welded titanium–stainless steel joint with V/Cu based composite filler metals. Vacuum. 2013;94:41–7. https://doi.org/10.1016/j.vacuum.2013.01.015.
153. Qian M, Schaffer GB. Sintering of aluminium and its alloys. In: Sintering of advanced materials. London: Elsevier; 2010. p. 291–323. https://doi.org/10.1533/9781845699949.3.291.
154. Judge WD, Bishop DP, Kipouros GJ. Industrial sintering response and microstructural characterization of aluminum powder metallurgy alloy alumix 123. Metallogr Microstruct Anal. 2017;6:375–82. https://doi.org/10.1007/s13632-017-0379-0.
155. Bishop DP, Caley WF, Kipouros GJ, Hexemer RL, Donaldson IW. Powder metallurgy processing of 2xxx and 7xxx series aluminium alloys. Can Metall Q. 2011;50:246–52. https://doi.org/10.1179/1879139511Y.0000000003.
156. Yadav Kaku SM, Raju V, Bharath K, Fuchs Godec R, Reddy Tiyyagura H. Evaluation of ZrB2 reinforced Al/Al alloy composite produced by powder metallurgy-vacuum arc melting technique: a unique approach. Vacuum. 2018;155:539–45. https://doi.org/10.1016/j.vacuum.2018.06.055.
157. Chattopadhyay AK, Sundarapandian P. Enhanced material properties of sintered aluminium powders. In: Advances in powder metallurgy and particulate materials, MPIF; 2010.

158. Wu L, Yang L, Liu C, Ma Y, Yu Z, Wang T, Liu W, Yan H. The coupling effect of vacuum, pressure and temperature on microstructure and mechanical properties of PM aluminum alloy. Vacuum. 2022;196:110728. https://doi.org/10.1016/j.vacuum.2021.110728.
159. Jayakumar K, Mathew J, Joseph MA, Kumar RS, Shukla AK, Samuel MG. Synthesis and characterization of A356-SiCp composite produced through vacuum hot pressing. Mater Manuf Process. 2013. https://doi.org/10.1080/10426914.2013.773012.
160. Chua AS, Brochu M, Bishop DP. Spark plasma sintering of prealloyed aluminium powders. Powder Metall. 2015;58:51–60. https://doi.org/10.1179/1743290114Y.0000000105.
161. Wu L, Yu Z, Liu C, Ma Y, Huang Y, Wang T, Yang L, Yan H, Liu W. Microstructure and tensile properties of aluminum powder metallurgy alloy prepared by a novel low-pressure sintering. J Market Res. 2021;14:1419–29. https://doi.org/10.1016/j.jmrt.2021.07.074.
162. Sweet GA, Brochu M, Hexemer RL, Donaldson IW, Bishop DP. Microstructure and mechanical properties of air atomized aluminum powder consolidated via spark plasma sintering. Mater Sci Eng A. 2014;608:273–82. https://doi.org/10.1016/j.msea.2014.04.078.
163. Płonka B, Senderski J. Advanced technologies used in the manufacture of products from aluminium alloys powder in extrusion process. Key Eng Mater. 2011;491:59–66. https://doi.org/10.4028/www.scientific.net/KEM.491.59.
164. Galanty M, Kazanowski P, Kansuwan P, Misiolek WZ. Consolidation of metal powders during the extrusion process. J Mater Process Technol. 2002;125–126:491–6. https://doi.org/10.1016/S0924-0136(02)00327-8.
165. Senderski J, Płonka B, Lech-Grega M, Boczkal S, Pachla W. Structure and mechanical properties AlZnMgZr alloy manufactured of powders. Arch Mater Sci Eng. 2009;39:97–102.
166. Płonka B, Boczkal S, Rajda M. Effect of manufacturing conditions on the utilitarian properties of AlCuMgMn(ZrSc) alloy consolidated from powder. In: Powder metallurgy world congress and exhibition, Yokohama, Japan; 2012.